

# Dimensionality e ffects in a disordered system in the vicinity of the Superconductor-to-Insulator Transition

Claire Marrache-Kikuchi

▶ **To cite this version:**

Claire Marrache-Kikuchi. Dimensionality e ffects in a disordered system in the vicinity of the Superconductor-to-Insulator Transition. Superconductivity [cond-mat.supr-con]. Université Paris Sud - Paris XI, 2014. tel-00929767

**HAL Id: tel-00929767**

**https://theses.hal.science/tel-00929767**

Submitted on 13 Jan 2014

**HAL** is a multi-disciplinary open access archive for the deposit and dissemination of scientific research documents, whether they are published or not. The documents may come from teaching and research institutions in France or abroad, or from public or private research centers.

L'archive ouverte pluridisciplinaire **HAL**, est destinée au dépôt et à la diffusion de documents scientifiques de niveau recherche, publiés ou non, émanant des établissements d'enseignement et de recherche français ou étrangers, des laboratoires publics ou privés.

# UNIVERSITÉ DE PARIS SUD
# U.F.R SCIENTIFIQUE D'ORSAY

## MÉMOIRE D'HABILITATION À DIRIGER DES RECHERCHES

Spécialité

**MATIÈRE CONDENSÉE**

par

**CLAIRE AKIKO MARRACHE-KIKUCHI**

Sujet :

# Dimensionality effects in a disordered system in the vicinity of the Superconductor-to-Insulator Transition

———-

# Effets dimensionnels dans un système désordonné au voisinage de la Transition Supraconducteur-Isolant

Soutenue le **10 Janvier 2014** devant le jury composé de :

| | |
|---|---|
| **Olivier BOURGEOIS** | Examinateur |
| **Louis DUMOULIN** | Examinateur |
| **Aharon KAPITULNIK** | Rapporteur |
| **Jérôme LESUEUR** | Examinateur |
| **Marc SANQUER** | Rapporteur |
| **Pascal SIMON** | Président |
| **Nandini TRIVEDI** | Rapporteur |

CSNSM

CENTRE DE SCIENCES NUCLEAIRES ET DE SCIENCES DE LA MATIÈRE
Université Paris-Sud - CNRS - IN2P3

# Contents


**Introduction** 1

**I Setting the context** 3

**1 Experimental and theoretical state-of-the-art** 4
1.1 Phenomenology of experimental systems . . . 4
1.1.1 Granular materials . . . 4
1.1.2 Homogeneous materials . . . 5
1.1.3 Homogeneous micro-cristalline materials . . . 6
1.2 Brief overview of the theoretical models . . . 6
1.3 Open questions . . . 9
1.4 Situation of our work . . . 9
1.4.1 Film synthesis and characteristics . . . 9
1.4.2 Quantum Phase Transitions in a-NbSi . . . 10
1.4.3 Tunable parameters for the QPTs . . . 10

**II Presentation of our work** 12

**2 Weakening superconductivity with disorder** 13
2.1 Destruction of superconductivity with disorder in a-$Nb_xSi_{1-x}$ films . . . 13
2.1.1 Presentation of the paper . . . 13
2.1.2 Paper ♯1 : Crauste et al., *J. Phys. : Conf. Series*, **150**, 042019, 2009 . . . 13
2.2 Destruction of superconductivity with disorder in Nb films . . . 16
2.2.1 Presentation of the paper . . . 16
2.2.2 Paper ♯2 : Couëdo et al., *J. Phys. : Conf. Series*, **400**, 022011, 2012 . . . 16

**3 SIT : Point of view of quantum phase transitions** 20
3.1 The Superconductor-to-Insulator Transition as a Quantum Phase Transition . . . 20
3.2 Scaling near a Quantum Phase Transition . . . 20
3.2.1 Presentation of the paper . . . 20
3.2.2 Paper ♯3 : Marrache et al., *Phys. Rev. B*, **78**, 144520, 2008 . . . 21
3.3 Dimensional crossover from 2D to 3D . . . 28
3.3.1 Presentation of the paper . . . 28
3.3.2 Paper ♯4 : Crauste et al., *to be published* . . . 28

**4 SIT : A closer look at the processes at play** 34
4.1 Annealing as a parameter to fine-tune the disorder . . . 34
4.2 What is the meaning of "disorder" ? . . . 35
4.2.1 Presentation of the paper . . . 35
4.2.2 Paper ♯5 : Crauste et al., *Phys. Rev. B*, **87**, 144514, 2013 . . . 35
4.3 What is the meaning of "disorder" ? (cont'd) . . . 44
4.3.1 Presentation of the paper . . . 44
4.3.2 Paper ♯6 : Crauste et al., *J. Phys : Conf. Series*, **400**, 022012, 2012 . . . 44

**5 Application to particle detectors** 47
5.1 Background on the CSNSM *Cryogenic Detectors Group* . . . 47
5.2 Challenges in CMB and sub-millimeter astroparticle detection . . . 49
5.2.1 Scientific challenges . . . 49
5.2.2 Instrumental challenges . . . 49

5.3 A proposal for a new kind of solid-state sub-millimeter particle detector . . . 52
5.3.1 Presentation of the proposal . . . 52
5.3.2 Paper ♯7 : Marnieros et al., *J. Phys. Conf. Series*, **150**, 012027, 2009 . . . 53
5.4 Thermometry for particle and light detectors : superconducting NbSi . . . 56
5.4.1 Presentation of the paper . . . 56
5.4.2 Paper ♯8 : Crauste et al., *J. Low Temp. Phys.*, **163**, 60, 2011 . . . 56

**6 Experimental development : a cryogen free dilution refrigerator 61**
6.1 Characteristics . . . 62
6.1.1 Pulse tube-based pre-cooling . . . 62
6.1.2 Double still technique . . . 62
6.1.3 Superconducting magnet in parallel to the dilution unit . . . 62
6.1.4 Magnet pre-cooling system . . . 63
6.1.5 Thermal switches . . . 64
6.2 Performances . . . 64
6.2.1 General performances . . . 64
6.2.2 Cooling down time . . . 66
6.3 Advantages . . . 66
6.4 Ongoing improvements . . . 66

**III Future Perspectives 68**

**7 Future work and outlook 69**
7.1 Elucidation of the effect of the thickness . . . 69
7.2 Study of the dynamic properties of disordered superconductors . . . 69
7.3 Probing the density of state near the SIT . . . 71
7.4 Influence of Coulomb interactions in disordered systems . . . 71
7.5 Characterization of the hypothetic metallic state(s) . . . 72
7.6 Towards an understanding of the specificity of the materials . . . 72
7.7 Nanostructured films . . . 72
7.8 Disordered materials on the insulating side . . . 73
7.9 Application to detectors : Kinetic Inductance Detectors . . . 74
7.10 Towards lower dimensions . . . 74

# Introduction

## General framework of the research

Low temperature properties of disordered materials still represent a challenging area of study in condensed matter physics although there has been more than four decades of research on this subject. Disorder can indeed profoundly affect the transport properties of numerous quantum systems : helium superfluid properties are modified when it goes through a porous medium, the superconducting ground state of some materials can change to metallic or insulating when the system disorder is sufficiently increased, the influence of disorder on the advent of high-temperature superconductivity is an object of concern for both applied and theoretical physics, and disorder has recently been proved to be an important tuning parameter in cold atomic systems. This is due to the multiple effects disorder can, a priori, have on quantum properties of materials :

i. it modifies and enhances quantum interferences
ii. in electronic systems, it enforces Coulomb interactions
iii. it works against the establishment of long-range coherence

Within this general framework, the interplay between superconductivity and disorder is an object of intense investigation ever since the pioneering work of Ma and Lee [Ma and Lee, 1985]. Indeed, superconductivity is deeply affected by the increase of the system disorder but in a way that is not fully understood yet. In particular, disorder is expected to modify the ground state of the system and make it transit to a metallic or insulating state, hence giving rise to Quantum Phase Transitions (QPT) [1]. The effect of this tuning parameter is all the more dramatic when the system dimensionality is reduced: 2D is believed to be the inferior critical dimension for the existence of both superconductivity and a metallic state [Abrahams et al., 1979].

As part of the ongoing effort to address this important condensed matter issue, our work aims at studying the interplay between superconductivity and disorder in two dimensional systems. The main objectives are to determine the possible two dimensional ground states and study the transitions between those fundamental states.

## Outline

In part I, I will try to put our work into perspective by presenting the main theoretical questions in the domain and the experimental state-of-the-art.

I will then (part II) present our work in more details. In chapter 2, I will concentrate on how, quantitatively, in two-dimensional films, a reduction of the film thickness results in a degradation of the superconducting properties. In chapter 3, I will focus on the Quantum Phase Transitions in these systems. In chapter 4, I will expand on one original way to tune the disorder in a-NbSi thin films : annealing. In chapter 5, I will show how these studies can have interesting applications for detectors in astrophysics or astroparticle experiments. At last, in chapter 6, I will detail the development of a cryogen-free cryostat we have recently undertaken.

I will end this manuscrit by a few perspectives in part III.

## Acknowledgments

The work reported in the following pages is not, of course, solely my work.

First and above all, it has all been possible thanks to the help and support of the *Cryogenic Detectors Group* of the CSNSM. More specifically, the samples have been synthesized and characterized by Laurent Bergé, Sophie Collin, Youri Dolgorouky, and Anne-Aëlle Drillien. Aurélie Gentils and the Semiramis group have performed TEM measurements (section 4.2). Emiliano Olivieri has been a great companion for building the cryogen-free

1. Quantum Phase Transitions are phase transitions occurring at T=0 and governed by quantum fluctuations. They are induced by a change of a parameter - such as disorder or magnetic field - in the Hamiltonian of the system. As a result, the ground state of the system is modified.

cryostat and, more generally, for various discussions on cryogenics and low level measurements. Louis Dumoulin has initiated and encouraged much of this research. I personally owe a lot to him, whether scientifically or personally. But the results, analysis, interactions and various thoughts are mainly due to the PhD students I have worked with : Olivier Crauste from 2006 to 2010, François Couëdo from 2010, and now Vincent Humbert since 2013.

I am grateful for the various collaborations and interactions outside the CSNSM I have enjoyed throughout the years, although I sometimes chose not to present the corresponding work in this manuscript :

- ⋆ **The Nanostructures à la Nanoseconde group at the Laboratoire de Physique des Solides -** and more specifically Julien Gabelli, Pascale Diener, who spent her postdoc between the LPS and the CSNSM, Marco Aprili and Bertrand Reulet for work related to GHz transport measurements (section 7.2).
- ⋆ **The Service de Cryogénie at the SPEC, CEA -** Patrick Pari, Philippe Forget and Matthieu de Combarieu have helped with the design, fabrication and tests of the cryogen-free dilution unit we have recently installed (chapter 6).
- ⋆ **Cryoconcept -** Julien Paris, Olivier Guia, Christian Laurent, Pascale Peron and Philippe Bonnet were extremely diligent, helpful and obliging for the installation of the cryogen-free cryostat.
- ⋆ **The Cristaux Électroniques at the Institut Néel -** and more specifically Julien Delahaye and Thierry Grenet on the relaxation of electron glasses (section 7.8).
- ⋆ **The Laboratoire de Transport Électronique Quantique et Supraconductivité -** and more specifically Claude Chapelier and Charlène Tonnoir for STM measurements (section 7.3).
- ⋆ **The Low Temperature Group at RIKEN (Japan) -** I have spent 18 very enjoyable and profitable months at RIKEN as a postdoc. I would more specifically like to thank Kimitoshi Kono and David Rees for the work we performed related to electron detection at the surface of superfluid $^3$He.
- ⋆ **Aharon Kapitulnik from Stanford University -** for discussions during his Senior Chair granted by the RTRA Triangle de la Physique.

I also gratefully acknowledge the support of the RTRA Triangle de la Physique (grant No. 2009-019T-TSI2D), of the ANR (projects POSTIT(2010), LUMINEU (2012), COCA(2012)), of P2IO (teaching project on cryogenics), and of the CNRS for the *Délégation* I enjoyed from September 2011 to September 2013.

# Part I

# Setting the context

# Chapter 1

# Experimental and theoretical state-of-the-art

## 1.1 Phenomenology of experimental systems

The experimental study of the destruction of superconductivity in thin films has given rise to a large literature for over 40 years. In this section, I will try to briefly overview what I feel are the main features of the experimental situation.

In two dimensions [1], the superconductor-to-insulator transition (SIT, see section 1.2) features depend crucially on the nature of the considered material, and above all of its morphology. Traditionally, a clear distinction is made between granular and homogeneous films which are thought to fall under different theoretical models. As explained below, these two main classes of materials also usually exhibit notably distinct behaviors when the transition is approached.

### 1.1.1 Granular materials

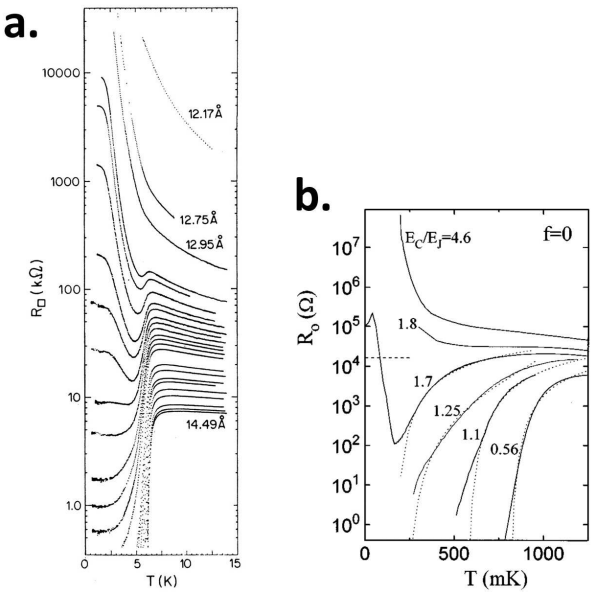



Figure 1.1: a. Resistance as a function of temperature for a-Ga films of different thicknesses (taken from [Jaeger et al., 1986]). b. Resistance as a function of temperature of Josephson junctions arrays with different values of the ratio between the charge and the Josephson energies (taken from [van der Zant et al., 1996]).

Granular materials are composed of superconducting islands, coupled by tunnel effect. The system ground state is then governed by a competition between the electrostatic charging energy and the inter-grain Josephson coupling.

1. The commonly accepted criterion two-dimensionality with respect to superconductivity is : $d < \xi_{SC}$, the superconducting coherence length.

Granular systems are characterized by a constant superconducting onset temperature $T_{c,onset}$, essentially corresponding to the critical temperature of each grain. When the film disorder is increased, the superconducting transition broadens (figure 1.1.a.) due to increasing fluctuations in the phase of the order parameter. These phase fluctuations are favored through the granular structure. Moreover, granular films often exhibit re-entrance features of the resistance, as the temperature is lowered, near the SIT. As disorder is further increased, the films become weakly insulating before exhibiting an exponential increase of the resistance as the temperature is lowered, in agreement with strong localization.

Experimentally, such systems are generally fabricated by quench-condensing metals on a substrate, without any particular precaution regarding the film wetting. The films then are a few tens of Å thick for the thinnest (Sn [Strongin et al., 1970], Au [Dynes et al., 1978], Al [Deutscher et al., 1980], Pb [Hebard and Vandenberg, 1980] amongst many others).

Let us note that Josephson junction arrays can be viewed as a extreme case of granular materials (figure 1.1.b.) [van der Zant et al., 1996].

### 1.1.2 Homogeneous materials

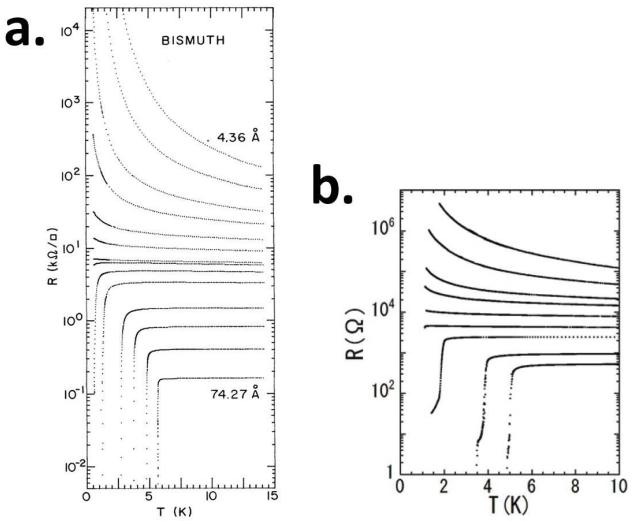



Figure 1.2: a. Evolution of the resistance with the temperature for a-Bi films (on a Ge underlayer) of different thicknesses. Taken from [Haviland et al., 1989]. The critical thickness for the SIT is 6.73 Å. b. Evolution of the resistance with the temperature for MoRu films of thicknesses ranging from 16.9 to 69.4 Å. The critical thickness is about 25 Å. Taken from [Hirakawa et al., 2008].

Homogeneous materials are disordered on an atomic scale. They present sharp superconducting transitions. When disorder is increased, there is usually no broadening of the transition (figure 1.7.a.).

Homogeneous materials include amorphous alloy films (a-MoGe, a-MoSi, a-NbSi, ...), metals deposited at low temperature on a a-Ge underlayer [2], and $InO_x$. These three categories of homogeneous films have nonetheless their own particular features vis-à-vis the SIT :

1. One important difference resides in the parameters that can induce a disorder-tuned SIT in these systems :
   - In ultra-thin metallic films, it is reasonable to assume that a thickness reduction does not change the material density of states.
   - Alloys, on the other hand, present numerous manners to tune the disorder : via the film thickness or their composition for instance. The stoichiometry permits to modify the bulk superconducting temperature $T_{c0}$ through the modification of the density of states.
   - Disorder in $InO_x$ films has also been introduced by annealing. This procedure has the effects of both reducing the oxygen content in the film [Gantmakher, 1998] and of reducing its volume [Ovadyahu, 1993].
2. In the case of ultra-thin metallic films, deemed to be homogeneous, one can note that the SIT occurs extremely rapidly [3]. Moreover, these films are usually a few monolayers-thick. By contrast, alloy thin films have thicker critical thicknesses of the order of a few tens of angströms (figure 1.7.b.).

2. A a-Ge underlayer increases the wetting of the deposited films, so that the sample thus synthesized are continuous, but highly disordered, thanks to the cryogenic deposition temperature.

3. Typically, in the disorder-induced SIT, it occurs for a thickness variation of the order of one tenth of angströms.

3. $InO_x$ films differ from alloy or metallic thin films in that they usually are thick ($d$>200Å) and therefore could be considered three-dimensional [Feigel'man et al., 2010]. Let us also note that they present a large negative magnetoresistance and spatial inhomogeneities of the superconducting order parameter, although the films are morphologically homogeneous, that distinguish it from the other two categories.

The latter point rises the question of the pertinence of differentiating materials through their morphological characteristics : if a morphologically homogeneous system can present an inhomogeneous electronic phase, what really distinguishes the different classes of materials ?

### 1.1.3 Homogeneous micro-cristalline materials

Micro-cristalline materials studied in the framework of the SIT are metallic nitrides (TiN and NbN). These films are made out of cristallites which size is about 300 Å in diameter [Baturina et al., 2007]. Electronic transport-wise, they behave like homogeneous systems (figure 1.3) in the sense that they do not present any re-entrance phenomena or any broadening of the superconducting transition when disorder is increased [Feigel'man et al., 2010, Baturina et al., 2007]. Like $InO_x$ films, TiN present a large negative magnetoresistance and spatial inhomogeneities of the superconducting order parameter.

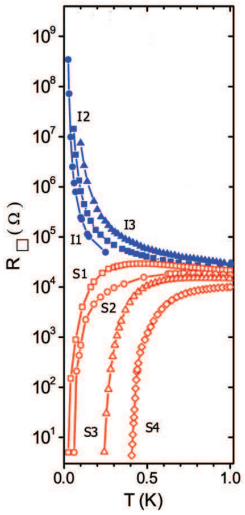



Figure 1.3: Evolution of the resistance with the temperature for TiN films close to the SIT. Taken from [Baturina et al., 2007].

## 1.2 Brief overview of the theoretical models

Until the 1980s, the influence of disorder on superconductivity was only taken into account by the theory of so-called "dirty" superconductors, based on Anderson's theorem [Anderson, 1959] where disorder was treated as a perturbation to the initial system and was not pair-breaking. Subsequently, several theories [Anderson et al., 1983, Ma and Lee, 1985, Kapitulnik et al., 1985] tried to understand how, in the 3D case, a disordered-tuned Anderson Metal-to-Insulator Transition in the normal state [Anderson, 1958] could affect superconductivity. The possible ground states for 3D disordered superconductors therefore depend on whether the destruction of superconductivity by disorder takes place before, at the same time or after the Anderson transition [Gantmakher and Dolgopolov, 2010]. This approach was then extended to any control parameter that could drive a superconducting ground state into a non-superconducting one.

In 2D, however, the situation is more complex. This dimension is particularly interesting to investigate the interplay between quantum interferences, Coulomb interactions and superconducting fluctuations : because of the reduced dimensionality, the possible ground states of the system are more strongly affected than in 3D by the modification of one of these parameters.

Historically, the theory of localization [Abrahams et al., 1979] predicted that non-interacting electrons would end up being localized, no matter how weak the disorder : in this picture, there is no possible metallic ground state in 2D. Hence, 2D systems were thought of either in terms of insulators or, if superconductivity was involved, of superconductors. Accordingly, the pioneering experimental work of Goldman's group [Haviland et al., 1989] interpreted the destruction of superconductivity in thin films in terms of a direct Superconductor-Insulator Transition.

Experimentally, it is clear that superconducting 2D systems experience a transition from a superconducting to an insulating ground state. However, in reduced dimensions, electrons are known to be prone to more important Coulomb interactions and quantum fluctuations. These two ingredients can in turn affect the system ground state and have even been proved to favor a metallic phase in some systems [4]. Experimentalists therefore disagree on whether the observed transition is direct ([Markovic et al., 1998, Bielejec and Wu, 2002] for eg.) or implies an intermediate metallic phase ([Yazdani and Kapitulnik, 1995, Marrache-Kikuchi et al., 2008] for eg.). In the same time, there have been extensive theoretical debates on the ground state emerging when superconductivity is suppressed [5] (see for example [Larkin, 1999, A. Kapitulnik and Chakravarty, 2001, Punnoose and Finkel'stein, 2005, Gantmakher and Dolgopolov, 2008]).

To this day, three possible phase diagrams are being considered (see Figure 1.4), each corresponding to a different theory. There has been experimental evidence, sometimes contradictory, supporting all different models. Let us now briefly overview these.

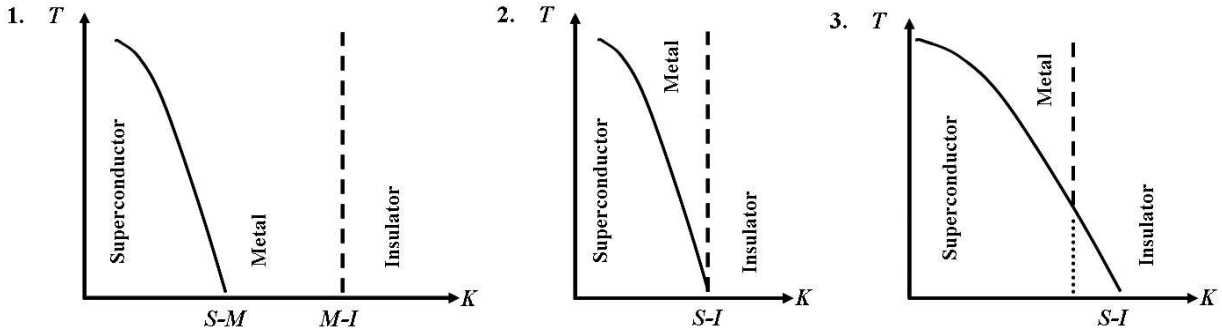



Figure 1.4: Possible phase diagrams for a 2D disordered system, tuned by a parameter $K$ (disorder, electric or magnetic field...). Taken from [Gantmakher and Dolgopolov, 2010].

- **Diagram n°2** corresponds to the one of the first models developed in the 90s to explain the SIT: the **"Dirty Boson Model"** (DBM) [Fisher and Lee, 1989]. In this picture, the system consists of interacting bosons in a disorder potential and the transition is direct between a superconducting state - consisting of localized vortices and condensed Cooper pairs - and an insulating state of localized Cooper pairs and condensed vortices. The metallic ground state is a singularity occurring exactly at the transition, for a universal sheet resistance $R_c = h/4e^2$. At the transition, the amplitude of the superconducting order parameter stays a priori finite, but superconductivity disappears due to important phase fluctuations. The DBM is therefore believed to be relevant for granular materials, Josephson junctions arrays or bosonic systems of cold atoms [Feigel'man et al., 2010, Giamarchi, 2009], although it has widely been applied to qualitatively describe homogeneous systems [Markovic et al., 1998, Yazdani and Kapitulnik, 1995, Marrache-Kikuchi et al., 2008, Bielejec and Wu, 2002] for eg.. However it presents a few drawbacks :
  - it fails to explain the behavior of homogeneous systems at intermediate temperatures (typically in the 100 mK - 1 K range)
  - it does not account for the wide range of experimental values of the critical exponents (as defined in section 3.2) or for the critical resistance (found to be non universal) [Bielejec and Wu, 2002, Yazdani and Kapitulnik, 199 Marrache-Kikuchi et al., 2008]
  - it cannot explain the magnitude of the giant negative magnetoresistance observed in some systems (figure 1.5) [Sambandamurthy et al., 2004, Baturina et al., 2007]
  - it cannot explain the important spatial inhomogeneities measured in the superconducting order parameter [Sacépé et al., 2008] (figure 1.6)

4. In 2D electron gases in Si-MOSFETs for example, the metallic phase is probably a consequence of strong Coulomb interactions [Kravchenko et al., 1994].

5. By an increase in the disorder, but also by the application of a magnetic field for example.

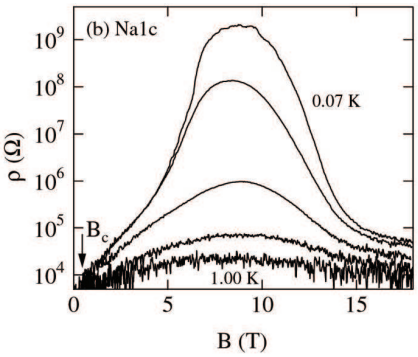



Figure 1.5: Resistance as function of the magnetic field for $InO_x$ films. Taken from [Sambandamurthy et al., 2004].

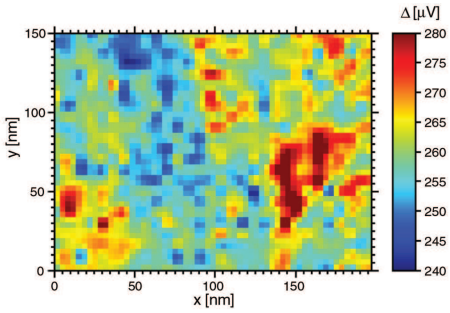



Figure 1.6: Spatial fluctuations of the superconducting gap in thin TiN films. Taken from [Sacépé et al., 2008].

- **Diagram n°3** can be accounted for by two very different models :
  - ⋆ The **fermionic scenario** developed by Finkel'stein [Larkin, 1999, Finkel'stein, 1987, Finkel'stein, 1994, Maekawa and Fukuyama, 1982] which explains the destruction of superconductivity through the competition between Cooper-pair attraction and disorder-enhanced Coulomb repulsion. It predicts a simultaneous vanishing of the superconducting critical temperature and of the order parameter at relatively large conductance, but, due to Anderson localization, the emerging 2D electronic state is expected to be insulating at T=0. This theory should essentially be applicable in the cases of homogeneously-disordered superconducting 1D wires or of 2D films. This scenario may account for the fermionic channel observed in some experiments and due to un-paired electrons below $T_c$ [Yazdani and Kapitulnik, 1995], but it fails to explain the superconducting behavior observed in low conductance 2D films [Marrache-Kikuchi, 2006, Sacépé et al., 2008] for eg., the giant negative magnetoresistance, or the spatial inhomogeneities of the superconducting order parameter.
  - ⋆ The **"pseudo-spin" scenario** has very recently been developed by Feigel'man and collaborators. It explains the SIT as a competition between Cooper pairing and localization [Feigel'man et al., 2010]. This is an extension of Ma and Lee's theory [Ma and Lee, 1985] that disregards Coulomb interactions and is believed to be valid for 3D homogeneous superconductors (although similar results are awaited in 2D). In this picture, the superconducting state consists in the pairing of weakly-localized electrons. At the transition, the superconducting order parameter is predicted to be extremely inhomogeneous as experimentally observed in InOx thin films [Sacépé, 2007]. On the insulating side, the material is a weak Anderson insulator, with a hard insulating gap due to Cooper interaction ; Cooper pairs are predicted to be pre-formed although they are localized and without macroscopic coherence. This theory explains the activated behavior observed in some insulators [Baturina et al., 2007, Ovadia et al., 2009] but does not yet describe the weak insulating behavior observed in other systems undergoing an SIT [Gantmakher, 2004, Marrache-Kikuchi et al., 2008]. Similar results have been observed via numerical simulations [Ghosal et al., 2001].
- **Diagram n°1** corresponds to a more prospective vision of the 2D disordered system implying the existence of a (quantum) metallic ground state. The ground-breaking work by Kravchenko and co-workers on clean 2D electron gases in Si-MOSFETs [Kravchenko1994] has shown that, contrary to what was expected from Anderson localization, there could be a metallic phase in 2D, provided that the Coulomb interactions were strong enough. Subsequent theoretical studies have shown that a 2D disordered metallic phase could be stabilized [Gantmakher2008] via either :
  - i. spin/orbit interactions
  - ii. Coulomb interactions [6]
  - iii. attractive interactions such as superconductivity [Feigel'man and Larkin, 1998, Feigel'Man et al., 2001, Spivak et al., 2001]
  - iv. or a coupling to a heat bath introducing dissipation [7] [A. Kapitulnik and Chakravarty, 2001].

  Experimentally, because such measurements can easily be impaired by artifacts, there has not been clear-cut proof for a 2D quantum metal. However, some systems exhibit a saturation of the resistance at very low temperature which might be interpreted as compelling evidence for such a ground state

6. A corresponding theory for disordered systems has been developed by Punnoose and Finkel'stein [Punnoose and Finkel'stein, 2005]
7. The metallic phase would then be stabilized by strong enough coupling to a heat dissipation bath [Das and Doniach, 1999].

[Yazdani and Kapitulnik, 1995, Marrache-Kikuchi, 2006, Eley et al., 2012]. The precise nature of this possible metal is still to be understood: it could be a fermionic metal [Punnoose and Finkel'stein, 2005] or a bosonic one [Das and Doniach, 1999]. The existence of a 2D metal in disordered system is therefore an open question. The meaning of "2D" would then also need to be clarified.

## 1.3 Open questions

The details of the QPTs governing the changes between the ground states raise a number of issues that have been at the centre of some controversies for the past few years [Larkin, 1999, Gantmakher and Dolgopolov, 2008]. However, as can be seen from the diversity of the above-described models, a complete and coherent picture of the SITs is still to be established. In my view, the following questions are still to be answered :

- ⋆ Is the SIT a direct transition ?
- ⋆ What is the nature of the insulating phase ?
- ⋆ Is the electronic state inhomogeneous ? If so, is this inhomogeneity inherent to the morphological disorder of the films, or is it due to mesoscopic fluctuations ?
- ⋆ Why are there different classes of materials ?
- ⋆ How can the disorder be quantified ?
- ⋆ What is the effect of a thickness reduction ? Is it analogous to an increase in disorder ?
- ⋆ What is the importance of Coulomb interactions ?
- ⋆ Do Cooper pairs survive in the insulating state ?
- ⋆ What are the dynamics of these systems near the transition ?

## 1.4 Situation of our work

As previously stated, 2D Quantum Phase Transitions are of particular interest in homogeneously disordered superconductors. Amorphous superconducting alloys are a well-known example of such systems. However, most amorphous materials that have been studied to date either do not have a controlled microscopic disorder - which would be extremely valuable for a precise monitoring of the effect of disorder - or suffer from experimental drawbacks that make them difficult to study. In this context, we chose to study amorphous $Nb_xSi_{1-x}$ films. Thanks to the different experimentally accessible control parameters, this compound is extremely versatile and its synthesis well controlled. We therefore believe that it may serve as a model for homogeneously disordered superconducting thin films.

### 1.4.1 Film synthesis and characteristics

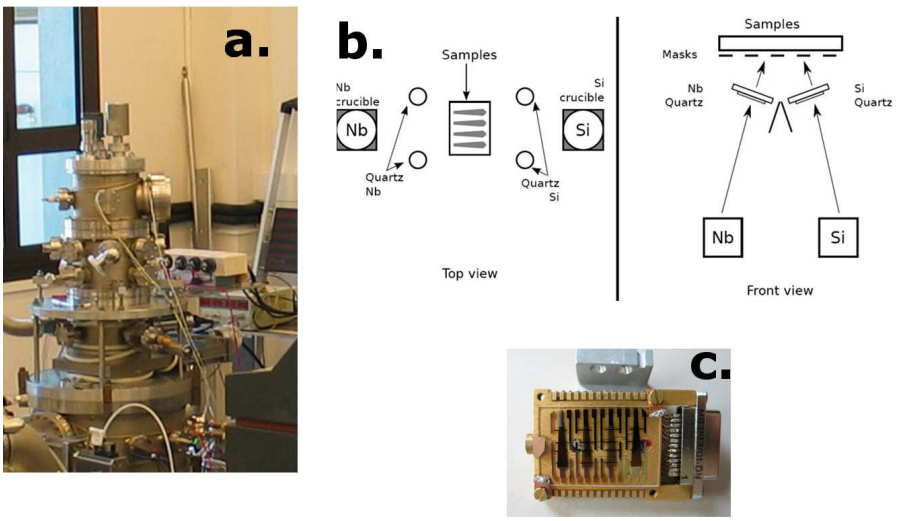



Figure 1.7: a. Ultra-high vacuum deposition chamber for a-NbSi at CSNSM. b. Schematic representation of the co-deposition geometry. c. Typical sample, mounted on a sample holder.

The a-$Nb_xSi_{1-x}$ films have been prepared at CSNSM, at room temperature[8] under ultrahigh vacuum by electron beam co-deposition of Nb and Si. The films are deposited onto sapphire substrates coated with a

8. a-NbSi films are stable at room temperature.

50-nm-thick SiO underlayer. Samples are also generally over-coated with a 250 Å-thick SiO layer for protection against oxydation.

The CSNSM group has been synthesizing a-NbSi films for a few years now. The experimental deposition apparatus to grow them is therefore well mastered, although there is a constant concern to improve the deposition technique. The deposition is controlled *in situ* by a special set of piezoelectric quartz in order to precisely monitor the composition and the thickness of the deposition. These two characteristics then are controlled *ex situ* by Rutherford back scattering (RBS) at the Aramis facility of CSNSM.

As will be seen in section 4.2, samples have been characterized by Atomic Force Microscopy and Transmission Electron Microscopy and showed no sign of morphological granularity nor inhomogeneity. Thin films have been measured to be continuous, structurally non-percolating and, a priori, homogeneously disordered even for thicknesses as low as 25 Å .

### 1.4.2 Quantum Phase Transitions in a-NbSi

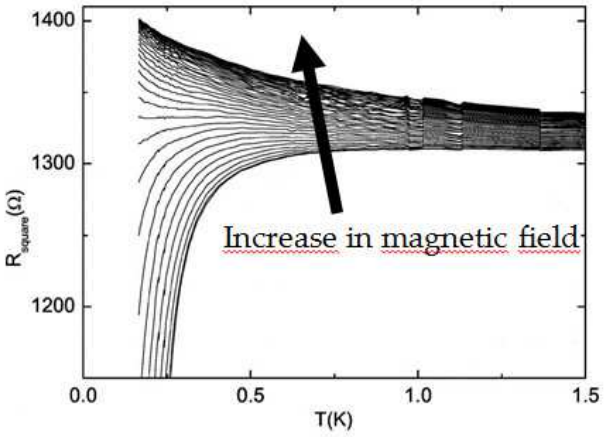



Figure 1.8: Magnetic field-tuned SIT in 2D a-NbSi thin films. Taken from [Aubin et al., 2006].

In 3D, NbSi thin films exist under the three possible ground states : superconducting, metallic and insulating, depending on the niobium concentration. In 2D, this material undergoes what we have so far interpreted as a SIT, that has been tuned either by a magnetic field (figure 1.8), or by varying the film thickness [Aubin et al., 2006, Marrache-Kikuchi et al., 2008].

Regarding the thickness-tuned transition, most materials investigated so far present two main disadvantages : either they are made ultrathin in order to destroy the superconducting ground state at zero magnetic field (Bi, Ta), with a film thickness in the nanometer range [Haviland et al., 1989, Qin et al., 2006] which drastically narrows the study area ; or, like $InO_x$, because of a low carrier density, the films are 3D rather than 2D with a thickness of several tens of nanometers [Shahar and Ovadyahu, 1992, Gantmakher et al., 2000]. For a-NbSi thin films, however, the typical critical thickness at which the 2D superconducting ground state is suppressed is of the order of 100 Å (see section 3.3), depending on the niobium concentration. At these thicknesses, unlike other systems, the films are 2D with respect to the superconducting correlation length and we need not worry about any continuity problems in the films.

Furthermore, we believe a-NbSi is an ideal system to address the question of a possible disordered metal in 2D. Indeed, some transport features close to the transition indicate that the observed SIT might actually not be direct but rather imply Superconductor-to-Metal-to-Insulator Transitions :

i. at very low temperature (7 - 100 mK) the measured resistances - both on the "superconducting" and the "insulating" sides - are astonishingly temperature independent and this effect appears to be intrinsic

ii. the "insulating" phase presents only weak temperature dependence unlike other systems, such as TiN for eg. [Sacépé et al., 2008]. This pleads in favor of a metal with quantum corrections rather than an actual insulator

### 1.4.3 Tunable parameters for the QPTs

Finally, let us stress that a-NbSi presents a number of tunable parameters that could allow us to modify the relative importance of Coulomb interactions, disorder and superconductivity. This should allow us to explore a larger portion of the parameter space than with other materials. The usual tuning parameters : the film thickness $d$, the application of a magnetic or electric field, are, naturally, available for this system. The magnetic field is

an important tool to probe the system normal state after quenching the superconductivity. The electric field modifies the Coulomb interactions in the material. This is especially important to test the "pseudo-spin" model which claims that these interactions do not play any role in the destruction of superconductivity. In addition to these important parameters, more original control knobs can also be adjusted in our system.

First, the composition $x$ of the alloy allows to control the density of states. Second, as will be seen in chapter 4, the film normal resistance can be modified via annealing (or ion implantation) while keeping a constant thickness. This additional tuning parameter provides a very convenient way to tune the disorder.

# Part II

# Presentation of our work

# Chapter 2

# Weakening superconductivity with disorder

In this chapter, I will present two conference papers on the thickness-induced destruction of superconductivity in two related systems : a-$Nb_xSi_{1-x}$ films and Nb films. Both papers examine how, quantitatively, in two-dimensional films, a reduction of the film thickness results in a degradation of the superconducting properties, namely in terms of a decrease of the superconducting critical temperature $T_c$.

In both papers, we have tried to analyze the obtained results within the framework of Finkel'stein's fermionic theory (see section 1.2) which prediction I will briefly remind here. For weakly disordered systems, where $k_F l \gg 1$ ($k_F$ is the Fermi wave vector and $l$ the elastic mean free path), Anderson's theorem [Anderson, 1959] claims that superconductivity is not affected by non-magnetic impurities. However, as disorder increases, this theorem does not hold : the elastic scattering caused by the disorder reduces the dynamical charge screening and thus enhances Coulomb interactions. This induces a $T_c$ reduction which Maekawa and Fukuyama [Maekawa et al., 1983] have calculated to the first order in $k_F l$. Finkel'stein [Finkel'stein, 1994] then completed this theory and described the entire $T_c$ reduction down to very disordered system ($k_F l \sim 1$). He derived the following prediction linking the superconducting critical temperature to the normal state resistance :

$$\frac{T_c}{T_{c0}} = \exp\left(-\frac{1}{\gamma}\right)\left[\left(1+\frac{\sqrt{r/2}}{\gamma - r/4}\right)\left(1-\frac{\sqrt{r/2}}{\gamma - r/4}\right)\right]^{1/\sqrt{2r}} \tag{2.1}$$

where $\gamma = 1/\ln\left(\frac{k_B T_{c0}\tau}{2\pi\hbar}\right)$, $r = \frac{e^2}{2\pi\hbar}R_\square$, $R_\square$ the normal sheet resistance, $\tau$ the mean free path time, and $T_{c0}$ the BCS superconducting critical temperature for the corresponding bulk (3D) material.

However, more than the actual analysis, I feel what is more interesting is the comparison between the two systems. As stated before, it is primordial to understand how different materials react in such different manners to an increase in disorder. The comparison between Nb and a-$Nb_xSi_{1-x}$ films is a small step towards this goal. In the future, we would very much like to investigate other systems to clarify our understanding of this issue.

## 2.1 Destruction of superconductivity with disorder in a-$Nb_xSi_{1-x}$ films

### 2.1.1 Presentation of the paper

The following paper, presented at the LT25 conference in August 2008 by Olivier Crauste, focuses on the $T_c$ reduction with decreasing thickness $d$ in a-$Nb_xSi_{1-x}$ films of different compositions $x$. The main result is the following :

- **Finkel'stein's theory explains qualitatively the observed $T_c$ reduction -** The general tendency of the $T_c = f(R_\square)$ is well described by equation 2.1. However, the fitting parameters imposed by the bulk superconducting temperature $T_{c0}$ and the mean free path time $\tau$ do not agree with the knowledge we have of a-$Nb_xSi_{1-x}$ films, in particular from specific heat measurements.

### 2.1.2 Paper ♯1 : Crauste et al., *J. Phys. : Conf. Series*, 150, 042019, 2009

# Thickness dependence of the superconductivity in thin disordered NbSi films

**O Crauste, C A Marrache–Kikuchi, L Bergé, D Stanescu and L Dumoulin**

C.S.N.S.M, CNRS-IN2P3, UMR 8609, Paris XI University, Orsay, France

E-mail: Olivier.Crauste@csnsm.in2p3.fr

**Abstract.** Superconducting a-$Nb_xSi_{1-x}$ thin films experience a lowering of the $T_c$ until the superconductivity disappears through a Superconductor–Insulator Transition (SIT). We here present transport measurements on 2D a-$Nb_xSi_{1-x}$ films, close to the SIT, for different compositions and thicknesses. We investigate the lowering of the $T_c$ in light of existing theories, especially the one developed by Finkel'stein.

## 1. Introduction

Since the pioneering work of Hebard et al. on InOx [1], it has been decades now that transport properties in disordered supraconducting thin films have aroused great excitation. These 2D systems, where the thickness $d_\perp$ is lower than the superconducting coherence length $\xi$, exhibit long studied Superconductor–Insulator Transitions (SIT) which can be induced by various external parameters such as the magnetic field, the disorder, etc. [2]. These SITs have been described by M.P.A. Fisher [3] and the "Dirty Boson Model" which analyses the transition in terms of Quantum Phase Transition.

When the thickness of such superconducting thin films is reduced, the superconductivity is progressively destroyed before the film undergoes a disorder–induced SIT and hence becomes insulating. M.P.A. Fisher's model well describes this transition but does not give a clear physical interpretation for the initial $T_c$ reduction.

Superconducting a-$Nb_xSi_{1-x}$ thin films have been shown to provide an interesting example of system undergoing a SIT [4]. In this paper, we focus on the undestanding of the $T_c$ reduction in this system before it turns to insulating.

## 2. Experimental Setup

The amorphous NbSi thin films have been prepared under ultrahigh vacuum by e-beam co-deposition of Nb and Si. Different series of four samples have been deposited onto sapphire substrates coated with a 50 nm-thick SiO underlayer. The stoichiometry and the thicknesses of the various samples are given in Table 1. The four films were synthesized during a single run in order to have the samples' niobium concentrations as similar as possible. We also took special care over the control of the sample's parameters : the evaporation was controlled *in situ* by a special set of piezo-electric quartz in order to precisely monitor the composition and the thickness of the deposition. These two characteristics were then controlled *ex situ* by Rutherford Back Scattering and the results well fitted with the *in situ* monitoring. Each samples' edges were etched by Reactive Ion Etching in order to suppress any edge effect that might affect the transport measurements.

We then measured the electrical transport properties of the samples with a dedicated dilution fridge down to 7 mK. All leads were filtered from RF at room temperature. Transport measurements were done with a TRMC2 measuring bridge. We double-checked our measurements by performing AC lock-in detection measurements. Moreover, in all cases, special care was taken to ensure we were not overheating the films.

Our samples are believed to be homogeneous as AFM and SEM measurements show no morphological granularity. Temperature dependance of the sheet resistivity shows sharp transitions (Figure 1) and no reentrant behavior as it is the case for granular systems [5]. Another argument for the samples' homogeneity is that the onset temperature of the superconductivity decreases as the film thickness is reduced.

© 2009 IOP Publishing Ltd


25th International Conference on Low Temperature Physics (LT25) IOP Publishing
Journal of Physics: Conference Series **150** (2009) 042019 doi:10.1088/1742-6596/150/4/042019

**Table 1.** Description of $Nb_xSi_{1-x}$ thin films : composition $x$, name, thickness $d_\perp$ and superconducting transition temperature $T_{cb}$ for bulk samples of the same stoichiometry.

| Composition | Name | $d_\perp$ [Å] | $T_{cb}$ [K] |
|---|---|---|---|
| $x = 14\%$ | OC02 | 75, 125, 175, 500 | 0.28 |
| | OC03 | 90, 105, 150, 175 | |
| $x = 15\%$ | CKJ1 | 125, 250, 500, 1000 | 0.59 |
| | CKJ2 | 25, 50, 75, 100 | |
| $x = 17\%$ | CKJ3 | 40, 50, 75, 125 | 0.8 |

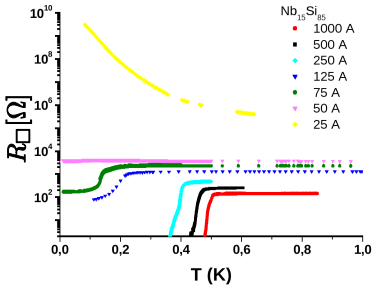



**Figure 1.** Resistance for $x = 15\%$. Our samples are assumed to be homogeneously disordered : there is no reentrant behavior, the transition is sharp and the onset of the superconductivity decreases with the thickness.

**Table 2.** Results obtained from least square fit of Eq 1.

| Composition | $\tau$ [s] |
|---|---|
| $x = 14\%$ | $1.2 \times 10^{-13}$ |
| $x = 15\%$ | $0.8 \times 10^{-13}$ |
| $x = 17\%$ | $1.4 \times 10^{-13}$ |

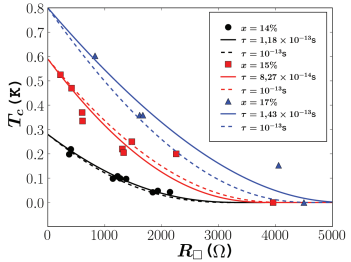



**Figure 2.** Decrease of $T_c$ vs $R_\square$. The symbols represent the experimental data. The solid lines are the least square fit of Eq 1. The dashed curves are obtained with $\tau = 10^{-13}$ s for the different compositions.

## 3. Theoretical background

The influence of the disorder on the superconductivity has been a long–standing problem. For weakly disordered systems, $k_F l \gg 1$ where $k_F$ is the Fermi wave vector and $l$ the elastic mean free path, Anderson's theorem claims that superconductivity is not affected by non-magnetic impurities. However, as the disorder increases, this theorem does not hold : the elastic scattering caused by the disorder reduces the dynamical charge screening and thus enhance the Coulomb interaction. This induces a $T_c$ reduction as Maekawa and Fukuyama [6] have explained within a linear approximation in the first order of $k_F l$. Finkel'stein [7] then completed this theory and described the whole reduction of $T_c$ down to very disordered system ($k_F l \approx 1$). He derives the following equation :

$$\frac{T_c}{T_{c0}} = \exp\left(-\frac{1}{\gamma}\right)\left[\left(1+\frac{\sqrt{r/2}}{\gamma - r/4}\right)\times\left(1-\frac{\sqrt{r/2}}{\gamma - r/4}\right)^{-1}\right]^{1/\sqrt{2r}} \quad (1)$$

where $\gamma = 1/\ln\left(\frac{k_B T_{cb}\tau}{2\pi\hbar}\right)$, $r = (e^2/2\pi\hbar)R_\square$ [8], $R_\square$ is the normal sheet resistance, and $T_{c0}$ is the BCS superconductivity transition temperature for the bulk material and $\tau$ the elastic mean free path time. This theory was applied on different systems : MoGe [7], Ta [8], TiN [9].

## 4. Thickness dependence of $T_c$

Since a-NbSi thin films are homogeneous and highly disordered ($k_F l \approx 1$), we have tried to see whether Eq 1 could account for the $T_c$ reduction we observe. We measured $R_\square$ and $T_c$, $T_{c0}$ was taken to be $T_{cb}$, the superconducting transition temperature measured for thicker samples, and $\tau$ was the fitting parameter. The mean free path times obtained by the least square fit of our experimental data are given in Table 2. The fits and the experimental data are shown on Figure 2. Since all $\tau$ have a value of roughly $10^{-13}$ s, we tried to perform a fit with a fixed $\tau$. The results is shown on Fig. 2 (dashed lines).

Let us compare the $\tau$ obtained by fitting the experimental data with Eq. 1 with what we can reasonably expect in this material. In our systems, the inter-atomic distance was measured to be of about 2.6 Å [10]. Therefore the mean free path can be expected to lie between 2.6 and 10 Å. Moreover specific heat measurements on NbSi films have given $c = 1.5\times10^{-5}$ J/K.cm$^3$ [11] which is a value comparable to that of gold. Taking into account that the effective mass might not be the same in Au and in NbSi, we have an acceptable range of Fermi velocity between $10^7$ and $2.10^8$ cm.s$^{-1}$. This leads to an acceptable range for the mean-free-path times between $10^{-16}$ and $10^{-14}$ s. The $\tau$ obtained from the fit is one order of magnitude above this acceptable range. Eq. 1 therefore does not describe satisfyingly our data.

However, Finkel'stein mentions a correction that has to be made for very disordered films. Indeed, for $l < d_\perp$, the mean free path time $\tau$ in Eq. 1 should be replaced by $\frac{d_\perp^2}{l^2}\tau$. One must note that this introduces an additional dependance on $l$ which value is not precisely known in our films. In order to fit our data, we must therefore make an hypothesis on the value of $l$ and adjust $\tau$ and $T_{c0}$. We performed the fits for two values of $l$ ($l$=2,65 Å and $l$=5 Å). The results are summarized in Figure 4 and the adjustment plotted together with the experimental data on Figure 3. Whatever the precise value of $l$, we now obtain mean free path times that are plausible. Both $\tau$ and $T_{c0}$ are found to be not significantly dependant on $l$. However, the $T_{c0}$ inferred from this fit are systematically lower than the $T_{cb}$ measured in bulk samples.

## 5. Conclusion

Our samples' behavior is qualitatively described by Finkel'stein theory provided that we take into account the correction necessary for very disordered thin films ($d_\perp > l$). This is in agreement





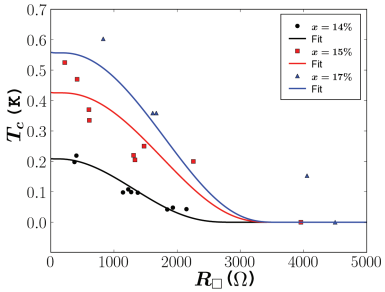



**Figure 3.** Decrease of $T_c$ vs $R_\square$. The solid lines are the least square fit of Eq 1 with the correction $\tau \to \frac{d_\perp^2}{l^2}\tau$. The fits performed for $l = 2.6$Å and $l = 5$Å are indistinguishable.

| Composition | $\tau(l = 2.65$Å$)$ | $\tau(l = 5.0$Å$)$ | $T_{c0}$ |
|---|---|---|---|
| $x = 14\%$ | $0.9\times10^{-16}$ s | $3.4\times10^{-16}$ s | 0.21 K |
| $x = 15\%$ | $1.8\times10^{-16}$ s | $6.5\times10^{-16}$ s | 0.43 K |
| $x = 17\%$ | $8.6\times10^{-16}$ s | $31\times10^{-16}$ s | 0.56 K |

**Figure 4.** Results obtained from least square fit of Eq 1 with the correction $\tau \to \frac{d_\perp^2}{l^2}\tau$. Two different values of $l$ are taken to perform the fit. $T_{c0}$ is now also a fitting parameter.

with the fact that a-NbSi is a strongly disordered system : for bulk $x = 14\%$ samples, the resistivity $\rho \simeq 1900\ \mu\Omega.\text{cm} \pm 100$, which is 10 times larger than the bulk resistivity in MoGe [7][12] ($\rho \simeq 160\mu\Omega.\text{cm}$). Quantitatively, however, the inferred mean free path time corresponds to what is expected for these films, but the $T_{c0}$ do not match the superconducting temperatures measured for 3D samples. Equivalently, this means that the theory doesn't account for thick samples. A possible explanation for this is that these thick samples approach the vicinity of the 2D-3D crossover which is the limit for Finkel'stein's theory (for $x$=15%, $T_{cb}$=0.59 K, $\xi_{eff} = \sqrt{\hbar v_F l/k_B T_c} = 409$ Å with $l$=2.6 Å and $v_F$=5×10$^5$ m.s$^{-1}$).

## References

[1] Hebard A F and Paalanen M A 1984 *Phys. Rev. B* **30** 4063
[2] Sondhi S L, Girvin S M, Carini J P and Shahar D 1997 *Rev. Mod. Phys.* **69** 315
[3] Fisher M P A 1990 *Phys. Rev. Letters* **65** 923
[4] Aubin H, Marrache-Kikuchi C A, Pourret A, Behnia K, Bergé L, Dumoulin L and Lesueur J 2006 *Phys. Rev.* B **73** 094521
[5] Haviland D B, Liu Y and Goldman A M 1989 *Phys. Rev. Lett.* **62** 2180
[6] Maekawa S and Fukuyama H 1983 *J. Phys. Soc. Jpn.* **52** 1352
[7] Finkel'stein A M 1994 *Physica* B **197** 636
[8] Astrakharchik E G and Adkins C J 1994 *Phys. Rev.* B **50** 13622
[9] Hadacek N, Sanquer M and Villégier J C 2004 *Phys. Rev.* B **69** 024505
[10] Hucknall P K, Walker C G H, Greig D, Matthew J A D, Norman D and Turton J 2004 *Surface and Interface Analysis* **19** 23
[11] Marnieros S, Bergé L, Juillard A and Dumoulin L 1999 *Physica B* **261** 862
[12] Graybeal J M and Beasley M R 1984 *Phys. Rev. B* **29** 4167

## 2.2 Destruction of superconductivity with disorder in Nb films

### 2.2.1 Presentation of the paper

In an attempt to complete our understanding of a-$Nb_xSi_{1-x}$, we initiated a brief study on this compound at the $x \to 100\%$ limit : pure Nb films. This was the subject of François Couëdo's 6 weeks Master Course internship.

Nb films proved to be difficult to synthesize : the vacuum level during the deposition is an important parameter, since Nb films are very sensitive to residual $O_2$ [1] and the reproducibility of the films were thus made difficult. We could however study the transport properties of four such films of thicknesses ranging from 25 to 263 Å, under a magnetic field up to 6 T.

The following paper, presented at the LT26 conference in August 2011 by François Couëdo, focuses on the $T_c$ reduction with decreasing thickness $d$ in Nb films and sketches a comparison between this system and a-$Nb_xSi_{1-x}$. The main results are the following :

1. **The phase diagram for Nb films in the ($d$,$H$) plane is inferred.**
2. **Finkel'stein's theory explains qualitatively the observed $T_c$ reduction -** As for a-$Nb_xSi_{1-x}$ films, the general tendency of the $T_c = f(R_\square)$ is well described by equation 2.1, but the fitted bulk superconducting temperature $T_{c0}$ and mean free path time $\tau$ are unrealistic. In particular, the mean free path time derived from equation 2.1 is two orders of magnitude larger than what is found in the literature.
3. **Failure of critical scaling near the transition -** The obtained results for Nb films have also been analyzed in the framework of the Dirty Boson Model (see section 1.2) where the destruction of superconductivity is described as a Quantum Phase Transition to a bosonic insulator through fluctuations of the phase of the order parameter. As such, scaling relations are predicted (see section 3.2), and have been tried on our data. Whatever the critical exponents, our data could not be made to collapse on two curves (one for the superconducting side, one for the insulating side).
4. **Comparison with a-$Nb_xSi_{1-x}$ -** These results show that the destruction of superconductivity in both systems cannot be explained by the same mechanisms :
   - For a-$Nb_xSi_{1-x}$, the greater $x$, the larger the critical sheet resistance at which superconductivity is completely destroyed. In other words, as the niobium composition is increased, so does the robustness of superconductivity to disorder. For Nb films, on the contrary, $T_c \to 0$ for a sheet resistance much smaller than the $x = 13.5\%$ a-$Nb_xSi_{1-x}$ sample.
   - The scaling analysis implied by the Dirty Boson Model works very well in the case of a-$Nb_xSi_{1-x}$ but not for pure niobium films.
   - These differences are intriguing and more investigation to understand them could provide indications on the underlying physical processes.

### 2.2.2 Paper ♯2 : Couëdo et al., *J. Phys. : Conf. Series*, 400, 022011, 2012

1. 1 atomic % of $O_2$ reduces the $T_c$ by 1 K [Crow et al., 1969].

# Superconductor–Insulator Transitions in Pure Polycrystalline Nb Thin Films

F.Couedo, O.Crauste, L.Bergé, Y.Dolgorouky, C.Marrache-Kikuchi and L.Dumoulin
CSNSM, Univ Paris-Sud, UMR8609, CNRS-IN2P3, Orsay, F-91405, France

E-mail: francois.couedo@csnsm.in2p3.fr

**Abstract.** We report on a study of the transport properties of Nb thin films. By varying the thickness of the films from 263 Å to 25 Å, we observed a depression of the superconductivity. Magnetic field was also applied up to 6 T, inducing the disappearance of the superconductivity and the onset of an insulating behavior. The results were compared to those we have already obtained on a highly disordered system, a-$Nb_xSi_{1-x}$, to understand whether the same mechanisms for the disappearance of the superconductivity could be at play in pure metallic thin films and in highly disordered systems.

## 1. Introduction

A usual measure of disorder for 2D systems is the sheet resistance $R_s = \frac{\rho}{d}$. By evaporating superconducting films of different thicknesses $d$, such that $d < \xi$ the coherence length, we can vary $R_s$ and thus modify the disorder of the samples [1]. Magnetic field is another well-known way to supress the superconducting coherence in 2D systems [2]. We have studied the effects of these two parameters on Nb films and have compared them to those that have been previously observed in amorphous $Nb_xSi_{1-x}$ thin films [3], [4].

## 2. Experimental Setup

Nb thin films with four different thicknesses (25, 57, 108, and 263 Å) were deposited during the same evaporation onto sapphire substrates by e-beam deposition. Pure metallic thin films evaporated at room temperature are usually polycrystalline [5]. SiO underlayer and overlayer (resp. 370 and 330 Å) were also deposited, respectively to ensure the smoothness of the Nb films and to prevent them against oxidation. Pressure during the evaporation was about $10^{-7}$ mbar for a deposition rate of 2 Å/s. The film thickness was controlled in situ by a set of piezoelectric quartz and ex situ by Rutherford Back Scattering. AFM measurements have been performed ex situ and showed no sign of coarse granularity (average surface roughness of $\sim$ 1 Å), hence guaranteeing the continuity of the films. As we will show, low temperature $R_s$(T) features do not show any sign of reentrance, characteristic of a granular systems. Nb films are therefore believed to be homogeneous and continuous. Moreover, the 108 Å-thick Nb film has a room temperature resistivity of 100 $\mu\Omega$.cm and a superconducting critical temperature $T_c$ of 3,1 K, which is comparable to other values found in the litterature for polycrystalline Nb thin films [6], [7].

Electrical measurements have been performed in a He-4 cryostat, down to 1,3 K. A magnetic field perpendicular to the film could be applied, operating up to 6 T. DC-resistances were measured with a standard four-probes method. The normal sheet resistances $R_{s,n}$ were measured at 25 K, where superconducting fluctuations are negligible. The superconducting critical temperature $T_c$ was determined as the midpoint between the temperatures at which the resistance is 10 % and 90 % of the normal sheet resistance.





## 3. Results and Analyses

From the $R_s$(T) characteristics of the films, we observe an increase of $R_{s,n}$ together with a decrease of the $T_c$ [Fig. (1a)]. Even for our thinnest film (25 Å) superconductivity persists. The small bumps in the characteristics below $T_c$ are due to edge effects caused by the shadow masks used during the film deposition. They are not considered relevant for our study.

Applying a perpendicular magnetic field to the sample plane is another way to reduce and eventually destroy superconductivity in thin films. By varying the magnetic field up to 6 T, for the different samples, we observed a change of sign of the Temperature Coefficient of Resistance $\frac{dR}{dT}$, revealing a likely destruction of the superconductivity and the onset of an insulating behavior [Fig. (1b)].

When we combine both thickness and magnetic field effects, we can establish the phase diagram for Nb thin films in the (H, d) plane. The ($H_c$, $d_c$) experimental points form a single critical line separating the superconducting ground state from the insulating one [Fig. (1c)].

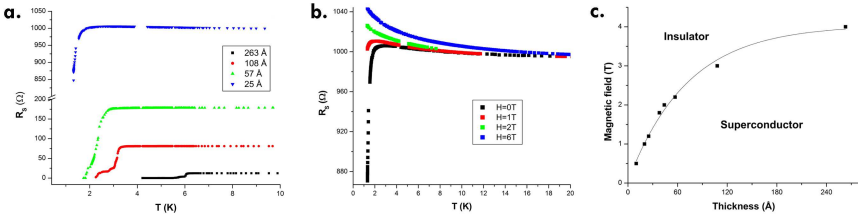



**Figure 1.** Sheet resistance as a function of temperature at H=0 for 25 Å- to 263 Å-thick Nb films (a) and for a 25 Å-thick Nb film at different magnetic fields (b). Phase diagram for Nb thin films in the (H, d) plane (c).

In order to compare the behavior of Nb thin films with disorder with that of higher disordered systems, such as previously studied a-$Nb_xSi_{1-x}$ films ($\rho_{300K} \sim 1000$ $\mu\Omega$.cm for a 100 Å-thick $Nb_{0.15}Si_{0.85}$ film), we have analysed our results with theoretical models usually considered in the problematic of 2D disordered superconductors [8].

### *3.1. Analysis of the observed disorder-induced $T_c$ reduction via amplitude fluctuations effects*

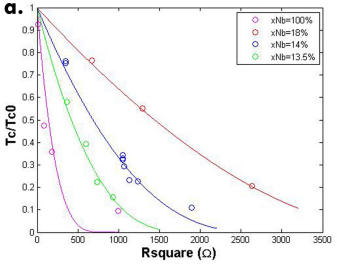
For 2D homogeneous disordered superconductors, Finkel'stein explained the destruction of the superconductivity by the disorder-induced weakening of the Coulomb interactions dynamical screening [9]. For sufficiently high disorder, Coulomb interactions are so reinforced that electron pairing is not efficient anymore : the amplitude of the superconducting order parameter $\phi(r) = \Delta e^{i\varphi(r)}$ then vanishes. Through renormalization group analysis, Finkel'stein established the evolution of the $T_c$ with disorder :

$$\frac{T_c}{T_{c0}} = \exp(-\frac{1}{\gamma})[(1+\frac{\sqrt{\frac{r}{2}}}{\gamma-\frac{r}{4}})(1-\frac{\sqrt{\frac{r}{2}}}{\gamma-\frac{r}{4}})^{-1}]^{\frac{1}{\sqrt{2r}}} \quad (1)$$

where $r = \frac{e^2}{2\pi\hbar} R_{s,n}$, $\gamma = \frac{1}{\ln(\frac{k_B T_{c0}\tau}{2\pi\hbar})}$, $T_{c0}$ the bulk $T_c$ and $\tau$ the elastic scattering time.

Figure (2a) shows an analysis of the $T_c$ reduction for both Nb and $Nb_xSi_{1-x}$ according to equation (1) [3]. The fit are obtained by optimizing $\tau$ and $T_{c0}$. These values can be compared to the expected ones, summarized in table (2c). For $Nb_xSi_{1-x}$ the value of $T_{c0}$ are in good agreement with the $T_c$ measured for thick films [10]. The obtained $T_{c0}$ for Nb is lower than the bulk value (9,22 K) but could be explained by a small oxygen contamination of our films : Nb is very sensitive to oxidation (1 atomic % of $O_2$ reduces the $T_c$ by 1 K [11]). However, the fitted values of $\tau$ are strikingly different from those that can reasonnably be expected for both systems. Moreover, $Nb_xSi_{1-x}$ present a complete destruction of superconductivity for larger values of $R_s$ than Nb films, thus implying that they are more robust to disorder-induced $T_c$ reduction, and so despite the lower value of their bulk $T_c$. This counter-intuitive result may imply that Finkel'stein analysis cannot describe the destruction of superconductivity in both systems.

**a.**




**b.**

| Material | $T_{c0\,fit}$ (K) | $\tau_{fit}$ (s) |
|---|---|---|
| Nb | 6.5 | $1.10^{-17}$ |
| $Nb_{0.18}Si_{0.82}$ | 1.098 | $8.10^{-14}$ |
| $Nb_{0.14}Si_{0.86}$ | 0.314 | $5.10^{-14}$ |
| $Nb_{0.135}Si_{0.865}$ | 0.216 | $1.8.10^{-14}$ |

**c.**

| Material | $v_F$ (cm.s$^{-1}$) | $D$ (cm$^2$.s$^{-1}$) | $l$ (Å) | $\tau$ (s) |
|---|---|---|---|---|
| $Nb_xSi_{1-x}$ | $0.4<v_F<1.2\times10^8$ [3] | 0.6 [4] | $1.5<l<5$ | $10^{-16} < \tau < 10^{-15}$ |
| Nb | $v_F \simeq 2.7\times10^7$ [11] | 1.6 | $l \simeq 18$ | $\tau \simeq 6.5\times10^{-15}$ |

**Figure 2.** Comparison of $\frac{T_c}{T_{c0}}$ vs $R_{s,n}$ for Nb and $Nb_xSi_{1-x}$ films (a). Symbols and solid lines respectively represent experimental data obtained by varying the film thickness and fits of formula (1). Tables (b) synthesizes the best fitting values and (c) the expected ones. $v_F$ and $D$ are taken from the literature or critical field measurements. $l$ and $\tau$ are calculated from these values.

### *3.2. Analysis of the H-induced SIT via phase fluctuations effects*

An alternative description of the superconductivity destruction in 2D disordered systems was established by Fisher [13]. Enhanced by disorder or magnetic field, phase fluctuations of the order parameter cause the loss of the macroscopic phase coherence, thus inducing a quantum phase transition from the superconducting to the insulating states (SIT). Sufficiently close to the critical point, the system resistance is then expected to obey the scaling relation :

$$R(\delta, T) = R_c f(\delta T^{-\frac{1}{\nu z}}) \quad (2)$$

where $\delta$ is the distance to the critical point, $\nu$ the correlation length exponent, $z$ the dynamical critical exponent and $R_c$ the critical resistance.

As previously shown on figure (1a), we do not observe a disorder-induced SIT at zero magnetic field. Therefore, in order to test Fisher's scenario, magnetic field has been applied to the Nb films to tune a SIT [Fig. (1b)]. We have plot the sheet resistance as a function of the scaling parameter $(H-H_c)T^{-\frac{1}{\nu z}}$ for different values of the critical exponents to see if the data could exhibit universal behavior. The best optimization, for the 25 Å-thick Nb film, is presented figure (3a), previous results for a 125 Å-thick $Nb_xSi_{1-x}$ film are shown figure (3b) [4]. $Nb_xSi_{1-x}$ data collapse onto two universal curves, representing the superconducting and insulating states, whereas the data for Nb films cannot, whatever the value of $\nu z$. First let us stress that this result shows that all data cannot be artificially renormalized. It thus reinforced the confidence we have on the universal behavior observed for $Nb_xSi_{1-x}$ films. Second, although the reason for which the scaling procedure fails for Nb films is a subject for future investigations, we note that Fisher's model implies a strong disorder, a condition which may not be met in polycrystalline Nb films.

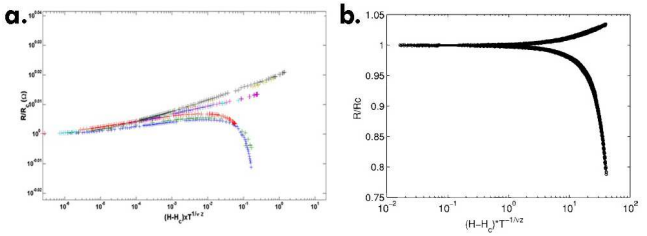



**Figure 3.** Sheet resistance as a function of the scaling variable $(H-H_c)T^{-\frac{1}{\nu z}}$, (a) for a 25 Å-thick Nb film ($\nu z = 0.22$) and (b) for a 125 Å-thick $Nb_{0.15}Si_{0.85}$ film ($\nu z = 0.67$).

## 4. Conclusions

We have presented a study of dc-measurements of Nb films, where thickness and magnetic field have been varied. Comparaison with a higher disordered system, a-$Nb_xSi_{1-x}$, shows that the destruction of superconductivity in both systems can probably not be explained by the same mechanisms, whatever the theoretical model, although there remains to understand why.

## 5. References

[1] Haviland D B, Liu Y and Goldman A M 1989 *Phys. Rev. Lett.* **62** 2180
[2] Hebard A and Paalanen M 1990 *Phys. Rev. Lett.* **65** 927
[3] Crauste O 2010 *PhD dissertation* Université Paris-Sud XI
[4] Aubin H, Marrache-Kikuchi C A, Pourret A, Behnia K, Bergé L, Dumoulin L and Lesueur J 2006 *Phys. Rev. B* **73** 094521
[5] Tu K N 2011, Electronic Thin - Film Reliability, *Cambridge University Press*
[6] Park S I and Geballe T M 1985 *Physica B* **135** 108
[7] Moehlecke S and Ovadyahu Z 1984 *Phys. Rev. B* **29** 6203
[8] Gantmakher V F and Dolgopolov V T 2010 *arXiv*:1004.3761
[9] Finkel'stein A M 1994 *Physica B* **197** 636
[10] Juillard A 1996 *Master dissertation* University Nancy I
[11] Crow J E, Strongin M, Thompson R S and Kammerer O F, 1969 *Phys. Lett.* **30A** 161
[12] Dalrymple B J, Wolf S A, Ehrlich A C and Gillespie D J 1986 *Phys. Rev. B* **33** 7514
[13] Fisher M P A 1990 *Phys. Rev. Lett.* **65** 923

**Acknowledgments**
This work has been partially supported by the ANR (grant No. ANR-06-BLAN-0326) and by the Triangle de la Physique (grant No. 2009-019T-TSI2D).

# Chapter 3

# SIT : Point of view of quantum phase transitions

## 3.1 The Superconductor-to-Insulator Transition as a Quantum Phase Transition

One way to address the issue of the Superconductor-to-Insulator Transition (SIT) is to consider it from the point of view of Quantum Phase Transitions (QPT). This is the angle I would like to develop in this chapter.

Classical Phase Transitions - such as the Superconductor-to-Normal metal Transition - occur at finite temperature. They are therefore ultimately driven by thermal fluctuations. By contrast, Quantum Phase Transitions occur at T = 0, in the absence of thermal fluctuations. The transition is then driven by an external parameter [Sachdev, 1999] which changes the ground state of the system. The SIT is, by definition, such a transition. In the vicinity of a QPT, the system behavior is governed by quantum fluctuations. At low enough temperature, the system quantum critical behavior is reminiscent of the T = 0 QPT. It is therefore possible to experimentally investigate a QPT, even though the system is not, strictly speaking, at the transition.

The analysis of the quantum critical behavior therefore is a powerful tool, first of all to assess the existence of a Quantum Critical Point (QCP). The quantitative analysis of the corresponding critical exponents (see section 3.2) also enables to distinguish between different theoretical models. In section 3.3, I will also broach the question of the relation between different QCPs, and more specifically, what becomes of the SIT as the system evolves from two- to three-dimensional.

Despite the very elegant underlying theoretical premises, considering the SIT only from the angle of QPTs has its drawbacks. Mainly, it consists in looking at the broad picture of what happens at the transition, without looking into the details of the microscopic mechanisms at play, except for their consequences in terms of criticality (critical exponents, values of the tuning parameters at the transition, ...). I feel that this way of addressing the subject would not be complete without a complementary closeup study of the problem. This will be the subject of the following chapter.

The two-dimensional (2D) Superconductor-to-Insulator Transition has been described as a Quantum Phase Transition between a superconductor and an insulating phase. In this chapter, we will stick to this description of the SIT. This is an important starting point of the subsequent analysis : it assumes that no other ground state is possible in 2D. In particular, it has been widely accepted that no metallic state can exist in this dimensionality, at least in the absence of strong Coulomb interactions. This comes from the fact that the localization in dimension 2 is then sufficient to prevent any T = 0 electronic conduction whatever the disorder level [Abrahams et al., 1979]. As we will see in the following chapters, the experimental situation might be more complex. But, for now, let us embrace this view.

## 3.2 Scaling near a Quantum Phase Transition

### 3.2.1 Presentation of the paper

The quantum critical behavior is governed by scaling laws that predict the system properties. For a SIT tuned by an external parameter $K$, in our case the application of a magnetic field or an increase of disorder, the temperature ($T$) dependence of the sheet resistance is solely determined by the distance to the critical point

$\delta = \frac{K-K_c}{K_c}$, $K_c$ being the critical value of the tuning parameter [Sondhi et al., 1997] :

$$R(\delta, T) = R_c f\left(\delta T^{-\frac{1}{\nu z}}\right)$$

$R_c$ then is the value of the sheet resistance at the transition. The critical exponents, $\nu$ - for the correlation length - and $z$ - for the dynamics -, determine the system's universality class and depend on the phenomena underlying the transition. For a bosonic system with long range Coulomb interactions, one expects $z = 1$ [Fisher et al., 1990]. For a weakly disordered system, the so-called "Harris criterion" predicts $\nu > 1$ [Chayes et al., 1986], but this criterion is not expected to hold for strongly disordered systems, such as a-$Nb_xSi_{1-x}$ thin films.

In collaboration with Hervé Aubin, Adrien Pourret, Kamran Behnia and Jérôme Lesueur at LPEM (ESPCI), we have previously shown that $Nb_xSi_{1-x}$ thin films present a magnetic field-tuned Superconductor-to-Insulator Transition [Aubin et al., 2006]. We had shown that the nature of the transition depended on the direction of the applied magnetic field with respect to the film plane. A parallel applied field causes the film to undergo a classical transition, whereas a perpendicular magnetic field leads to a QPT.

The following paper extends the analysis of these experiments to the thickness-tuned SIT under a finite magnetic field. It adresses the following issues :

1. **Analysis of the QPT -** Sample thickness is a parameter that is experimentally complicated to tune : fabricating microscopically identical films, which only differ by their thickness is challenging. In our case, we synthesized four samples in a single run in order for them to be as identical as possible. However, performing a convincing scaling analysis of the thickness-tuned SIT with only four samples is difficult.
   The following paper explores some variations on the scaling analysis near a QCP in order to interpolate the system's behavior between the discrete values of the film thickness we experimentally have access to. In the case of the thickness-tuned SIT under nonzero magnetic field, we show that the only relevant parameter for scaling *all* our data is the distance to the transition $\delta_d = \frac{|d-d_c(H)|}{d_c(H)}$, whatever the actual value of the magnetic field $H$. As expected, the critical thickness $d_c(H)$ decreases as $H$ increases. Since the magnetic field can be continuously varied, a single sample can therefore, by a change of $H$, be tuned to be more or less close to $d_c(H)$ and hence to the QCP.
2. **Critical exponents -** The scaling procedure enabled us to determine the critical exponents product $\nu z$. It is very different from what is found in the literature (see section 1.1 for a comparison) : we find $\nu_H z \simeq 0.7$ for the magnetic field-tuned SIT and $\nu_d z \simeq 0.4$ for the thickness-tuned SIT under finite $H$.
   Finding different critical exponents for these two transitions signifies that they belong to different universality classes. This is a first argument advocating that the thickness reduction plays a special role in the SIT. We shall expand more on this subject later on (see section 4.2.2).
   However a value such as $\nu_d z \simeq 0.4$ is particularly low, since most systems exhibit a critical exponents product larger than 1, and cannot be explained by existing theoretical models.
3. **Phase diagram in the ($d$,$B$) plane -** Beyond any consideration regarding the scaling theory, the paper establishes the phase diagram in the ($d$, $H$) plane for a-$Nb_xSi_{1-x}$ films.
4. **Value of the critical resistance $R_c$ -** We show that the value of the sheet resistance at the SIT varies widely (almost by a factor of 4, from 350 Ω to 1300 Ω) when the magnetic field changes from 5 to 11 kOe. These values of $R_c$ are well below the value of $R_c = \frac{h}{4e^2} = 6,47$ kΩ expected by the Dirty Boson Model [Cha et al., 1991]. This indicates that this model, based on the duality between vortices and Cooper pairs in the insulating and superconducting phases, might not capture all the physics at play in our system.

### 3.2.2 Paper ♯3 : Marrache et al., *Phys. Rev. B*, 78, 144520, 2008

# Thickness-tuned superconductor-insulator transitions under magnetic field in *a*-NbSi

C. A. Marrache-Kikuchi*
*CSNSM (CNRS-UMR8609), Université Paris Sud, Bat. 108, 91405 Orsay Campus, France*

H. Aubin, A. Pourret, K. Behnia, and J. Lesueur
*Laboratoire Photons et Matière (CNRS), ESPCI, 10 rue Vauquelin, 75231 Paris, France*

L. Bergé and L. Dumoulin
*CSNSM (CNRS-UMR8609), Université Paris Sud, Bat. 108, 91405 Orsay Campus, France*
(Received 2 May 2008; revised manuscript received 2 October 2008; published 30 October 2008)

We have studied the thickness-induced superconductor-to-insulator transition in the presence of a magnetic field for *a*-NbSi thin films. Analyzing the critical behavior of this system within the "dirty boson model," we have found a critical exponent product of $\nu_d z \sim 0.4$. The corresponding phase diagram in the $(H,d)$ plane is inferred. This small exponent product, as well as the nonuniversal value of the critical resistance found at the transition, calls for further investigations in order to thoroughly understand these transitions.

DOI: 10.1103/PhysRevB.78.144520 PACS number(s): 74.25.−q, 74.40.+k, 71.30.+h, 64.60.−i

## I. INTRODUCTION

Low-temperature transport in disordered conducting materials implies quantum interferences, Coulomb repulsion, and superconducting fluctuations. Since two dimensions (2D) is the lower critical dimension for the existence of both the superconducting and the metallic states, transport properties of such disordered thin films have attracted continuous attention since the 1960s in order to understand what ground states are allowed in those systems and study the nature of the quantum phase transitions between the different phases.[1–3]

Quantum phase transitions (QPT) occur when a parameter in the Hamiltonian is varied, resulting in a change in the system's ground state. These transitions, therefore, take place at zero temperature and are driven by quantum fluctuations, contrary to classical phase transitions, which are controlled by thermal fluctuations. Near a QPT, the quantum fluctuations have a characteristic length scale—the correlation length $\xi$—diverging as $\xi \propto \delta^{-\nu}$, where $\nu$ is the correlation length critical exponent, $\delta_K = \frac{|K-K_c|}{K_c}$ is the distance of the considered system to the $K$-driven transition, and $K$ is an experimentally tunable parameter which critical value is $K_c$. The fluctuations are also characterized by a vanishing frequency $\Omega \propto \xi^{-z}$, where $z$ is the dynamical critical exponent. The two critical exponents $\nu$ and $z$ define the universality class to which the transition belongs.

In the case of superconductor-to-insulator transitions (SITs) in disordered thin films, the tunable parameter in the Hamiltonian can be the disorder or the magnetic field $H$. The most popular theoretical model to explain these SITs is the "dirty boson model" developed by M.P.A. Fisher.[2] In this model, the coherence of the superconducting state is destroyed by quantum fluctuations of the order parameter's phase, and the system amounts to interacting bosons in the presence of disorder. The superconducting and insulating phases are then dual to one another: the superconducting phase consists of localized vortices and condensed Cooper pairs, whereas the insulating phase is characterized by condensed vortices and localized Cooper pairs. Both disorder and magnetic-field-driven transitions have similar description within this frame: in the quantum regime, for dc measurements, the sheet resistance obeys a scaling law that is solely dependent on the variable $\delta * T^{-1/\nu z}$ (Refs. 1 and 2),

$$R(\delta,T) = R_c f(\alpha \delta T^{-1/\nu z}), \tag{1}$$

where $R_c$ is the critical sheet resistance and $f$ is a universal scaling function having a unique constraint: $f(0)=1$. $\alpha$ is a nonuniversal constant.[4] $z=1$ is expected due to the long-range Coulomb interactions and the dirty boson model predicts $\nu > \frac{2}{d} = 1$, as well as a universal value of the system's sheet resistance at the transition $R_c = R_Q = \frac{h}{4e^2} = 6500\ \Omega$.[3] Despite obeying to the same scaling laws [Eq. (1)], the field-induced transition and the disorder-induced transitions have different physical grounds: in the magnetic-field-induced SIT, the vortex density increases with the magnetic field until they delocalize and Bose condense; in the disorder-induced SIT at zero field, the Bose condensation is undergone by the vortex/antivortex pairs. These two SITs, hence, have no reason to have the same critical exponents.[3]

Experimentally, number of disordered superconducting films experiences a SIT when submitted to a perpendicular magnetic field. However, they do not all behave in the same way. Following Gantmakher's[5] comment, one can separate them into two different categories. Some compounds exhibit an insulating phase in which low-temperature resistance is only 10% above their high-temperature resistance. This behavior resembles more the one of a conductor in the presence of weak localization than the one of an actual insulator.[6] This is the case of $Mo_xGe_{1-x}$,[7] $Mo_xSi_{1-x}$,[8] Be,[9] *a*-Bi,[10] or $Nd_{2-x}Ce_xCuO_{4+y}$.[5] Other systems, such as amorphous indium oxyde[11] or TiN,[12] have, in the same conditions, a much more important increase in resistance—up to a factor of 10. Their resistances then have an exponential increase with the temperature.[11,13] The renormalization analysis of these field-induced SIT gives $0.75 \leq \nu_H z \leq 1.35$, independently of the above-mentioned categories.

 ©2008 The American Physical Society

The experimental realizations of the thickness-induced SIT, where tuning the system's thickness is taken to be a mean of varying its disorder, are far more rare because of the experimental difficulty of synthesizing microscopically identical films, which only differ by their thicknesses. In the case of this transition, the distinction previously made no longer exists: all studied compounds show a drastic increase in resistance of many orders in magnitude when their thickness is lowered.[10] However, one can make another distinction. Some systems, such as *a*-Bi,[10] are very sensitive to any thickness variation: a fraction of angstrom difference engenders resistance increases of several orders of magnitude at low temperature. This behavior is comparable to the one observed in granular systems.[14] On the other hand, systems such as MoC present a more progressive thickness dependence.[15] Values of the critical exponents have only been reported for *a*-Bi (Ref. 10): $\nu_d z \sim 1.3$.

Whichever the parameter tuned to induce the SIT, and contrary to the predictions of the dirty boson model, experiments show an important variation in the values of the critical sheet resistance at the transition $R_c$.[7–10,12,16] Within one system, $R_c$ can vary between 2000 Ω to 9000 Ω (Ref. 9), depending on the applied magnetic field or the normal resistance of the sample. Theories introducing a fermionic channel of electronic conduction have been developed to explain the nonuniversality of $R_c$,[7] but these are not entirely satisfactory since they do not account for values of $R_c$ larger than $R_Q$.[10]

As one can see, all the experimental realizations of the SITs in thin disordered films show a large variation in the measured critical exponents, as well as in the critical resistance. This has led to the questioning of the dirty boson model. Some have suggested a percolation-based mechanism,[17] others the contribution of fermions to the conduction near the transition.[7] Moreover, the flat $R(T)$ curves found near the transition have put into question Fisher's picture of a unique metallic separatrix between the superconducting and insulating regimes. Some[18] have suggested the existence of an intermediate metallic phase—the Bose metal.

In this context, it seemed to us particularly interesting to provide another example of such transition. 2D $Nb_xSi_{1-x}$ films are interesting systems for this study. We have previously shown that these films experience a magnetic-field-tuned SIT (Ref. 19) with a product of critical exponents $\nu_H z=0.67$, in agreement with other experimental data[20] but in contradiction with the dirty boson model. In this paper, we concentrate on the thickness-driven SIT in this compound. The following sections will be organized as follows: first, Sec. II will detail the experimental procedures. Section III will explain the finite-size scaling method we have used to analyze our results concerning the disorder-induced transition under nonzero magnetic fields, and show that we have obtained surprisingly small critical exponents for the transition. Combining this analysis with our previously obtained results,[19] we infer the phase diagram for $Nb_xSi_{1-x}$ (Sec. IV). Finally, Sec. V will provide a discussion on the interpretation of these sets of experiments on disordered superconducting thin films and on the domain of validity of the dirty boson model.

## II. EXPERIMENTAL PROCEDURE

The NbSi films have been prepared under ultrahigh vacuum by electron beam (e-beam) codeposition of Nb and Si. A series of four samples with stoichiometry $Nb_{0.15}Si_{0.85}$ and thicknesses of 100, 50, 25, and 12.5 nm has been deposited onto sapphire substrates coated with a 50-nm-thick SiO underlayer. The films were synthesized during a single run in order to have the samples' niobium concentrations as similar as possible. We also took special care over the control of the sample's parameters: the evaporation was controlled *in situ* by a special set of piezoelectric quartz in order to precisely monitor the composition and the thickness of the deposition. These two characteristics were then controlled *ex situ* by Rutherford back scattering (RBS), and the results were well fitted with the *in situ* monitoring. Samples of the same stoichiometry with thicknesses down to 2.5 nm have been characterized by atomic force microscopy and showed no sign of morphological granularity nor inhomogeneity. The superconducting transitions of these samples in zero magnetic field are a few tens of mK sharp and show no sign of reentrant behavior as usually observed for granular systems. Besides, all samples showed the same resistivity at high temperature within 4%. All these arguments lead us to think that our samples are homogeneous in composition, nongranular, and only differ from one another by their thickness. This conclusion is corroborated by a transmission electron microscopy (TEM) study,[21] showing that only $Nb_xSi_{1-x}$ alloys annealed at 500 °C present Nb-rich clusters. The electrical characteristics of the four films were measured down to 150 mK using a dilution refrigerator. A perpendicular magnetic field could be applied and was made to vary between 5 and 11 kOe. Resistance measurements were performed using a standard ac lock-in detection technique operated at 23 Hz. A current of 100 nA was applied to the sample, which is within the linear regime of the *I-V* characteristics for the considered films. All electrical leads were filtered from radio frequency at room temperature.

## III. *d*-INDUCED TRANSITION

Before describing the renormalization procedure we have used and the results thus obtained, let us establish the dimensionality of our samples. In our system, the mean free path $l$ is of the order of the interactomic distance: $l \simeq 2.65$ Å (Ref. 22) and, hence, much smaller than the superconducting coherence length $\xi_0$ given by the Bardeen Cooper Schrieffer theory [$\xi_0=0.18\frac{\hbar v_F}{k_B T_{c0}}$, where $v_F$ is the Fermi velocity estimated to be $2\times10^8$ cm s$^{-1}$ (Ref. 23)]. In the "dirty" limit the effective coherence length of the system is given by $\xi_{\mathrm{eff}}=\sqrt{\xi_0 l}$. We also have to consider the dephasing length, which acts near the SIT as a cutoff length due to the finite temperature:[2,3,11] $L_\Phi=\frac{\hbar^2}{m_e k_B \xi_{eff} T}$, where $m_e$ is the mass of the electron. The smallest length between $L_\Phi$ and $\xi_{\mathrm{eff}}$, hence, determines the dimensionality of the film. The different relevant lengths are given in Table I. The films with thicknesses ranging from 12.5 to 50 nm can be considered to be 2D, whereas the 100 nm film is three dimensions (3D). In the renormalization procedure, we shall focus on the 2D films so

TABLE I. Relevant parameters for our samples: the thickness $d$, the superconducting transition temperature $T_{c0}$, the BCS coherence length $\xi_0$, the effective coherence length $\xi_{\text{eff}}$, and the dephasing length $L_\Phi$ at 0.3 K.

| $d$ (nm) | $T_{c0}$ (mK) | $\xi_0$ ($\mu$m) | $\xi_{\text{eff}}$ (nm) | $L_\Phi$(0.3 K) (nm) |
|---|---|---|---|---|
| 12.5 | 213 | 12.8 | 58.2 | 50 |
| 25 | 347 | 7.9 | 45.7 | 64 |
| 50 | 480 | 5.7 | 38.9 | 75 |
| 100 | 530 | 5.2 | 37.1 | 79 |

that the resistances mentioned below are sheet resistances. Let us also note that, in what follows, we used the usual convention found in the SIT-related literature:[24] the term "superconducting" applies to curves that have a positive temperature coefficient of resistance (TCR: $\frac{dR}{dT}$), and, by contrast, we shall label as "insulating" all curves having a negative TCR.

As shown by the rarity of experimental data concerning the thickness-induced SIT, it is difficult to obtain a series of samples that are identical except for their thickness: unlike the magnetic field, $d$ cannot be tuned continuously. We have, therefore, developed an analysis method, which enables us to interpolate the system's transport behavior between the discrete values of $d$ we experimentally have access to.

All four samples were superconducting at zero magnetic field (inset of Fig. 1) and were progressively tuned through the transition by a finite $H$. For each value of $H$, all four samples were studied (Fig. 1), and the diagram $(R,d)$ traced for different temperatures presents a crossing point (Fig. 2). This is the signature of the QPT (Ref. 10) and allows us to estimate the critical thickness $d_c$ associated to the magnetic field $H$. We repeat this process for all values of $H$, obtaining a collection of critical parameters couples $(d_c,H)$.

When $H$ is fixed, the thickness-induced transition is solely governed by the distance to the transition $\delta_d=\frac{|d-d_c|}{d_c}$. If these

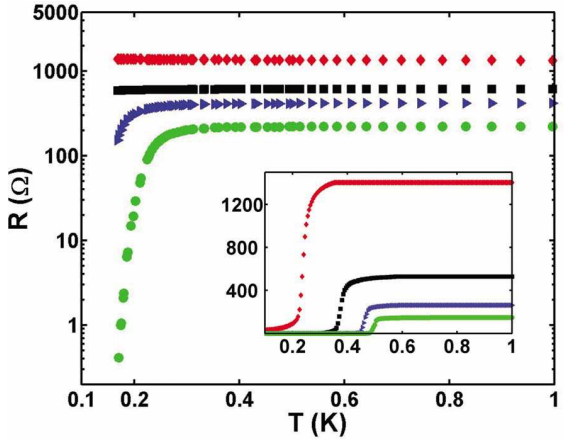



FIG. 1. (Color online) Resistance per square as function of temperature for $H=6.8$ kOe. The curves for all four samples are represented. For this particular value of the magnetic field, the 25-, 50- and 100-nm-thick films are superconducting, whereas the 12.5-nm-thick film is insulating. Inset: The same data at zero magnetic field.

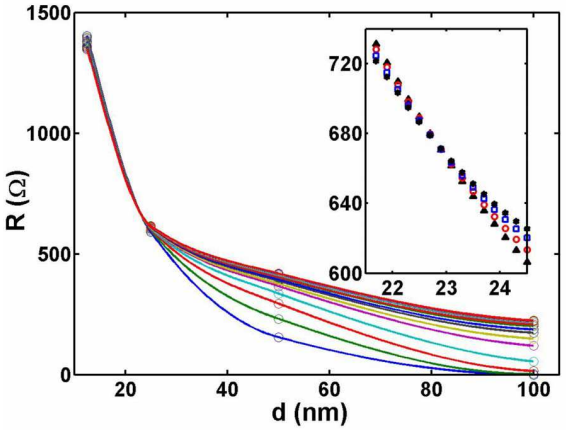



FIG. 2. (Color online) Resistance per square as function of sample thickness for $H=6.8$ kOe. The curves are represented for 16 different values of the temperature between 168 and 831 mK. Inset: the same data are shown around the crossing point at about $d_c=23$ nm for four particular temperatures: $T=168$, 186, 239, and 831 mK. This crossing point is interpreted as the signature of a QPT.

$d$-driven transitions all belong to the same universality class, independent of the particular value of $H$, the only relevant parameter for the scaling of all our data is the value of $\delta_d=\frac{|d-d_c(H)|}{d_c(H)}$. This means that *all* curves $R(\frac{|d-d_c(H)|}{d_c(H)},T)$ should collapse on two universal curves. Note that the renormalized quantity we consider is $R$ and not $\frac{R}{R_c}$ as in Ref. 10, for we do not find a universal critical resistance.[4] For each individual sample, this means that by tuning $H$, $d_c$ is made to vary and so does $\delta_d$. In other words, the thickness $d$ being fixed, the critical thickness $d_c$ is changed via the magnetic field. Since the only relevant parameter for the scaling is the distance $\delta_d$ to the transition, this situation is ultimately equivalent to having a fixed critical thickness and variable sample thicknesses (as in Ref. 10 for example).

For each sample, the results were analyzed using two independent scaling methods.[7,10] First, for the derivative method, we plot $\frac{DR}{D\delta_d}|_{\delta_d=0}\propto R_c T^{-\frac{1}{\nu_d z}} f'(0)$ as function of $\frac{1}{T}$, which, in a log-log diagram, gives a straight line of slope $\frac{1}{\nu_d z}$ (left insert Fig. 3). The second method consists in numerically finding $t(T)$ such that $R[\delta_d,t(T)]=R_c f[\delta_d t(T)]$ and that $t(T)$ yields the best collapse between the data measured at the temperature $T$ and the data measured at our lowest temperature (150 mK). To obey the scaling law [Eq. (1)], $t(T)$ should be of the form $T^{-1/\nu_d z}$, and we can, hence, infer the value of $\nu_d z$ (right insert Fig. 3).

For all 2D samples, we obtained a product of critical exponents of $\nu_d z=0.4\pm0.15$;. We can check this value of the exponent product by plotting $R$ as function of $\delta_d * T^{-1/\nu_d z}$ (Fig. 3) for the 25-nm-thick sample. All data superimpose nicely in the ranges $0.16\leq T\leq 0.35$ K and $|\delta_d|\leq 1$, forming two curves only: one representing the superconducting behavior and the other the insulating side of the transition. $|\delta_d|=1$ still exhibits a critical behavior since the corresponding data collapse on the same curves. It is quite surprising that the scaling continues to work that far from the critical

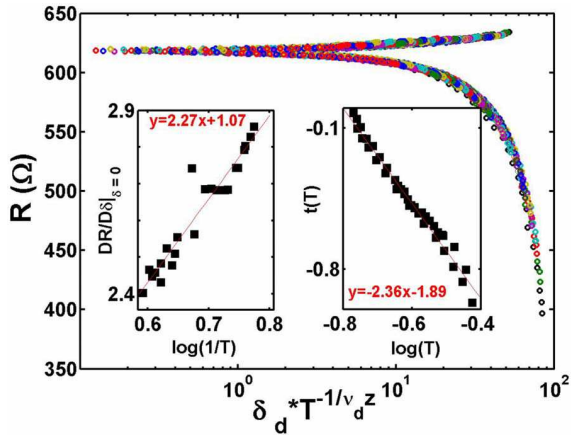



FIG. 3. (Color online) Renormalization of the resistance $R$ for the critical exponents $\nu_d z=0.4$ for the 25-nm-thick sample. Each color is affected to a particular value of $\delta_d$. Left inset: determination of the critical exponent product by the derivation method. Right inset: determination of the critical exponent product by the $t(T)$ minimization method.

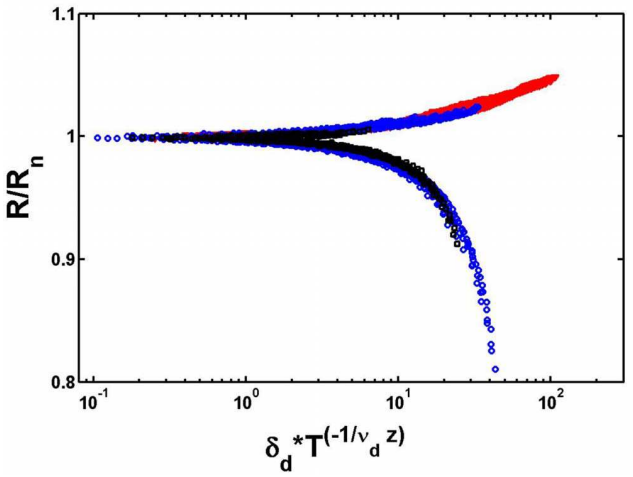



FIG. 4. (Color online) Renormalization of the renormalized resistance $\frac{R}{R_n}$ for the critical exponents $\nu_d z=0.4$ for the 12.5- (triangles), 25- (circles), and 50- (squares) nm-thick samples.

point. The analysis performed on the 12.5-nm- and the 50-nm-thick samples gave the same value of the product $\nu_d z$ within the uncertainty.

This far, we have only considered the renormalization of the resistance for one sample at a time. In order to compare the critical behavior of the different samples, we have to take into account their different normal resistances. We, therefore, have to compare the quantity $\frac{R}{R_n}$, where $R_n$ is the resistance taken at high temperature, typically at 1K. This procedure is not usual in the literature and directly derives from the fact that, in our experiment, $R_c$ is not universal and varies over one order of magnitude (see Sec. V). The scaling of $\frac{R}{R_c}$ then has no significance.[4]

We then looked for a critical exponent product that allowed *all* curves from *all* samples to collapse. For each sample, we adjusted the nonuniversal parameter $\alpha$ of Eq. (1) for the curves to superimpose. We found $\alpha_{12.5\ \mathrm{nm}}=1.9$, $\alpha_{25\ \mathrm{nm}}=0.9$, and $\alpha_{50\mathrm{nm}}=0.5$ for a product of $\nu_d z=0.4\pm0.1$. The corresponding criteria for the renormalization are then very clearly defined: (i) the magnetic field was made to vary between 5.1 and 10.5 kOe by increments of 0.1 kOe; all critical points $(d_c,H_c)$ corresponding to these fields have been taken into account; (ii) the only constraint on the distance to the transition is $\delta<0.8$; (iii) $0.17<T<0.39$ K. The result of the renormalization is given in Fig. 4. This graph is particularly remarkable: even if our samples have normal resistances varying by nearly one order of magnitude, the corresponding resistances all collapse on a single renormalization plot.

## IV. PHASE DIAGRAM

The renormalization method has enabled us to measure a number of critical parameter couples $(H_c,d_c)$, although we only had four different samples. We can, hence, draw part of the phase diagram for $Nb_xSi_{1-x}$ thin films (Fig. 5). The line formed by the critical points separates an insulating region at high fields, and small thicknesses form a superconducting region at low field and large thicknesses. Of course, these critical points coincide with those determined from the magnetic-field-induced SIT.[19] As for $a$-Bi,[10] depending on the parameter tuned to cross this line, the critical exponent product found is different: $\nu_H z=0.7$ when the field is varied, whereas a variation in the sample's thickness gives $\nu_d z=0.4$. We, thus, confirm that these two SITs belong to two separate universality classes.

## V. DISCUSSION

First let us comment on the value found for the critical exponent product. For $a$-NbSi in a thickness-induced SIT, we have found $\nu_d z=0.4$. This value is surprising when compared

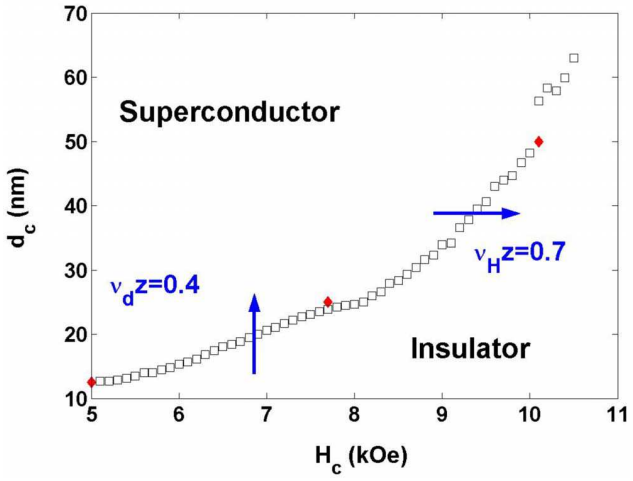



FIG. 5. (Color online) Phase diagram for a-$Nb_{15}Si_{85}$ in the $(H_c,d_c)$ plane. The open symbols were obtained from the thickness-tuned SIT, whereas the full symbols were obtained in Ref. 19 for the magnetic-field-tuned transition.

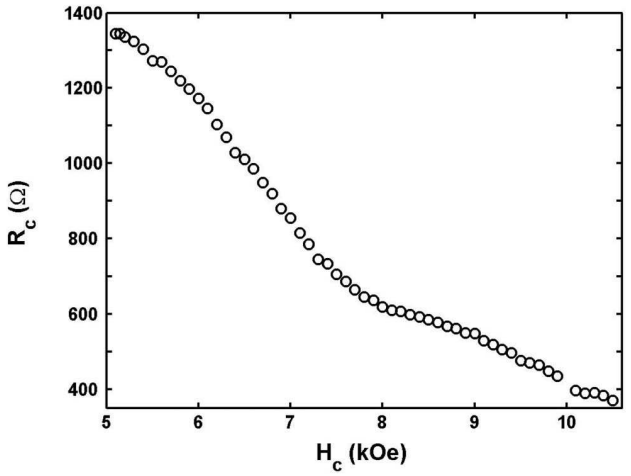



FIG. 6. Critical resistance as function of the critical field for *a*-NbSi films.

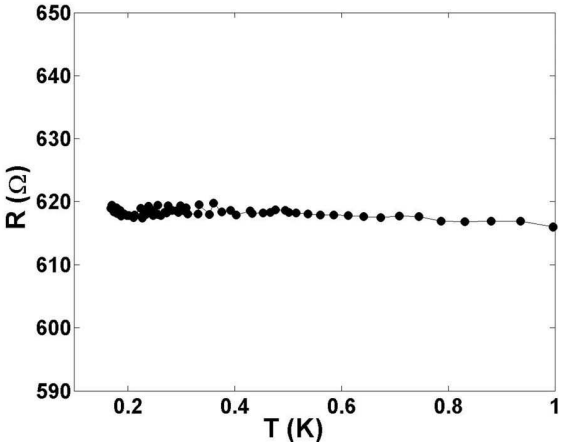



FIG. 7. Resistance as function of the temperature for the 50-nm-thick sample at $H=7.9$ kOe. Over one decade variation in temperature, the film's resistance only varies within 3.5 Ω (0.5% in relative value), which is our experimental uncertainty in this range.

to other critical exponents found by other groups, thin *a*-Bi films for instance, for which $\nu_d z=1.4$. At this point, we do not have any clear explanation for this important difference. However, $\nu_d z=1.4$ is close to what is predicted for classical 2D percolative systems ($\nu_d=4/3$), and *a*-Bi thin films present a thickness-induced SIT for very shallow thicknesses (a few angstroms, 20 Å at most). In this sense also, our system is particularly interesting since it allows 2D samples to experience a thickness-driven SIT at reasonable thicknesses, where the roughness of the film, the surface state of the substrate, or the microscopic details of the film's growth should not be important factors. $\nu_d z=0.4$ is also surprisingly small considering the theoretical predictions that have been made to this day.[1] Although the exact value of this product might be affected by the uncertainty on the determination of the exponents ($\pm 0.1$) and by the small number of samples we have, at any rate, we can confidently say that $\nu_d z<1$, which is inconsistent with the dirty boson model. If we assume that $z=1$, the consequence of this is that $\nu_d<1$. Many authors have pointed to the fact that this violates the so-called "Harris criterion" ($\nu>2/d$).[25] However, this criterion is valid for small disorder, and since our system consists in amorphous films in which the mean free path is of the order of the interatomic distance, it is not all that shocking that the value found for the localization length exponent does not obey this inequality.[26]

Another point that has much been discussed related to the dirty boson model is the value of the critical sheet resistance. In this set of experiments, we show that $R_c$ varies over a large range when either the magnetic field or the thickness is varied (Fig. 6).

Until now, we have analyzed our results by comparing them to the dirty boson model. Although the renormalization procedure works remarkably well for all systems studied to date—which means the SIT is indeed a QPT (Ref. 1)—two important predictions of this model ($\nu>2/d$ and $R_c=h/4e^2$) are not verified by *a*-NbSi thin films, as well as in other systems [*a*-Bi,[10] *a*-Be,[9] NdCeCuO,[27] MoGe,[28] InOx,[13,16] TiN,[12] and MoSi (Ref. 8)]. One might, therefore, put this model into question. Tunneling effect experiments suggest[29–31] that, for homogeneous systems, amplitude fluctuations of the order parameter play a role even in the vicinity of the SIT: when the films' thicknesses decrease, the superconducting gap $\Delta$ and the critical temperature decrease together, monotonically, such that $2\Delta/T_c \simeq$ constant. In this picture, near the SIT, the amplitude of the superconducting order parameter can become very small, whereas an essential point in the dirty boson model is that its amplitude is finite near the transition. The same studies show that, even in the "superconducting"—in the previously-defined sense of the TCR—region, the one-particle density of state is not zero, meaning that there are normal excitations coming from electrons that are not involved in any Cooper pair. This would mean that amplitude fluctuations of the system must be taken into account for a correct description of the transition, which is not the case in M.P.A. Fisher's model. The suggestion by some authors that other phase(s) may be involved in between the superconducting and the insulating regimes is particularly interesting. Some have suggested a vortex-liquid phase,[32,33] which has recently[34] been linked to the problem of anomalous Nernst effect in the cuprates. As recent measurements on amorphous superconductors have shown,[35–37] Nernst effect is a very sensitive probe of amplitude fluctuations[35,36] and phase fluctuations[37] of superconducting order parameter. These last works suggest that measurements of the Nernst effect should be a relevant probe to test the existence of this vortex-liquid phase. However, there have not been clear predictions on how the thickness variation should affect this phase. Also very appealing is the suggestion that there is a bosonic metallic phase, such as the Bose metal,[18] involved. This hypothesis is very interesting, in particular when one takes a close look at the resistive behavior of our films. Indeed, at low temperatures, the resistance of some samples seem to saturate at a finite value (Fig. 7), displaying a large temperature range where the resistance is independent of the temperature. However, a study at lower temperatures should be undertaken to confirm this tendency. Let us restate that the qualification of insulating or superconducting have been arbitrarily attributed to $\frac{\partial R}{\partial T}<0$ (respec-

tively, $\frac{\partial R}{\partial T} > 0$) curves without any other ground than the assumption made by the dirty boson model that only these two phases existed. All these arguments (the amplitude fluctuations of the order parameter, a possible fermionic channel, and the suggestion of a Bose metal) plead in favor of a reconsideration of the dirty boson model and further experimental investigations of these systems.

In conclusion, we have studied the thickness-induced SIT in the presence of a perpendicular magnetic field on $a$-$Nb_{15}Si_{85}$ thin films of thicknesses ranging from 12.5 to 100 nm. We have found the signature of a QPT when the sample thickness is lowered. The corresponding critical exponent product is $\nu_d z \simeq 0.4 \pm 0.1$. This value is different from the one found in the analysis of the magnetic-field-induced transition in the same compound for which $\nu_H z = 0.65$. These two SITs, therefore, belong to two different universality classes. However, the very small value of $\nu_d z$ cannot be explained by the existing models for this transition. Further experimental investigations are needed to understand the growing discrepancies between the various experimental results and between these results and the theory.

## ACKNOWLEDGMENT

We are grateful to acknowledge stimulating discussions with M. V. Feigelman, S. Okuma, C. Chapelier, and Y. Avishai.

*Claire.Marrache@csnsm.in2p3.fr

[1] S. Sondhi, S. Girvin, J. Carini, and D. Shahar, Rev. Mod. Phys. **69**, 315 (1997).
[2] M. P. A. Fisher, Phys. Rev. Lett. **65**, 923 (1990).
[3] M. P. A. Fisher, G. Grinstein, and S. M. Girvin, Phys. Rev. Lett. **64**, 587 (1990).
[4] M. C. Cha, M. P. A. Fisher, S. M. Girvin, M. Wallin, and A. P. Young, Phys. Rev. B **44**, 6883 (1991).
[5] V. Gantmakher, Physica C **404**, 176 (2004).
[6] M. Steiner and A. Kapitulnik, Physica C **422**, 16 (2005).
[7] A. Yazdani and A. Kapitulnik, Phys. Rev. Lett. **74**, 3037 (1995).
[8] S. Okuma, T. Terashima, and N. Kokubo, Solid State Commun. **106**, 529 (1998).
[9] E. Bielejec and W. Wu, Phys. Rev. Lett. **88**, 206802 (2002).
[10] N. Marković, C. Christiansen, A. M. Mack, W. H. Huber, and A. M. Goldman, Phys. Rev. B **60**, 4320 (1999).
[11] V. Gantmakher, M. Golubkov, V. Dolgopolov, G. Tsydynzhapov, and A. Shashkin, JETP Lett. **71**, 160 (2000).
[12] T. Baturina, J. Bentner, C. Strunk, M. Baklanov, and A. Satta, Physica B (Amsterdam) **359-361**, 500 (2005).
[13] A. F. Hebard and M. A. Paalanen, Phys. Rev. Lett. **65**, 927 (1990).
[14] H. M. Jaeger, D. B. Haviland, B. G. Orr, and A. M. Goldman, Phys. Rev. B **40**, 182 (1989).
[15] S. J. Lee and J. B. Ketterson, Phys. Rev. Lett. **64**, 3078 (1990).
[16] M. A. Steiner, G. Boebinger, and A. Kapitulnik, Phys. Rev. Lett. **94**, 107008 (2005).
[17] Y. Dubi, Y. Meir, and Y. Avishai, Phys. Rev. Lett. **94**, 156406 (2005).
[18] D. Das and S. Doniach, Phys. Rev. B **60**, 1261 (1999).
[19] H. Aubin, C. A. Marrache-Kikuchi, A. Pourret, K. Behnia, L. Berge, L. Dumoulin, and J. Lesueur, Phys. Rev. B **73**, 094521 (2006).
[20] N. Marković, C. Christiansen, and A. M. Goldman, Phys. Rev. Lett. **81**, 5217 (1998).
[21] D. Querlioz, E. Helgren, D. Queen, F. Hellman, R. Islam, and D. Smith, Appl. Phys. Lett. **87**, 221901 (2005).
[22] P. Hucknall, C. Walker, D. Greig, J. Matthew, D. Norman, and J. Turton, J. Phys.: Condens. Matter **4**, 1131 (1992).
[23] S. Marnieros, Ph.D. thesis, University of Paris-XI, 1998.
[24] N. Marković, C. Christiansen, G. Martinez-Arizala, and A. M. Goldman, Phys. Rev. B **65**, 012501 (2001).
[25] J. T. Chayes, L. Chayes, D. S. Fisher, and T. Spencer, Phys. Rev. Lett. **57**, 2999 (1986).
[26] Y. Avishai (private communication).
[27] V. Gantmakher, S. Ermolov, G. Tsydynzhapov, A. Zhukov, and T. Baturina, JETP Lett. **77**, 424 (2003).
[28] N. Mason and A. Kapitulnik, Phys. Rev. B **65**, 220505(R) (2002).
[29] R. C. Dynes, A. E. White, J. M. Graybeal, and J. P. Garno, Phys. Rev. Lett. **57**, 2195 (1986).
[30] J. M. Valles, R. C. Dynes, and J. P. Garno, Phys. Rev. B **40**, 6680 (1989).
[31] J. M. Valles, R. C. Dynes, and J. P. Garno, Phys. Rev. Lett. **69**, 3567 (1992).
[32] J. A. Chervenak and J. M. Valles, Phys. Rev. B **54**, R15649 (1996).
[33] S. Okuma, M. Kobayashi, and M. Kamada, Phys. Rev. Lett. **94**, 047003 (2005).
[34] P. Anderson, Nat. Phys. **3**, 160 (2007).
[35] A. Pourret, H. Aubin, J. Lesueur, C. Marrache-Kikuchi, L. Berge, L. Dumoulin, and K. Behnia, Nat. Phys. **2**, 683 (2006).
[36] A. Pourret, H. Aubin, J. Lesueur, C. A. Marrache-Kikuchi, L. Berge, L. Dumoulin, and K. Behnia, Phys. Rev. B **76**, 214504 (2007).
[37] P. Spathis, H. Aubin, A. Pourret, and K. Behnia, Europhys. Lett. **83**, 57005 (2008).

## 3.3 Dimensional crossover from 2D to 3D

### 3.3.1 Presentation of the paper

Previous studies in our group have established the possible ground states for a-$Nb_xSi_{1-x}$ three-dimensional (3D) films [Dumoulin et al., 1993, Dumoulin et al., 1996, Marnieros, 1998] [1] (see figure 3.1) :

- $x < 9\%$ **- Anderson insulator.** The considered films are amorphous and with a mean free path of the order of the inter-atomic distance. The insulator therefore stems from the localization of wave functions, due to disorder.
- $9\% < x < 12\%$ **- Metal.** The metallic state corresponds to a 3D weakly-localized behavior.
- $12\% < x$ **- Superconductor.**

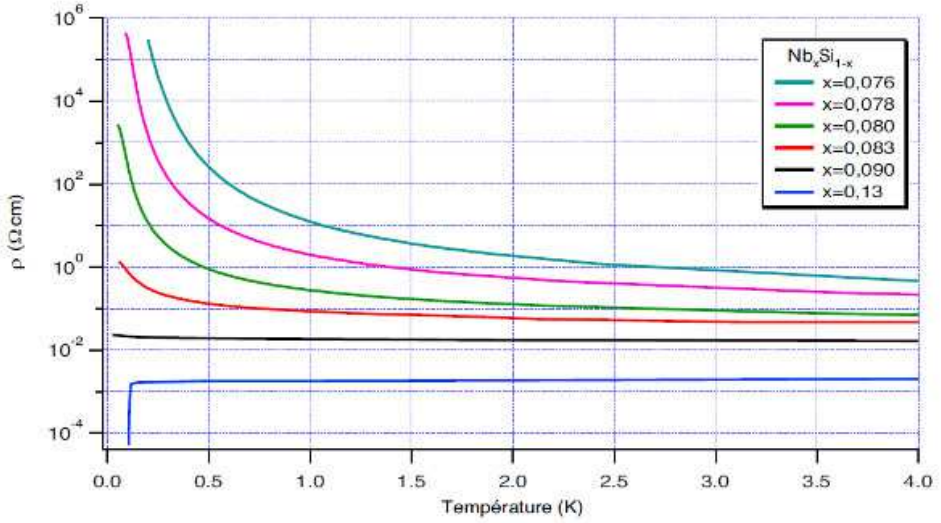



Figure 3.1: Evolution of the ground state of a-$Nb_xSi_{1-x}$ 3D films ($d = 1000$ Å) for different niobium compositions ranging from 7.6% to 13%. Taken from [Marnieros, 1998].

Moreover, we have seen in the previous section (3.2) that two-dimensional (2D) a-$Nb_xSi_{1-x}$ films present a Superconductor-to-Insulator Transition (SIT). This system, in 2D, thus has two possible ground states [2].

The following paper is the result of the work of Olivier Crauste and François Coüedo. It adresses the issue of the dimensional crossover between the 3D and the 2D situations. It therefore focuses on the thickness-tuned SIT in 2D films, as the niobium composition varies. The main results are the following :

1. **The evolution of the critical thickness $d_c$ is established as a function of $x$ -** The film stoichiometry can be modified to tune the robustness of the superconductive state, or, in other words, the bulk superconducting critical temperature $T_{c0}$. $d_c$ decreases as the niobium content of the film increases.
2. **The phase diagram in the ($d$,$x$) plane is inferred -** Large critical thicknesses can be obtained, while remaining 2D. This is an advantage of alloys such as a-$Nb_xSi_{1-x}$ films, where the bulk superconducting critical temperature can be tuned. This makes a-$Nb_xSi_{1-x}$ a model system to study the thickness-tuned SIT. The origin of the strong responsiveness of a-NbSi films to a change in thickness is a open question.
3. **The SIT in 2D connects with the 3D Superconductor-to-Metal Transition**.

### 3.3.2 Paper ♯4 : Crauste et al., *to be published*

1. These results were mainly in agreement with previous measurements on this system [Hertel et al., 1983]. The slight differences in critical compositions are thought to arise from the film synthesis method. In the case of reference [Hertel et al., 1983], the films were sputtered, whereas our films are co-deposited.
2. If we take it for granted that metallic states are theoretically forbidden in 2D.

# Destruction of superconductivity in disordered materials : a dimensional crossover

O. Crauste, F. Couëdo, L. Bergé, C.A. Marrache-Kikuchi,* and L. Dumoulin
*CSNSM, CNRS-UMR8609, Université Paris Sud, Bat. 108, 91405 Orsay Campus, France*
(Dated: October 14, 2013)

The disorder-induced Superconductor-to-Insulator Transition in amorphous $Nb_xSi_{1-x}$ two-dimensional thin films is studied for different niobium compositions $x$ through a variation of the sample thickness $d$. We show that the critical thickness $d_c$, separating a superconducting regime from an insulating one, increases strongly with diminishing $x$, thus attaining values of over 100 Å. The corresponding phase diagram in the $(d, x)$ plane is inferred and related to the three-dimensional situation. The two-dimensional Superconductor-to-Insulator Transition well connects with the three-dimensional Superconductor-to-Metal Transition.

PACS numbers: 68.35.Rh, 71.30.+h, 73.43.Nq, 73.50.-h, 74.25.-q, 74.40.Kb, 74.78.-w, 74.81.Bd

*Introduction.-* In disordered systems, the electronic ground state is the result of a competition between Coulomb interaction, disorder, which eventually leads to localization of charge carriers, and, when relevant, superconductivity. In this conflict between antagonistic forces, dimensionality plays a special role and determines what ground states are allowed. Indeed, in three-dimensional systems, two distinct quantum phase transitions, the Metal-to-Insulator Transition (MIT) [1–3] and the Superconductor-to-Metal Transition, separate the three possible ground states ; whereas in two dimensions, the system can only exhibit a direct Superconductor-to-Insulator Transition (SIT), since metals are theoretically forbidden in the absence of strong electron-electron interactions [4–6]. One important question is then to understand how the three ground states (superconducting, metallic and insulating) that are possible in bulk systems evolve when the thickness is reduced. More specifically, is an initially three-dimensional superconducting system affected by a thickness reduction in a universal manner or does this effect depend on the initial strength of the superconductivity?

The thickness-tuned SIT in thin alloy films provides an interesting way to address this question. Indeed, in bulk systems, the different ground states can be continuously explored through a change of stoichiometry. For example, in our system of interest, amorphous $Nb_xSi_{1-x}$ (a-NbSi), bulk films ($d \gtrsim 1000$ Å) are superconducting for $x \gtrsim 12.6\%$, metallic for $9\% \lesssim x \lesssim 12.6\%$, and insulating below $x \simeq 9\%$ [7–9]. In the two-dimensional limit, the sample thickness $d$ is one of the parameters tuning the SIT : starting from a superconducting thin film, a reduction of $d$ progressively drives the system towards an insulating state, which it reaches below a critical thickness $d_c$ [10, 11]. For instance, pure niobium films ($x = 100\%$) are superconducting until $d_c = 7$ Å [12, 13]. For a-NbSi alloys of lower niobium content, one can wonder whether $d_c$ depends on the composition $x$ and hence on the bulk superconducting temperature $T_{c0}$.

In the present letter, we focus on the thickness-induced SIT in two-dimensional a-NbSi films. We will present the variation of the critical thickness with the composition and consider the corresponding two-dimensional phase diagram in relation with the three-dimensional one.

*Experimental.–*a-NbSi films have been prepared at room temperature and under ultrahigh vacuum (typically a few $10^{-8}$ mbar) by electron beam co-deposition of Nb and Si, at a rate of about 1 Å.s$^{-1}$. The evaporation rates of each source were monitored in situ by a dedicated set of piezo-electric quartz in order to precisely monitor the composition and the thickness of the films during the deposition. These were also corroborated ex situ by Rutherford Backscattering Spectroscopy (RBS) measurements [14]. The films were deposited onto sapphire substrates coated with a 250 Å-thick SiO underlayer designed to smooth the substrate surface. The samples were subsequently protected from oxydation by a 250 Å-thick SiO overlayer. The samples studied here have Nb concentrations ranging from 13.5% to 18% and thicknesses varying from 20 to 500 Å. Similar films have been measured to be continuous, amorphous and structurally non-granular at least down to a thickness of $d =$ 25 Å [15].

Transport measurements were carried out down to 10 mK in a dilution refrigerator, using a TRMC2 resistance measurement bridge and standard AC lock-in detection techniques. The applied polarisation has been checked to be sufficiently low to avoid any parasitic effect. All electrical leads were filtered from RF at room temperature.

*Determination of $d_c$.-* We have considered the evolution of the superconducting properties of two-dimensional a-NbSi thin films as the thickness is lowered, for different values of the composition $x$ (see figure 1 for the different sheet resistances $R_\square(T)$ corresponding to $x$=18%). The SIT occurs at a critical thickness $d_c$ characterized by a change in the Temperature Coefficient of Resistance (TCR = $\frac{dR}{dT}$) at low temperature : a positive TCR corresponds to a superconducting ground state, whereas a negative TCR is taken to be characteristic of an insulator [16, 17]. For each value of $x$, we have determined $d_c$ through two methods.

First, by plotting the evolution of the sheet resistance

*Electronic address: Claire.Marrache@csnsm.in2p3.fr

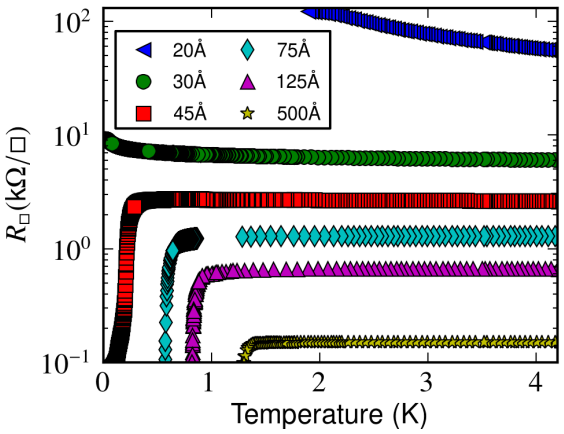



FIG. 1: Sheet resistance as a function of temperature for a-$Nb_{18}Si_{82}$ samples of thicknesses ranging from 20 to 500 Å. The SIT is tuned through a change in sample thickness and occurs in the interval at $d_c = 34 \pm 2$ Å.

$R_\square$ with the thickness for different temperatures (see figure 2). The crossing point, $(d_c, R_{\square,c})$, where $R_{\square,c}$ is the critical sheet resistance at the transition, signals the transition between a superconducting and an insulating phase [11, 18, 19].

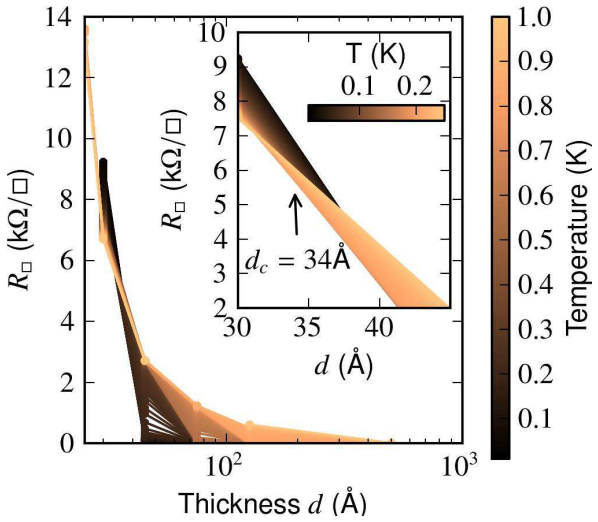



FIG. 2: Sheet resistance as a function of the thickness for different temperatures ranging from 10 mK to 1 K for $x = 18\%$. The crossing point provides $d_c$ and $R_{\square,c}$ at the transition. For $x = 18\%$, $d_c = 34 \pm 2$ Å. Inset : same data, centered around $d = 34$ Å, for 10 mK $< T <$ 250 mK.

The second estimation of $d_c$ derives from the evolution of the superconducting critical temperature $T_c$ with the thickness. Indeed, as has been reported in other two-dimensional systems [20, 21], at a given composition, we observe a relation between $T_c$ and $d$ : as the sample thickness is decreased, $T_c$ decreases linearly with $1/d$, as shown figure 3. The interpretation of this relation is beyond the scope of this paper. However, from the extrapolation to $1/d \to 0$, one can infer $T_{c0}$, the superconducting critical temperature of the bulk film corresponding to the same composition (figure 4.a.). The values of $T_{c0}$ thus obtained are in very good agreement with what has previously been measured in bulk samples [22]. From the extrapolation to $T_c \simeq 0$, one can deduce the critical thickness at which superconductivity is suppressed in thin a-NbSi films.

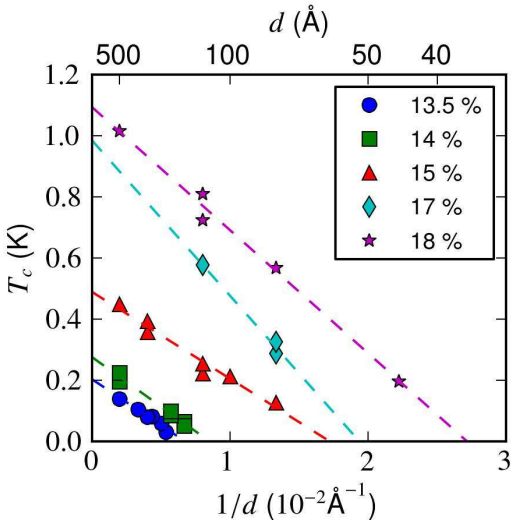



FIG. 3: Evolution of the superconducting critical temperature $T_c$ with the inverse of the thickness $d$ for the different samples studied. The dashed lines are best linear fits to $T_c = f(1/d)$.

Both evaluations of $d_c$ are given figure 5 and are in good agreement with one another. The obtained values of $d_c$ are large ($d_c > 30$ Å), which is particularly convenient to study the disorder-tuned SIT at thicknesses where the continuity of the films is secured.

Even at these large values of $d_c$, the films can be considered two-dimensional from the point of view of superconductivity. Indeed, for a-NbSi films of a similar composition, the superconducting coherence length $\xi_{SC}$ has been measured to be larger than 100 Å [23]. Moreover, a *minimal* estimate of $\xi_{SC}$ can be derived from Ginzburg-Landau theory in the dirty limit : $\xi_{SC} = 0.36\sqrt{\frac{3}{2}\frac{2\pi\hbar^3}{k_B T_{C0} m R_{\square,c} e^2}}$, where $m$ is the electron mass, $e$ its charge, and $R_{\square,c}$ the sheet resistance of the critical film. The dependance of this evaluation of $\xi_{SC}$ with $x$ is given figure 4.b. We have $d \lesssim \xi_{SC}$, which is the commonly accepted criterion of 2D superconductivity [24], for all samples except those of thickness 500 Å.

*Critical resistance.-* In the literature, some importance has been given to the value of the normal sheet resistance for the critical sample. Indeed, $R_{\square,c} = \frac{h}{e^2 (k_F l)_c}$ has been deemed to be a direct measurement of the disorder $(k_F l)_c$ at the SIT [16, 25]. Predictions on this quantity depend on the underlying theoretical scenario for the SIT. In the bosonic scenario, developed by M.P.A. Fisher, where the insulator is a localized state for Cooper pairs, the

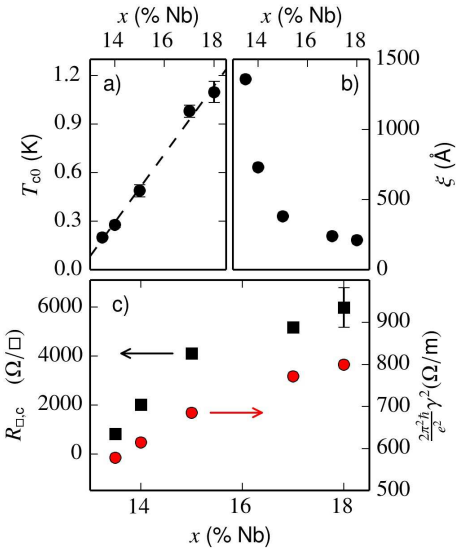



FIG. 4: a. Bulk superconducting critical temperature ($T_{c0}$) for different compositions. The dotted line corresponds to the best linear fit : $T_{c0} = 0.210(x - 12.6)$. b. Evolution of the superconducting coherence length $\xi_{SC}$ with the composition $x$ (see text). c. Evolution with $x$ of the critical sheet resistance $R_{\square,c}$ (squares) estimated from the crossing point in the $R_\square(d)$ plot. For comparison an estimate of $\frac{2\pi^2\hbar}{e^2}\gamma^2$ by Finkel'stein's fermionic scenario is given (circles).

critical resistance should be universal and of value the quantum resistance $R_Q = \frac{h}{4e^2} \simeq 6.5\text{k}\Omega/\square$ [16, 26]. In the fermionic scenario, superconductivity is destroyed to give rise to a fermionic insulating state at $d_c = \frac{e^2}{2\pi^2\hbar}R_\square \sim \gamma^2 = \left(\ln\left(\frac{k_B T_{c0}\tau}{\hbar}\right)\right)^{-2}$, where $\tau$ is the mean-free path time [25].

The experimental evolution of $R_{\square,c}$ with the composition for a-NbSi thin films is given figure 4.c. As can be seen, $R_{\square,c}$ is non universal and varies by a factor of 7 for the considered composition range. The fact that $x$ can be tuned in a-NbSi films allows to span this large range of $R_{\square,c}$ in a single compound. As observed in other systems [27, 28], $R_Q$ does not seem to play any specific role, contrary to the prediction of the bosonic scenario. Figure 4.c also gives the evolution of $\gamma^2$ predicted by Finkel'stein's fermionic theory, with $\tau = 5.10^{-16}$ s, evaluated from previous measurements [8]. As can been seen, there is a qualitative agreement between Finkel'stein's predictions and our experimental data, but there is no quantitative one, as was shown in [29].

The above-mentioned theoretical predictions therefore do not fully describe the evolution of $R_{\square,c}$ in a-NbSi thin films. We interpret this as yet another indication that $R_\square$ is not the only relevant parameter for our system. Indeed, we have shown [15] that, in the SIT, the thickness played a role distinct from a modification of the microscopic disorder, for example tuned by a small change in the film composition. The destruction of superconductivity in the thickness-tuned transition then cannot be fully predicted by the sole knowledge of the sheet resistance. This specificity of the thickness role remains however to be understood.

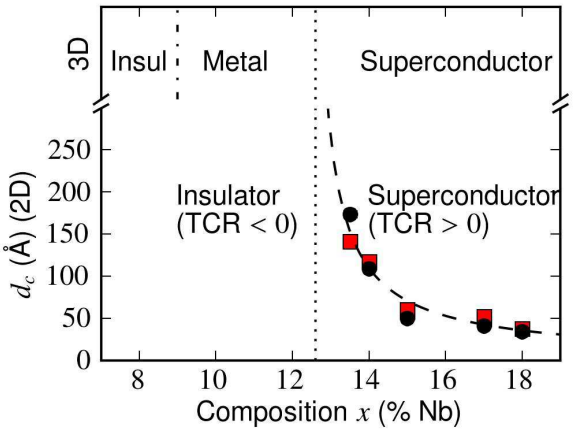



FIG. 5: Phase diagram as a function of the composition $x$ and the thickness $d$. The black dots corresponds to the estimation of $d_c$ as the value at which the $R_\square(d)$ cross at different temperatures. The red dots corresponds to the value obtained by the extrapolation of $T_c(1/d) \to 0$. The dashed line corresponds to the best fit of the scaling law $d_c = f(x)$ (see text for details).

*Phase diagram.*- Figure 5 summarizes the results under a phase diagram in the ($d$,$x$) plane, featuring the superconducting and insulating phases. Let us highlight some of the features of this diagram :

First, the critical thickness can be tuned by a variation in the film composition : $d_c$ seems to diverge as $x$ decreases. The corresponding evolution can be captured by a power law : $d_c = d_0 \times \left(\frac{x - x_c}{x_c}\right)^\alpha$. Taking into account the uncertainty on the determination of $d_c$, the best fit (dashed line in figure 5) gives $d_0 = 17 \pm 7$ Å, $\alpha = -0.9 \pm 0.1$ and $x_c = 12.4 \pm 0.6\%$. This equation can be extrapolated to $x = 100\%$ where it gives $d_c = 5 \pm 2$ Å, in agreement with what is found in the literature for pure Nb films [12, 13].

Second, the critical thicknesses thus obtained can be as large as a few hundreds of angströms. As far as we know, these are the largest critical thicknesses obtained for a two-dimensional SIT : $d_c$ is usually of a few monolayers for pure metal films [10, 30–33] or a few tens of angströms for other alloys [34–36].

Third, the critical line separating the superconducting and insulating phases in two dimensions clearly extrapolates with the Superconductor-to-Metal boundary in the three-dimensional limit. Indeed, $x_c$, at which $d_c \to +\infty$, can be compared to the composition at which superconductivity ceases to exist in bulk films (linear fit of figure 4.a : $T_{c0} = 0$ for $x_{c0} = 12.6 \pm 0.8\%$). Both values of $x_c$ coincide within error bars.

*Discussion.*- The present work is therefore an original study of the variation of $d_c$ with a parameter driving the SIT in two dimensions, here the alloy composition

$x$. Some hypothesis can be put forward to explain the remarkable result of the divergence of $d_c$ near a critical value of $x$.

If one assumes that the principal effect of $x$ is to modify the material density of state at the Fermi level and therefore $T_{c0}$ (figure 4.a), one could expect a correlation between $d_c$ and $T_{c0}$ : the lower $T_{c0}$, the larger the critical thickness. Compiling the experimental results obtained on pure metals does not permit to validate this hypothesis. Indeed, thickness reduction has most often been studied on superconducting materials with large $T_{c0}$, such as Pb [37], Nb [12], a-Bi [10]. Metallic films with $T_{c0}$ lower than 1 K (W, Ir, Ti, Al [30]) exhibit, before the destruction of superconductivity, an increase of $T_c$ when the film thickness is reduced. This entangles the impact of disorder with an increase of surface effects on the phonon spectrum [38], making experiments more complicated to interpret. The tunability of $T_{c0}$ through $x$ is specific to alloys such as a-NbSi, and has enabled us to carry out a systematic study of the SIT critical thickness with $T_{c0}$ *within the same material*. In the present study, $x$ only varies from 13.5% to 18% in a structurally disordered compound, so that films of different compositions are very similar, material-wise. A correlation between $T_{c0}$ and $d_c$, if confirmed, would be an original result, calling for an in-depth study.

Another hypothesis is to relate the divergence of $d_c$ with the proximity of the MIT in the corresponding three-dimensional material. Indeed, bulk a-NbSi presents anomalies in the density-of-state, related to the correlation pseudo-gap that develops near the MIT [9]. It would be interesting to relate the divergence of $d_c$ to the opening of this pseudo-gap and to the associated correlation length [39]. This assumption will be tested in future tunneling experiments.

Regarding the continuity in the phase diagram between the bulk metal and the two-dimensional insulating state - characterized, as is usual in the literature, by a negative TCR - the crucial issues then are : first to understand what microscopic differences exist between those two states. For instance, the nature of the two-dimensional insulator is still a debated question [3]. Second : how does the three-dimensional metal transit to an insulating ground state at lower dimension and at what lengthscale. Further investigations on this point are under way.

*Conclusion.-* We have studied the thickness-tuned SIT in amorphous $Nb_xSi_{1-x}$ thin films and established the phase diagram when the composition of the alloy is varied. The critical thickness below which the system is insulating is correlated with the bulk superconducting critical temperature, and diverges in the vicinity of the critical composition at which the Superconductor-to-Metal Transition occurs in bulk films. The tunability of a-NbSi, and notably the possibility of modifying its bulk superconducting critical temperature, makes it a model system to study the SIT.

**Acknowledgments**

This work has been partially supported by the Agence Nationale de la Recherche (grants No. ANR-06-BLAN-0326 and ANR-2010-BLANC-0403-01), and by the Triangle de la Physique (grant No. 2009-019T-TSI2D).

[1] D. Belitz and T. Kirkpatrick, Rev. Mod. Phys. **66**, 261 (1994).
[2] F. Evers and A. D. Mirlin, Rev. Mod. Phys. **80**, 1355 (2008).
[3] V. Dobrosavlejevic, N. Trivedi, and J. Valles, *Conductor Insulator Quantum Phase Transitions* (OUP Oxford, 2012).
[4] E. Abrahams, S. Kravchenko, and M. Sarachik, Rev. Mod. Phys. **73**, 251 (2001).
[5] M. V. Feigel'man, L. B. Ioffe, V. E. Kravtsov, and E. A. Yuzbashyan, Phys. Rev. Lett. **98**, 027001 (2007).
[6] V. L. Pokrovsky, G. M. Falco, and T. Nattermann, Phys. Rev. Lett. **105**, 267001 (2010).
[7] L. Dumoulin, L. Bergé, J. Lesueur, H. Bernas, and M. Chapellier, J. Low. Temp. Phys. **93**, 301 (1993).
[8] O. Crauste, Ph.D. thesis, Paris-Sud, Orsay (2010).
[9] D. Bishop, E. Spencer, and R. Dynes, Sol. St. Elec. **28**, 73 (1985).
[10] D. Haviland, Y. Liu, and A. Goldman, Phys. Rev. Lett. **62**, 2180 (1989).
[11] C. Marrache-Kikuchi, H. Aubin, A. Pourret, K. Behnia, J. Lesueur, L. Bergé, and L. Dumoulin, Phys. Rev. B **78**, 144520 (2008).
[12] A. Asamitsu, M. Iguchi, A. Ichikawa, and N. Nishida, Physica B **194-196** (1994).
[13] N. Nishida, S. Okuma, and A. Asamitsu, Physica B **169**, 487 (1991).
[14] J. Walls, ed., *Methods of Surface Analysis* (Cambridge University Press, 1989).
[15] O. Crauste, A. Gentils, F. Couedo, Y. Dolgorouky, L. Bergé, S. Collin, C. Marrache-Kikuchi, and L. Dumoulin, Phys. Rev. B **87**, 144514 (2013).
[16] M. Fisher, Phys. Rev. Lett. **65**, 923 (1990).
[17] R. Schneider, A. Zaitsev, D. Fuchs, and H. v. Lohneysen, Phys. Rev. Lett. **108**, 257003 (2012).
[18] A. Hebard and M. Paalanen, Phys. Rev. Lett. **65**, 927 (1990).
[19] N. Markovic, C. Christiansen, and A. Goldman, Phys. Rev. Lett. **81**, 5217 (1998).
[20] M. Stewart, H. Nguyen, S. Hollen, A. Yin, J. Xu, and J. Valles, Physica B **469**, 774 (2009).
[21] J. Simonin, Phys. Rev. B **33**, 7830 (1986).
[22] A. Juillard, Master's thesis, École des Mines de Nancy (1996).
[23] A. Pourret, H. Aubin, J. Lesueur, C. Marrache-Kikuchi, L. Bergé, L. Dumoulin, and K. Behnia, Nature Physics **2**, 683 (2006).
[24] M. V. Feigel'man and M. A. Skvortsov, Phys. Rev. Lett. **109**, 147002 (2012).

[25] A. Finkel'stein, Physica B **197**, 636 (1994).
[26] M. Cha, M. Fisher, S. Girvin, M. Wallin, and A. Young, Phys. Rev. B **44**, 6883 (1991).
[27] A. Yazdani and A. Kapitulnik, Phys. Rev. Lett. **74**, 3037 (1995).
[28] N. Markovic, C. Christiansen, A. Mack, W. Huber, and A. Goldman, Phys. Rev. B **60**, 4320 (1999).
[29] O. Crauste, C. Marrache-Kikuchi, L. Berge, D. Stanescu, and L. Dumoulin, in *Journal of Physics: Conference Series* (IOP Publishing, 2009), vol. 150, p. 042019.
[30] M. Strongin, R. Thompson, O. Kammerer, and J. Crow, Phys. Rev. B **1**, 1078 (1970).
[31] S. Qin, J. Kim, Q. Niu, and C. Shih, Science **324**, 1314 (2009).
[32] D. Eom, S. Qin, M.-Y. Chou, and C. K. Shih, Phys. Rev. Lett. **96**, 027005 (2006).
[33] Y. Li, C. L. Vicente, and J. Yoon, Physical Review B **81**, 20505 (2010).
[34] S. Lee and J. Ketterson, Phys. Rev. Lett. **64**, 3078 (1990).
[35] J. Graybeal and M. Beasley, Phys. Rev. B **29**, 4167 (1984).
[36] A. Hirakawa, K. Makise, T. Kawaguti, and B. Shinozaki, J. Phys. : Condens. Matter **20**, 485206 (2008).
[37] H. Jaeger, D. Haviland, B. Orr, and A. M. Goldman, Phys. Rev. B **40**, 182 (1989).
[38] D. Belitz, Phys. Rev. B **35** (1987).
[39] W. McMillan, Physical Review B **24**, 2739 (1981).

# Chapter 4

# SIT : A closer look at the processes at play

The point of view of Quantum Phase Transitions, explored in the previous chapter, is a powerful but very global approach of the Superconductor-to-Insulator Transition. As stated above, the analysis of the critical exponents and of the critical values of the different parameters ($d_c$, $H_c$, $R_c$, ...) can help determine the universality class to which the system belongs, but only indirectly leads to a physical picture of the processes involved.

Without discarding the upsides of the general theory of Quantum Phase Transitions, we wished to balance it with a more microscopic approach, where we focused on the study of the influence of different parameters (thickness, composition, ...) on the superconducting properties of the film ($T_c$, $R_\square$, ...). The ultimate aim of such a study is to guide us in our reconstruction of a plausible scenario for the destruction of superconductivity in disordered systems.

## 4.1 Annealing as a parameter to fine-tune the disorder

To study the influence of disorder, knowing how to tune and characterize disorder is, by definition, a crucial issue.

The disorder level $W$ is usually defined by the product $k_F l$ of the Fermi wavevector $k_F$ and of the elastic mean free path $l$ [Lee and Ramakrishnan, 1985]. In two dimensions, a simple Drude estimation of the sheet resistance gives :

$$R_\square = \frac{h}{e^2 k_F l} \tag{4.1}$$

This has led to the idea that $R_\square$ is a direct measurement of the disorder level in thin films, whatever the mean used to vary $W$.

In an ideal experiment, one would like to compare samples with different levels of disorder, *caeteris paribus*. This means that the experimental bias chosen to tune $W$ must not affect the system in any other aspect. Experimentally, however, it is not easy to find such a parameter. As mentioned in section 1.1, most experimental studies on the disorder-induced SIT have tuned the disorder via a variation of the film thickness. With Louis Dumoulin, we felt that this way of modifying the system disorder was not entirely without significance. Indeed, a-NbSi films with thicknesses ranging from 20 Å to 200 Å are all in the two-dimensional limit [1], but such a large change in $d$ could very well impact the dimensionality of other phenomena, such as Coulomb interactions or weak localization, that are also important to consider. We therefore looked for other experimental parameters that could be employed to change the disorder.

In our system of interest, a-$Nb_xSi_{1-x}$, the composition could be varied : a change in $x$ tunes the density of states and therefore modifies $k_F$. However, a tuning parameter that modifies the mean free path $l$ without changing the DOS nor the film thickness is even more appropriate : the disorder effect can then be observed on the same compound (same $k_F$), at fixed thickness. Annealing meets these requirements.

Previous studies have shown that annealing is a convenient experimental knob that can modify the conductivity in amorphous compounds. In InOx films [Shahar and Ovadyahu, 1992], annealing slightly changes the film volume and the oxygen content, thus rendering the compound more metallic, similar to a change in stoichiometry. In semiconductor-based amorphous thin films, such as a-$Al_xGe_{1-x}$ [Lesueur et al., 1985] or a-$Nb_xSi_{1-x}$ [Marnieros, 1998], however, annealing does not change the nature of the compound. In those systems, annealing gives the atoms sufficient energy to evolve towards thermodynamical equilibrium, through *sub-atomic*

1. The commonly accepted criterion two-dimensionality with respect to superconductivity is : $d < \xi_{SC}$, the superconducting coherence length.

relaxations of their position [2]. This has been shown to increase the local resistivity [Béal and Friedel, 1964]. Annealing thus is equivalent to a reduction of the mean free path, and does not affect the composition nor the thickness of the films. It therefore allows the fine-tuning of disorder on a *single* sample.

In sections 4.2 and 4.3, we will compare the change in disorder induced by annealing with the one derived from a change in thickness or composition. We have also used annealing as a tool for applications, to adjust the superconducting properties of thermometric thin films. This will be discussed in chapter 5.

## 4.2 What is the meaning of "disorder" ?

### 4.2.1 Presentation of the paper

As mentioned in the previous section, in a-$Nb_xSi_{1-x}$, we dispose of three different ways of varying the sheet resistance $R_\square$ : the composition $x$, the thickness $d$ and the annealing temperature $\theta_a$. The aim of this work is to examine whether those three parameters have the same effect on the superconducting properties of the studied thin films. The ultimate question we try to address is : do they all affect the disorder in the same way ?

The following paper is principally the result of the work of François Couëdo and Olivier Crauste, with an important contribution, for microscopic characterization of the samples, of Aurélie Gentils. The main results are the following :

1. Before examining the effect of annealing on a-NbSi films, we checked that this process does not modify the microscopic structure of the samples. Through AFM [3], TEM [4], and complementary transport measurements, we showed that **a-NbSi thin films remain continuous, amorphous and morphologically homogeneous** until an annealing temperature $\theta_{a,c}(d)$ which is thickness-dependant but is above 200 °C for thicknesses above 50 Å.
2. ***x* and $\boldsymbol{\theta_a}$ affect the films superconducting properties in a similar way** : the sole knowledge of the sheet resistance is then sufficient to fully determine the $T_c$ reduction with respect to the bulk superconducting temperature.
3. The effect of the thickness reduction is however distinct. $\boldsymbol{R_\square}$ **then is not the relevant parameter to fully describe the disorder**. In other words, what is named "disorder" in the literature most likely groups different phenomena : some of them captured by the sheet resistance : they affect $k_F l$ ; others, like the thickness, are independent, although they indirectly affect $R_\square$ through a mechanism that remains to be determined.

### 4.2.2 Paper ♯5 : Crauste et al., *Phys. Rev. B*, 87, 144514, 2013

2. For moderate annealing, no segregation or recristallisation occurs, as we will see.
3. Atomic Force Microscopy.
4. Transmission Electron Microscopy.

# Effect of annealing on the superconducting properties of $a$-$Nb_xSi_{1-x}$ thin films

O. Crauste, A. Gentils, F. Couëdo, Y. Dolgorouky, L. Bergé, S. Collin, C. A. Marrache-Kikuchi,* and L. Dumoulin
*Centre de Spectrométrie Nucléaire et de Spectrométrie de Masse, Centre National de la Recherche Scientifique, Unité Mixte de Recherche 8609, Université Paris Sud, Bat. 108, 91405 Orsay Campus, France*
(Received 8 October 2012; revised manuscript received 20 March 2013; published 23 April 2013)

$a$-$Nb_xSi_{1-x}$ thin films with thicknesses down to 25 Å have been structurally characterized by transmission electron microscopy measurements. As-deposited or annealed films are shown to be continuous and homogeneous in composition and thickness, up to an annealing temperature of 500 °C. We have carried out low-temperature transport measurements on these films close to the superconductor-to-insulator transition (SIT) and shown a qualitative difference between the effect of annealing or composition and a reduction of the film thickness on the superconducting properties of $a$-NbSi. These results question the pertinence of the sheet resistance $R_\square$ as the relevant parameter to describe the SIT.

DOI: 10.1103/PhysRevB.87.144514 PACS number(s): 74.25.−q, 68.37.Lp, 68.37.Ps, 68.55.−a

## I. INTRODUCTION

The interplay between superconductivity and disorder is a long-standing problem.[1–6] One of the first steps toward its understanding was given by the so-called Anderson theorem,[7] which states that weak nonmagnetic disorder has no effect on the superconducting critical temperature $T_c$. However, this limit is rarely ever attained in real samples. Moreover, numerous experiments have subsequently shown that microscopic interactions relate to the level of disorder in a more complex manner.[8,9] Despite a few decades of both theoretical and experimental efforts, this problem remains unsolved and is still a major issue in solid-state physics.[10]

The effects of disorder on superconductivity are all the more dramatic in two dimensions, which is the lowest dimension for the existence of either a metal or a superconductor. In two dimensions, as the microscopic disorder is increased, superconducting thin films evolve toward an insulating state. This change in ground state has commonly been described as a superconductor-to–insulator transition (SIT) and results from the competition between disorder-induced localization of charge carriers and the formation of a coherent state of condensed Cooper pairs.[10,11] Within these theoretical descriptions, the physical properties of the films should only depend on the sheet resistance $R_\square \propto \frac{1}{k_F l}$ (Refs. 5 and 12), where $k_F$ is the Fermi wave vector and $l$ is the mean free path.

The disorder-induced SIT has been studied experimentally in several systems.[5,13–18] In these studies, the experimental tuning parameter is usually a variation in the sample thickness. How exactly a reduction in sample thickness affects $R_\square$ is, however, unclear: although both processes affect $R_\square$, a change in the film microscopic disorder and a reduction of the sample thickness might be different in nature. Varying the sample thickness around typical values of a few tens of angströms may change the relative influence of the surface, as has been previously suggested,[19,20] or even modify the effective dimensionality of the system. The study of the influence of microscopic disorder on superconducting properties in samples of the *same* thickness might therefore help disentangle the complex effects gathered under the generic term of "disorder."

Our system of interest is amorphous $Nb_xSi_{1-x}$ ($a$-NbSi), which is known to undergo a disorder-driven SIT for two-dimensional (2D) samples where the film thickness $d < \xi_{SC}$, the superconducting coherence length.[21] The aim of this paper is to investigate the effect of annealing (up to 250 °C), as another way to vary $R_\square$, on the SIT. With this approach, annealing is a new parameter that allows us to microscopically finely modify the film disorder within the same sample, without changing its thickness. We will first show that these moderate thermal treatments do not measurably affect the structure of the samples (Sec. III). We will then focus on the modifications thus induced on their superconducting properties (Sec. IV). Section V will aim at providing a possible interpretation of this effect.

## II. EXPERIMENTAL PROCEDURE

All $a$-NbSi films have been prepared at room temperature and under ultrahigh vacuum (typically a few $10^{-8}$ mbar) by electron beam codeposition of Nb and Si, at a rate of the order of 1 Å $s^{-1}$. We have shown special care in the control of the sample parameters: the evaporation was controlled *in situ* by a special set of piezo-electric quartz in order to precisely monitor the composition and the thickness of the films during the deposition. In order to check *ex situ* these two parameters, Rutherford backscattering spectroscopy (RBS)[22] measurements were systematically undertaken and the results well fitted with the *in situ* monitoring. Due to heating during the deposition process, the equivalent annealing temperature of the as-deposited films has been estimated at 70 °C and confirmed by low-temperature measurements of the conductivity (see Sec. IV A).

Films for *transport measurements* were deposited onto sapphire substrates coated with a 250-Å-thick SiO underlayer designed to smooth the substrate surface. The samples were subsequently protected from oxidation by a 250-Å-thick SiO overlayer. The Nb concentrations ranged from 13.5 to 18% and the film thicknesses ranged from 20 to 500 Å. Each film has been annealed, by steps, from 70 to 250 °C, for 1 h, under a flowing $N_2$ atmosphere. To prevent any thermal shock, the samples were slowly cooled to room temperature.

Atomic force microscopy (AFM) and transmission electron microscopy (TEM) measurements have been carried out on $Nb_{18}Si_{82}$ films of thicknesses down to 25 Å, close to the lowest sample thickness studied by transport measurements (20 Å).

 ©2013 American Physical Society

Although the transport samples were of different compositions, it is reasonable to assume that the film stoichiometry does not affect its structure, at least in the considered range of niobium concentrations ($13.5 < x < 18\%$).

Samples for *AFM measurements* were deposited onto a silicon wafer, overcoated with a native silicon oxide layer. The *a*-NbSi samples were not covered by a SiO overlayer, in order to accurately characterize the film morphology.

*TEM studies* were performed on films evaporated onto commercial 250-Å-thick $SiO_2$ membranes, using a Tecnai $G^2$ FEI microscope operated at 200 keV. Energy filtered transmission electron microscopy (EFTEM) measurements have also been performed on this microscope, using a GATAN Tridiem imaging filter. As-deposited *a*-NbSi films were only covered by their native oxide layer. In order to assess the influence of the annealing temperature on the film structure, samples capped with 100 Å of SiO have been synthesized and embedded within a heating TEM sample holder in order to perform *in situ* measurements. This way, TEM annealed samples closely resembled the analogous transport samples. Moreover, this thin capping layer prevented any contamination of the *a*-NbSi film during the annealing, which ranged from 70 to 700 °C. The annealing took place inside the vacuum chamber and lasted 15 min. Since the characteristic time for annealing-induced relaxation is smaller than 1 min,[23–25] this duration is sufficient to obtain the same microscopic state of the material as for the transport samples.

Transport measurements were carried out down to 10 mK in a dilution refrigerator, using a TRMC2 resistance measurement bridge and standard ac lock-in detection techniques. The current applied to the sample was well within the linear regime of the I-V characteristics for the considered films. All electrical leads were filtered from rf at room temperature.

## III. STRUCTURE OF *a*-$Nb_xSi_{1-x}$ THIN FILMS

The characterization of disordered thin-film morphology is especially relevant for the study of the SIT, since the physical mechanisms explaining the destruction of superconductivity may differ for granular and morphologically homogeneous systems.[10,26] We have therefore conducted AFM and TEM measurements on our as-deposited *a*-NbSi films in order to verify their continuity, amorphousness, and nongranularity (Sec. III A) down to $d = 25$ Å.

Since annealing plays an important role in the present work, we have extended TEM measurements to films that were annealed *in situ* from 70 to 700 °C (Sec. III B). We will show that we observe, through this technique, no structural change in *a*-NbSi films up to an annealing temperature of 500 °C.

### A. Morphology of as-deposited films

#### 1. Transport measurements

Before describing the microscopy measurements we have performed, we would like to emphasize that transport measurements are very sensitive to the sample structure and can thus give us some information on the microscopic nature of *a*-NbSi.

Figure 1 shows the low-temperature characteristics of three $Nb_{18}Si_{82}$ films for thicknesses of 125, 75, and 45 Å. As has been previously measured in other *a*-NbSi samples,[21] the sheet resistance $R_\square(T)$ shows no sign of reentrance as is usually observed for granular systems[27] when the thickness is lowered. Moreover, the superconducting transitions are a few tens of mK sharp, as is usual for homogeneous films.

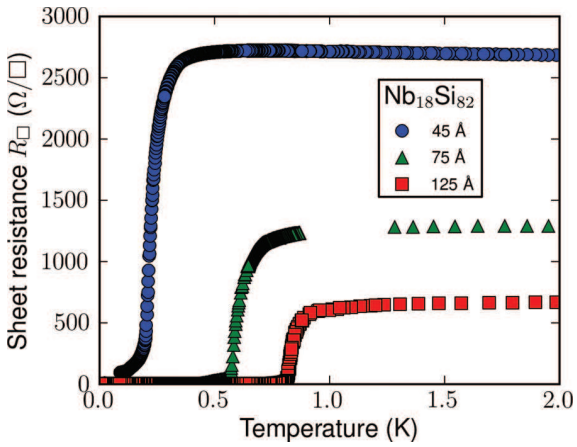



FIG. 1. (Color online) Sheet resistance as a function of temperature for $Nb_{18}Si_{82}$ samples of thicknesses ranging from 45 to 125 Å. The 25-Å-thick sample of the same composition was found to be insulating.

We have also measured the electron-phonon coupling constant to be $g_{e-ph} \simeq 50$ W $K^{-5}$ $cm^{-3}$ at 100 mK, which is very similar to the values obtained in bulk metallic *a*-NbSi.[28] This is another indication that all the film volume participates to the conduction and that there are no percolating structures.

#### 2. AFM measurements

We have performed AFM measurements on films of thicknesses down to 25 Å. All measured films were continuous, on a macroscopic scale, within the precision of the apparatus ($\simeq$20 nm in the sample plane). As we will see in the next paragraph, TEM observations will confirm this.

The sample surface was moreover found to be very smooth, with a RMS roughness limited by the AFM resolution ($\simeq$1 Å in height). This is yet another strong indication of the nongranularity of *a*-NbSi films down to these thicknesses.

#### 3. TEM measurements

TEM measurements were destined to confirm, with a better spatial resolution, the AFM results, namely, the continuity and homogeneity of our films. For practical purpose, as stated in Sec. II, the *a*-NbSi films were evaporated onto $SiO_2$ membranes for these observations.

Figures 2(b) and 2(c) shows a TEM image, along with the corresponding diffraction pattern, of a 25-Å-thick (100-Å-thick) $Nb_{18}Si_{82}$ film deposited onto such a $SiO_2$ membrane. Samples have been imaged at different positions, and no noticeable spatial difference either in the TEM images or the diffraction spectra was observed.

Due to the grainlike structures present on the TEM image of the commercial $SiO_2$ membrane [Fig. 2(a)], which are most probably due to mechanical stress effects, we estimate that we cannot visualize structures in *a*-NbSi films smaller than 20 Å in size. However, the TEM resolution is good enough

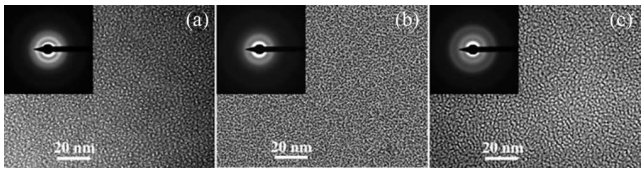



FIG. 2. TEM images of (a) the $SiO_2$ membrane that serves as substrate to TEM measurements and (b) 25- and (c) 100-Å-thick $Nb_{18}Si_{82}$ film deposited onto the membrane. Insets: Corresponding electronic diffraction patterns.

for us to be confident that our films contain no discontinuities or granular structures larger than this limit, as confirmed by transport measurements (Sec. IV).

Besides, the diffraction spectrum for the 100-Å-thick sample attests to the amorphousness of this film. In the case of the 25-Å-thick film, the diffraction spectrum is more difficult to interpret due to the ratio of the film thickness to the membrane thickness, but it is reasonable to assume that films thinner than 100 Å do not contain any crystallites, since they would also have been imaged in the 100-Å-thick sample. This will also be confirmed by conductivity measurements (Sec. IV A).

#### *4. Composition homogeneity*

In order to check the uniformity of the film composition along the sample and to confirm its homogeneity in thickness, we have performed EFTEM measurements on the 25-Å-thick $Nb_{18}Si_{82}$ TEM sample. We have considered the 34- and 99-eV energy edges for Nb and Si, respectively, using a 20-eV slit. The results are shown in Fig. 3. Any local difference in the EFTEM signal can be attributed to a change in niobium concentration or in the film thickness. Each measurement was performed for different focuses and no visible structure remained, leading us to conclude the samples are very homogeneous both in composition and thickness. We estimate that any difference in the number of Nb atoms larger than $\pm 0.1\%$ can be detected by this experimental setup with a spatial resolution of 10 Å.

### B. Annealed films

As previously stated, the present work focuses on the SIT in *amorphous* NbSi films. Exposed to sufficiently high temperature, bulk ($d > 500$ Å) NbSi is known to crystallize.[23,29] In order to use annealing as a relevant tuning parameter for our system, we therefore first had to establish the maximum temperature at which the amorphous character of these thin films is preserved.

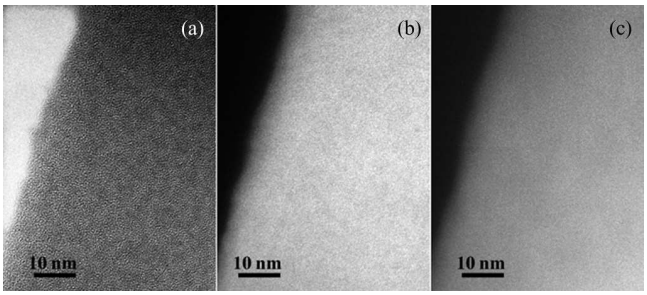



FIG. 3. (a) TEM image of a 25-Å-thick $Nb_{18}Si_{82}$ film deposited onto a $SiO_2$ membrane. The image is taken near a membrane edge (left). (b) EFTEM image of the same region of the sample for a Nb 34-eV M x ray. (c) EFTEM image of the same region of the sample for a Si 99-eV L x ray.

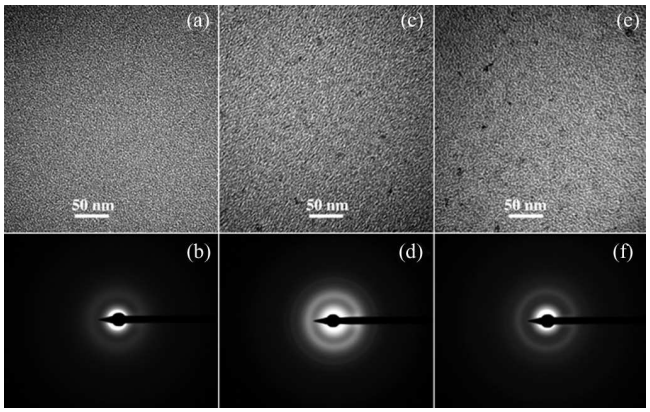



FIG. 4. TEM images and diffraction patterns of a 25-Å-thick $Nb_{18}Si_{82}$ sample after a (a) and (b) 200 °C annealing, (c) and (d) 500 °C annealing, and (e) and (f) 700 °C annealing.

For this, we have performed TEM and diffraction measurements on a 25-Å-thick $Nb_{18}Si_{82}$ sample, that was annealed *in situ* at regularly spaced temperatures ranging from 70 to 700 °C.

The results are summarized Fig. 4. We have found no significant change in the film structure until an annealing temperature of 500 °C, consistent with the results obtained for bulk samples.[23] Above this value, TEM images show the emergence of regions with a higher electron density. These have typical sizes of 50–100 Å. Moreover, clearly defined fine spotless rings appear in the diffraction pattern. These signal the appearance of small cubic face centered structures (lattice parameter $a \simeq 4.31$ Å) compatible with the formation of partially crystallized nanometric particles of $Nb_3Si$ ($a = 4.20$ Å). As the annealing temperature is further increased, the crystallites grow in size, but no additional feature appears on the diffraction pattern.

Considering our experimental resolution, we can be confident that no crystallites over 20 Å in size appear before an annealing temperature of 500 °C or else they would have been imaged. However, because we deal with very thin samples and very few Nb atoms, we cannot rule out that precursors to this crystallization, of size smaller than 20 Å, appear at lower annealing temperatures. This point will be further discussed in Sec. IV A.

## IV. EFFECT OF ANNEALING ON THE TRANSPORT PROPERTIES OF *a*-NbSi

As-deposited *a*-NbSi films can exhibit superconducting, metallic, or insulating behaviors, depending, notably, on the niobium content $x$.[30–32] In particular, for $x \gtrsim 12\%$, *a*-NbSi films are superconducting. As an illustration, the evolutions of the 4-K conductivity $\sigma$ and of the superconducting critical temperature $T_c$ with $x$ are given in Fig. 5 for *bulk* samples. As can be seen, for three-dimensional *a*-NbSi films, the conductivity and $T_c$ increase linearly with $x$, in accordance

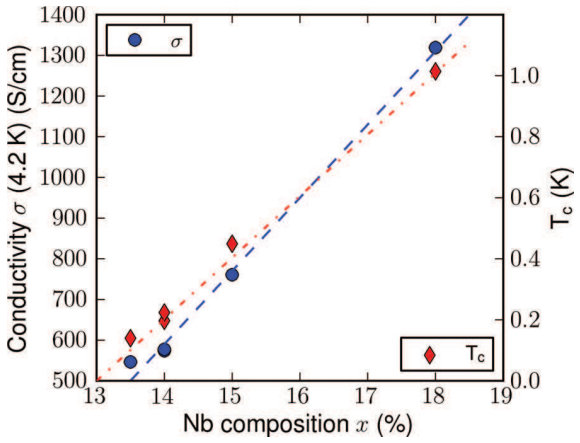



FIG. 5. (Color online) Evolution of the 4.2-K conductivity $\sigma_{4K}$ (blue dots) and of $T_c$ (red diamonds) with the alloy composition $x$. The lines are guides to the eye.

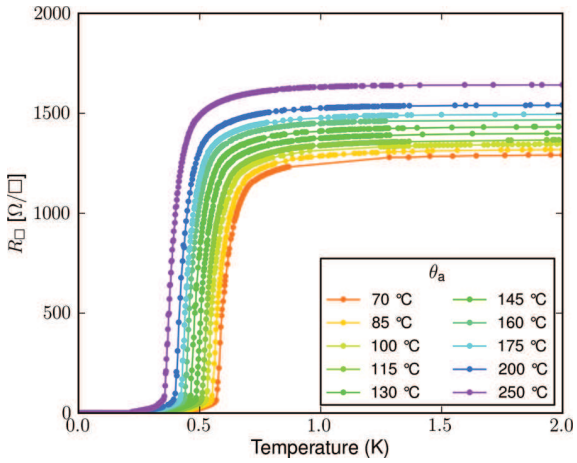



FIG. 6. (Color online) Evolution of the low-temperature transport properties of a 75-Å-thick $Nb_{18}Si_{82}$ film for $70 < \theta_a < 250\,^{\circ}C$.

with previous studies on $a$-NbSi near the metal-to-insulator transition.[33] This dependence is known to reflect the change in density of states induced by a change in Nb composition.

To study the effect of the annealing temperature on the superconducting properties of two-dimensional $a$-NbSi thin films, we have considered samples of two different niobium compositions, $x = 13.5$ and 18%, allowing us to span the portion of the phase diagram where $0.14 \leqslant T_{c,\mathrm{bulk}} \leqslant 1$ K. The superconducting films have thicknesses ranging from 45 to 500 Å. We can estimate the superconducting coherence length $\xi_{SC} \simeq \sqrt{\frac{0.18\hbar v_F l}{k_B T_c}}$ to be of the order of 260 to 930 Å depending on the film $T_c$, taking the mean free path to be the interatomic distance $l = 2.65$ Å[34] and $v_F \simeq 2.10^8$ cm s$^{-1}$,[35] in excellent agreement with the estimate of the Ginzburg-Landau coherence length obtained by Nernst effect in films of similar composition.[36,37] Except for the 500-Å-thick films, the films all have $d < \xi_{SC}$, as can be seen from Table I, which is the commonly accepted criterion for 2D superconductivity.[38] The

TABLE I. 4.2-K conductivity $\sigma$ and superconducting coherence length $\xi_{SC}$ of the different as-deposited samples. (N.S. = non-superconducting.)

| $x$ (%) | $d$ (Å) | $\sigma$ ($\times 10^2$ S cm$^{-1}$) | $T_c$ (K) | $\xi_{SC}$ (Å) |
|---|---|---|---|---|
| 13.5 | 50 | 3.1 | N.S. | |
| 13.5 | 75 | 4.2 | N.S. | |
| 13.5 | 100 | 4.6 | N.S. | |
| 13.5 | 200 | 5.4 | N.S. | |
| 13.5 | 250 | 5.4 | 0.080 | 930 |
| 13.5 | 300 | 5.6 | 0.104 | 815 |
| 13.5 | 500 | 5.5 | 0.140 | 703 |
| 18 | 20 | 0.91 | N.S. | |
| 18 | 25 | 3.8 | N.S. | |
| 18 | 30 | 5.5 | N.S. | |
| 18 | 45 | 8.4 | 0.196 | 594 |
| 18 | 75 | 10.3 | 0.568 | 349 |
| 18 | 125 | 11.9 | 0.724 | 309 |
| 18 | 125 | 12.2 | 0.809 | 292 |
| 18 | 500 | 13.2 | 1.015 | 261 |

transport properties of these films have been studied at low temperature, for annealing temperatures, $\theta_a$ ranging from room temperature to 250 °C.

In this work, we have focused on the effect of moderate annealing on $a$-NbSi films. It is important to restate that, in the range of $\theta_a$ considered, the samples remain amorphous. We therefore do not consider the situation where the annealing induces partial or total crystallization of the film. Within this regime, the effect of increasing $\theta_a$ on superconducting $a$-NbSi films is twofold: the normal resistance increases and $T_c$ decreases, as is shown for a typical sample in Fig. 6. In the following sections we will detail these effects.

### A. Evolution of film conductivity

For thick samples ($d > 150$ Å), the conductivity of as-deposited $a$-NbSi only depends on the alloy composition. For thinner films, the conductivity decreases with the thickness (Table I), as could be expected from the Fuchs law[39] combined with localization and interaction effects.[40]

When moderately annealed, the conductivity of $a$-NbSi decreases almost linearly with the annealing temperature $\theta_a$ and $\sigma^*_{4K}(\theta_a) = \frac{\sigma_{4K}(\theta_a)}{\sigma_{4K}(\theta_a = 70\,^{\circ}C)}$ is a function independent of the film thickness at fixed composition (Fig. 7). This linear behavior of $\sigma^*_{4K}$ with $\theta_a$ gives us ground to consider $\theta_a$ as a characterization of the disorder level in the sample, albeit not being an intrinsic relevant physical parameter.[41] Moreover, from this linear relation between $\sigma^*_{4K}$ and $\theta_a$, we can verify that the effective annealing temperature of as-deposited films indeed is 70 °C.

Strongly annealed samples deviate from this trend: when a film is annealed over a critical temperature $\theta_{a,c}(d)$, its conductivity increases with $\theta_a$. We interpret this to be the onset of compositional ordering which eventually leads to crystallization, as has been observed in Ref. 29. We have seen no sign of crystallites by TEM measurements (Sec. III B), which leads us to think that these crystallites, if any, are small (<20 Å). Thinner films are, for geometrical reasons, more sensitive to the formation of a small portion of a more metallic phase, crystalline or not, which could explain the thickness dependence of $\theta_{a,c}$.

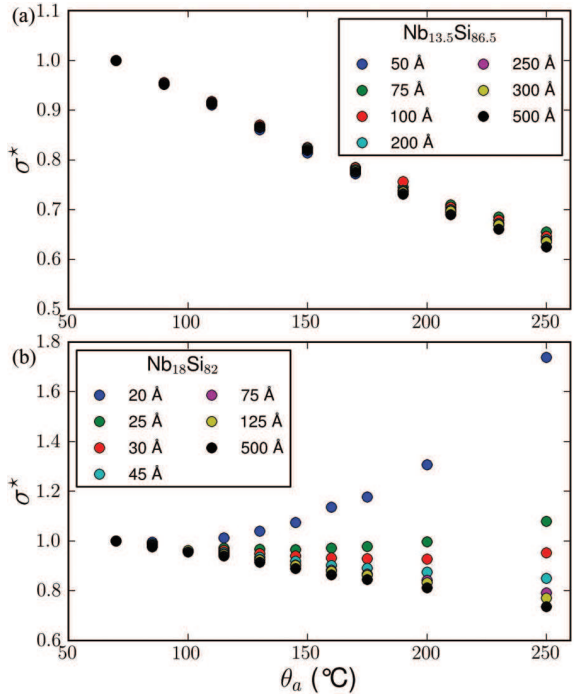



FIG. 7. (Color online) Evolution of the normalized 4.2-K conductivity $\sigma^*_{4K}(\theta_a) = \frac{\sigma_{4K}(\theta_a)}{\sigma_{4K}(\theta_a=70\,^\circ\mathrm{C})}$ with the annealing temperature for the (a) $Nb_{13.5}Si_{86.5}$ samples and the (b) $Nb_{18}Si_{82}$ samples.

These results show that transport measurements are extremely sensitive to the sample microscopic structure. Any deviation from the common $\sigma^*_{4K}(\theta_a)$ law was therefore considered to be the indication that, at a given thickness, the sample structure moved away from amorphousness and/or composition homogeneity. In the rest of this paper, the corresponding data will thus not be taken into account.

### B. Evolution of superconducting properties

Figure 8 shows the evolution of $T_c^* = \frac{T_c(\theta_a)}{T_c(\theta_a=70\,^\circ\mathrm{C})}$ as a function of $\theta_a$. As mentioned earlier, increasing $\theta_a$ tunes the sample closer to the SIT and $T_c$ therefore is a decreasing

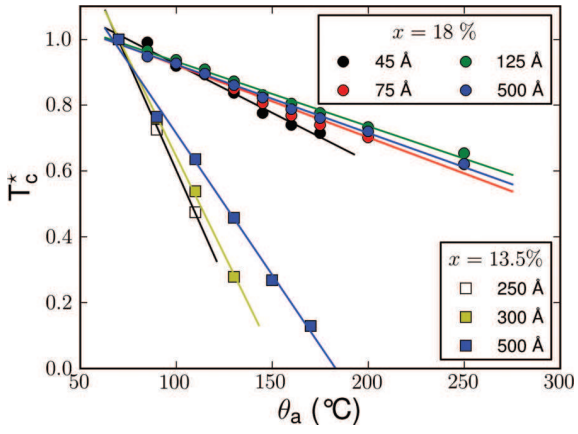



FIG. 8. (Color online) Evolution of the normalized superconducting critical temperature $T_c^* = \frac{T_c(\theta_a)}{T_c(\theta_a=70\,^\circ\mathrm{C})}$ with the annealing temperature for $Nb_{13.5}Si_{86.5}$ (squares) and $Nb_{18}Si_{82}$ (circles) samples.

function of $\theta_a$. Moreover, $|\frac{dT_c^*}{d\theta_a}|$ is smaller for large values of $x$: for samples with higher Nb content, the superconductivity is stronger and the effect of annealing is less felt.

## V. DISCUSSION ON THE EFFECT OF ANNEALING

Annealing of amorphous metallic alloys has been studied in the context of their interest as engineering materials.[23,41–46] It has been shown that their properties, whether mechanical, magnetic, or electrical, could be altered even by relatively low-temperature annealing which still preserved their amorphousness.

Although the study of microscopic changes induced by annealing is beyond the scope of this article, it should nonetheless be mentioned that the effects of such thermal treatments have been found to be threefold.[47] The first effect consists in diffusion processes. The other two effects can be attributed to structural relaxations, either chemical or topological. These are collective phenomena which redistribute quenched-in defects into lower energy configurations. Nominally, the material undergoes an extensive rearrangement of neighboring atoms without change in the mean nearest-neighbor distance.[48] The structural relaxations can either be compositional—introducing chemical short-range ordering (CSRO)—or topological—introducing topological short-range ordering (TSRO) where the relative positions of the atoms are rearranged regardless of their chemical nature.

In the case of $a$-NbSi thin films, for the considered range of annealing temperatures ($\theta_a < 250\,^\circ$C), it is reasonable to rule out significant diffusion processes. Indeed, these have measurable effects only for annealing temperatures typically above 1000 °C: in a compound similar to $a$-NbSi, the diffusion constant of an ion at 250 °C has been measured to be of about $4 \times 10^{-19}$ cm$^2$ s$^{-1}$.[49] For an annealing time of 1 h, the effective length covered by the atoms can therefore be estimated to be of the interatomic distance, at most. Moreover, the diffusion of atoms from the $SiO_2$ under- and/or overlayers into the $a$-NbSi film of interest is negligible: the kinematics of oxygen diffusion in silicon are very slow.[50] In addition, at temperatures above 1000 °C, far above our maximum annealing temperature, silicon atoms tend to diffuse from Si layers into $SiO_2$[51] rather than the contrary. Niobium atoms should also not be impacted by this very limited diffusion, thanks to their sparsity.

Second, as explained in the previous sections and verified in the literature,[23,29] $a$-NbSi thin films remain amorphous, for $\theta_a < \theta_{a,c}$, and there is no sign of chemical segregation within the films. Given the compositions we are working with, it is therefore reasonable to assume that CSRO does not affect the films' macroscopic properties and only plays a non-negligible role for temperatures higher than $\theta_{a,c}$.

TSRO, however, might provide a plausible explanation for the effect of annealing in $a$-NbSi films. Indeed, these relaxation processes induce atomic movements on lengthscales *a priori* smaller than the interatomic distance. Béal and Friedel[52] have theoretically studied the effect of such relaxation processes on the diffusion induced by pairs of scatterers and shown that this reorganization toward a local order always leads to an increase of the local resistivity. In systems close to the metal-to-insulator transition, as is $a$-NbSi in these conditions, this effect can be dramatic since a small increase in local resistivity can

translate into important effects on the macroscopic properties of the films.[53]

Last, it is important to note that previous studies have concluded that annealing $a$-NbSi up to $\theta_a = 260\,^{\circ}$C induces no change in the carrier density.[29]

For the purpose of our analysis, we will limit ourselves to the macroscopic effects of these annealing treatments. As previously seen, annealing modifies the samples' macroscopic conductivity. It can therefore be seen as a tuning parameter for disorder.

In disordered superconducting films, there have been numerous attempts to link the superconducting properties to the film disorder, measured by the product $k_F l$. In two-dimensional systems, $R_\square = \frac{h}{e^2}\frac{1}{k_F l}$, so that the square resistance has often been put forward as a way to quantify the mean sample disorder.

Theoretically, the Kosterlitz-Thouless critical temperature was predicted to be driven by $R_\square$ in disordered superconducting thin films.[54–56] In Maekawa and Fukuyama's theory explaining the initial effects of disorder on the $T_c$[3] through a purely fermionic scenario implying an increase of Coulomb interactions as $R_\square$ grows larger, $\frac{\Delta T_c}{T_c}$ is a function of $R_\square$ as well. The extension of this theory by Finkelstein[57] also relates a reduction in $T_c$ to the sole $R_\square$ for a given compound. Another scenario, of a bosonic nature, predicts a change in ground state from superconducting to insulating at large disorder for a universal critical sheet resistance $R_{\square,c}$,[58] which is temperature independent within the quantum critical region. The close link between a film sheet resistance and its critical temperature has also been underlined in recent theoretical reviews.[59,60]

Numerous experiments have confirmed the correlation between $T_c$ and $R_\square$ in very different disordered systems: InOx,[61] $a$-Ga,[62] MoC,[16] and NbN[63] for example. In these experiments, the disorder was made to vary through a change in the film thickness. Even more convincing were the results grouping different compounds or different ways of tuning the disorder, which showed a strikingly similar destruction of superconductivity when $R_\square$ grew: Strongin *et al.*[9] showed the same $T_c$ reduction with $R_\square$ for Bi and Pb films; Valles *et al.*[64] did so for Pb and Sn films; Graybeal *et al.*[40,65] presented similar results for $a$-MoGe films of different compositions and thicknesses. Shahar and Ovadyahu[5] also showed evidence for a well-defined $T_c(R_\square)$ relationship for InOx films of different oxygen contents.

In the following, we will show that our results are in contradiction with these previous studies, and that the reduction of the film thickness does not affect the superconducting properties in the same way as the composition $x$ or the annealing temperature $\theta_a$ does. In other words, $R_\square$ is not, in our system, a relevant parameter to describe the superconductor-to-insulator transition.

### A. Comparison between the effects of $x$ and $\theta_a$

Annealing and the film composition both modify the disorder parameter $R_\square \propto \frac{1}{k_F l}$: the film composition influences the density of states and hence modifies $k_F$, whereas annealing changes the effective mean free path $l$ through a variation of local conductivity. It can therefore be expected that, at fixed thickness $d$, these two tuning parameters have the same influence on the destruction of superconductivity. This effect can be seen on Fig. 9(a): the depletion of $T_c$ relates one to one with the square resistance $R_\square$ as the SIT is approached either through annealing (each color symbolizing one annealing temperature) or through a composition change (each composition being represented by a different symbol).

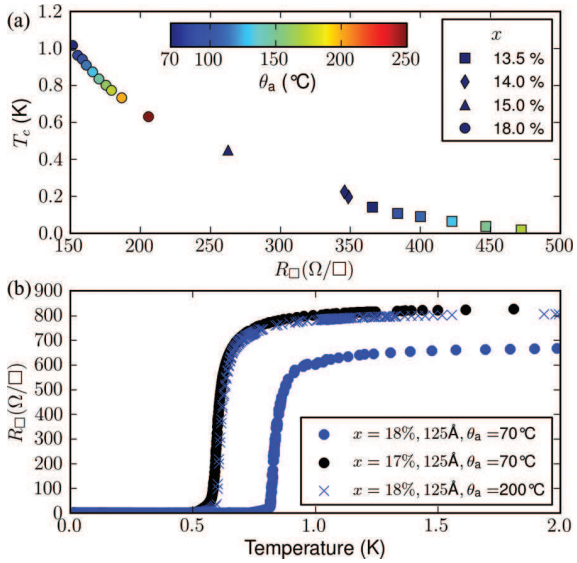



FIG. 9. (Color online) (a) $T_c$ as a function of the disorder parameter $R_\square$ for several 500-Å-thick samples. Each symbol represents one composition and each color one annealing temperature. The samples of $x = 14$ and 15% have been previously studied[21,66] and are given for comparison. (b) Annealing and a change in composition affecting the superconducting properties in the same way: starting from a 125-Å-thick $Nb_{18}Si_{82}$ sample (blue circles), the superconductivity can be weakened in the same manner ($T_c$ and $R_\square$) by annealing (blue crosses) or by a change of composition (red circles).

The fact that, at a given sample thickness, $T_c$ is entirely determined by $R_\square$ can also be seen in Fig. 9(b): starting from a 125-Å-thick $Nb_{18}Si_{82}$ sample, one can achieve the same reduction in $T_c$ *and the same* $R_\square$ with a $\theta_a = 200\,^{\circ}$C annealing *or* with a reduction of the composition to $x = 17\%$.

At fixed thickness, $R_\square$ can therefore be considered to be a relevant parameter to describe the SIT.

### B. Comparison between the effects of $d$ and $\theta_a$

The comparison between the effects of annealing with those induced by a reduction of the sample thickness is, however, more difficult: how a change in $d$ affects $R_\square$ is unclear. In a similar manner as the preceding, let us compare the effects of both parameters on $T_c$. As can be seen Fig. 10(a) , there is *no* one-to-one relationship between $T_c$ and $R_\square$: at a given composition $x$, the $T_c$ reduction induced by the annealing $|\frac{dT_c}{d\theta_a}|$ is much more important than the thickness-induced effect ($|\frac{dT_c}{dd}|$).

Again, Fig. 10(a) shows that, starting from a 125-Å- thick $Nb_{18}Si_{82}$ sample, one can achieve the same reduction in $T_c$ with a $\theta_a = 200\,^{\circ}$C annealing or a reduction of the thickness to $d = 75$ Å. However, the corresponding $R_\square$ differ by a factor of almost 2 in the two cases. In other words, the knowledge of

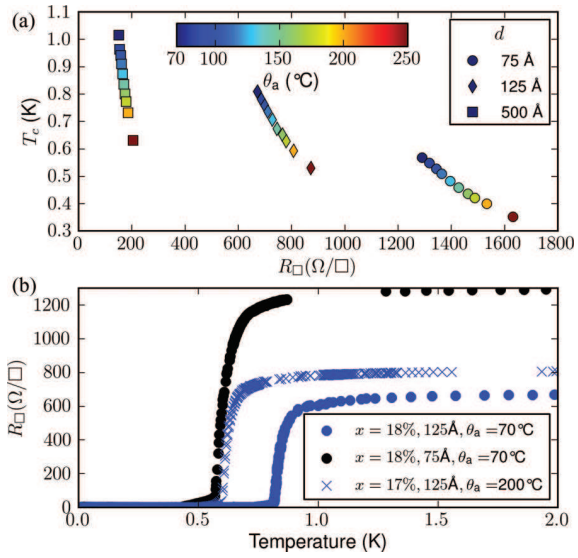



FIG. 10. (Color online) (a) $T_c$ as a function of the disorder parameter $R_\square$ for several $Nb_{18}Si_{82}$ samples. Each symbol represents one thickness and each color one annealing temperature. (b) Annealing and a change in thickness affecting the superconducting properties in different ways: starting from a 125-Å-thick $Nb_{18}Si_{82}$ sample (blue circles), $T_c$ can be weakened by annealing (blue crosses) or by a reduction of thickness (red circles). The corresponding square resistances are, however, different.

$R_\square$ is not sufficient to predict the superconducting behavior of the films when $d$ is made to vary.

### C. Quantifying disorder

The results of the two previous sections are summarized in Fig. 11. The critical temperatures for all superconducting films are plotted with respect to the corresponding $\frac{1}{R_\square}$ for both compositions ($x = 13.5$ and 18%) and for different annealing temperatures. Whereas samples of 500 Å follow the same $T_c$ suppression law, as was suggested by Ref. 5, the trend seems

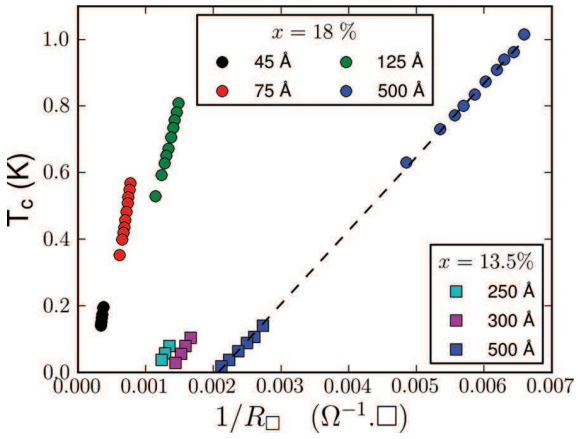



FIG. 11. (Color online) $T_c$ as a function of $R_\square$ for all films studied. Films of a given thickness follow the same trend regarding the suppression of superconductivity (the black dashed line is a guide to the eye).

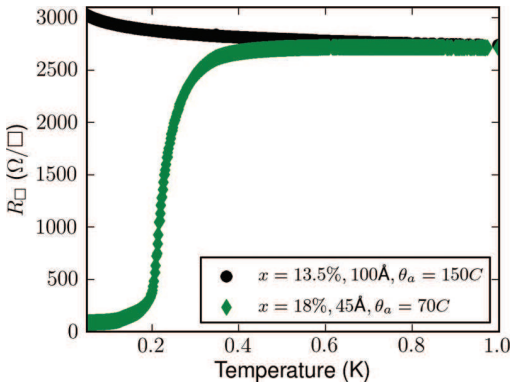



FIG. 12. (Color online) Transport properties of two films with the same $R_\square$. Despite having the same disorder parameter $\frac{1}{R_\square}$, these two films are on opposite sides of the SIT.

to be specific to each of the considered film thicknesses, and no universal behavior could be determined.

As a prominent illustration of this point, two films of the same $R_\square$ have been found to be on opposite sides of the superconductor-to-insulator transition, as shown in Fig. 12. This contradicts the theoretical predictions that $R_\square$ solely determines the ground state near the SIT.[4,10]

## VI. CONCLUSION

We have studied the disorder-tuned suppression of superconductivity in $a$-NbSi films, through the variation of thickness, composition, and annealing. We have shown that moderate annealing weakened superconductivity in these films, while the chemical composition of the films was unchanged and they remained amorphous. The suppression of superconductivity through a variation of composition or of annealing temperature could be explained, at a given thickness, through a single parameter $R_\square$. However, the effect of thickness reduction could not be satisfactorily explained this way. These arguments imply that $R_\square$ is not the relevant parameter to fully describe the disorder in the vicinity of a SIT. The transition tuned by the reduction of the sample thickness seems to play a special role, distinct from the effect of a modification of the microscopic disorder, here tuned by the annealing temperature. To the best of our knowledge, this difference remains to be understood.

Let us end with the mention that, for the different applications of superconducting films, it is particularly interesting to have an extrinsic parameter, like annealing, which could be used to fine tune their properties, mainly the normal resistance $R_{\square,n}$ and the superconducting critical temperature $T_c$, after the thin-film synthesis. We can cite the example of transition edge sensors, the operating temperature of which could thus be finely adjusted to the need of the considered experiment.[66]

## ACKNOWLEDGMENTS

We gratefully thank Odile Kaitasov and Erwan Oliviero for their assistance in the TEM and EFTEM measurements. We acknowledge the help of Cyril Bachelet for RBS measurements. We are also indebted to Marie-Odile Ruault for many fruitful discussions. This work has been partially supported

by the Agence Nationale de la Recherche (ANR) (Grants No. ANR-06-BLAN-0326 and No. ANR-2010-BLANC-0403-01) and by the Triangle de la Physique (Grant No. 2009-019T-TSI2D).

*claire.marrache@csnsm.in2p3.fr


[1] D. Belitz and T. R. Kirkpatrick, Rev. Mod. Phys. **66**, 261 (1994).
[2] Y. Imry and M. Strongin, Phys. Rev. B **24**, 6353 (1981).
[3] S. Maekawa and H. Fukuyama, J. Phys. Soc. Jpn. **51**, 1380 (1982).
[4] M. P. A. Fisher, Phys. Rev. Lett. **65**, 923 (1990).
[5] D. Shahar and Z. Ovadyahu, Phys. Rev. B **46**, 10917 (1992).
[6] B. Sacépé, T. Dubouchet, C. Chapelier, M. Sanquer, M. Ovadia, D. Shahar, M. Feigel'man, and L. Ioffe, Nature Physics **7**, 239 (2011).
[7] P. Anderson, J. Phys. Chem. Solids **11**, 26 (1959).
[8] H. Suhl and M. Maple, *Superconductivity in d- and f-Band Metals* (Academic, New York, 1980).
[9] M. Strongin, R. Thompson, O. Kammerer, and J. Crow, Phys. Rev. B **1**, 1078 (1970).
[10] M. Feigel'man, L. Ioffe, V. Kravtsov, and E. Cuevas, Ann. Phys. **325**, 1390 (2010).
[11] S. Sondhi, S. Girvin, J. Carini, and D. Shahar, Rev. Mod. Phys. **69**, 315 (1997).
[12] G. Bergmann, Phys. Rep. **4**, 159 (1976).
[13] G. Deutscher, B. Bandyopadhyay, T. Chui, P. Lindenfeld, W. L. McLean, and T. Worthington, Phys. Rev. Lett. **44**, 1150 (1980).
[14] H. M. Jaeger, D. B. Haviland, B. G. Orr, and A. M. Goldman, Phys. Rev. B **40**, 182 (1989).
[15] N. Markovic, C. Christiansen, and A. M. Goldman, Phys. Rev. Lett. **81**, 5217 (1998).
[16] S. J. Lee and J. B. Ketterson, Phys. Rev. Lett. **64**, 3078 (1990).
[17] E. Bielejec and W. Wu, Phys. Rev. Lett. **88**, 206802 (2002).
[18] N. Hadacek, M. Sanquer, and J. C. Villégier, Phys. Rev. B **69**, 024505 (2004).
[19] B. Keck and A. Schmid, J. Low Temp. Phys. **24**, 311 (1976).
[20] E. Montroll, J. Chem. Phys **18**, 183 (1950).
[21] C. A. Marrache-Kikuchi, H. Aubin, A. Pourret, K. Behnia, J. Lesueur, L. Bergé, and L. Dumoulin, Phys. Rev. B **78**, 144520 (2008).
[22] *Methods of Surface Analysis*, edited by J. Walls (Cambridge University Press, Cambridge, 1989).
[23] D. Querlioz, E. Helgren, D. Queen, F. Hellman, R. Islam, and D. Smith, Appl. Phys. Lett. **87**, 221901 (2005).
[24] M. T. Myers, S. Charnvanichborikarn, L. Shao, and S. O. Kucheyev, Phys. Rev. Lett. **109**, 095502 (2012).
[25] J. Lesueur, Ph.D. thesis, Paris XI, Orsay, 1985.
[26] J. M. Valles, R. C. Dynes, and J. P. Garno, Phys. Rev. Lett. **69**, 3567 (1992).
[27] D. B. Haviland, Y. Liu, and A. M. Goldman, Phys. Rev. Lett. **62**, 2180 (1989).
[28] S. Marnieros, L. Bergé, A. Juillard, and L. Dumoulin, Phys. Rev. Lett. **84**, 2469 (2000).
[29] F. Nava, P. Psaras, H. Takai, K. Tu, S. Valeri, and O. Bisi, J. Mater. Res. **1**, 327 (1986).
[30] L. Dumoulin, L. Bergé, J. Lesueur, H. Bernas, and M. Chapellier, J. Low Temp. Phys. **93**, 301 (1993).
[31] E. Helgren, G. Gruner, M. R. Ciofalo, D. V. Baxter, and J. P. Carini, Phys. Rev. Lett. **87**, 116602 (2001).
[32] P. Lee and T. Ramakrishnan, Rev. Mod. Phys. **57**, 287 (1985).
[33] D. Bishop, E. Spencer, and R. Dynes, Sol. St. Elec. **28**, 73 (1985).
[34] P. Hucknall, C. Walker, D. Greig, J. Matthew, D. Norman, and J. Turton, J. Phys.: Cond Mat. **4**, 1131 (1992).
[35] S. Marnieros, Ph.D. thesis, Paris XI, Orsay, 1998.
[36] A. Pourret, H. Aubin, J. Lesueur, C. Marrache-Kikuchi, L. Berge, L. Dumoulin, and K. Behnia, Nature Physics **2**, 683 (2006).
[37] A. Pourret, H. Aubin, J. Lesueur, C. A. Marrache-Kikuchi, L. Berge, L. Dumoulin, and K. Behnia, Phys. Rev. B **76**, 214504 (2007).
[38] M. Feigel'man and M. Skvortsov, Phys. Rev. Lett. **109**, 147002 (2012).
[39] K. Chopra, *Thin Film Phenomena* (McGraw-Hill, New York, 1969).
[40] J. M. Graybeal and M. R. Beasley, Phys. Rev. B **29**, 4167 (1984).
[41] J. Lesueur, L. Dumoulin, and P. Nedellec, Phys. Rev. Lett. **55**, 2355 (1985).
[42] J. Gilman, Phys. Today **28**, 46 (1975).
[43] S. Kim, D. H. Shin, D. Y. Shin, C. O. Kim, J. H. Park, S. B. Yang, S.-H. Choi, S. J. Yoo, and J.-G. Kim, J. of Nanomaterials **2012**, 572746 (2012).
[44] G. Legeay and X. Castel, Thin Solid Films **520**, 4021 (2012).
[45] S. Moon, M. Lee, and C. Grigoropoulos, J. Heat Transfer **124**, 253 (2002).
[46] E. Guillotel, L. Zeng, E. Helgren, F. Hellman, R. Islam, and D. Smith, J. Appl. Phys. **101**, 023908 (2007).
[47] T. Egami, J. Mater. Sci. **13**, 2587 (1978).
[48] T. Egami, Mat. Res. Bull. **13**, 557 (1978).
[49] D. Gupta, K. Tu, and K. Asai, Phys. Rev. Lett. **35**, 796 (1975).
[50] R. Devine, D. Mathiot, W. Warren, D. Fleetwood, and B. Aspar, Appl. Phys. Lett. **63**, 2926 (1993).
[51] R. Tromp, G. W. Rubloff, P. Balk, F. K. LeGoues, and E. J. van Loenen, Phys. Rev. Lett. **55**, 2332 (1985).
[52] M. Béal and J. Friedel, Phys. Rev. **135**, A466 (1964).
[53] E. Abrahams, P. W. Anderson, D. C. Licciardello, and T. V. Ramakrishnan, Phys. Rev. Lett. **42**, 673 (1979).
[54] M. R. Beasley, J. E. Mooij, and T. P. Orlando, Phys. Rev. Lett. **42**, 1165 (1979).
[55] B. Halperin and D. Nelson, J. Low Temp. Phys. **36**, 599 (1979).
[56] A. T. Fiory, A. F. Hebard, and W. I. Glaberson, Phys. Rev. B **28**, 5075 (1983).
[57] A. Finkelstein, Physica B **197**, 636 (1994).
[58] M. P. A. Fisher, G. Grinstein, and S. M. Girvin, Phys. Rev. Lett. **64**, 587 (1990).
[59] A. Larkin, Ann. Phys. **8**, 785 (1999).
[60] V. F. Gantmakher and V. T. Dolgopolov, Phys. Usp. **53**, 1 (2010).
[61] A. T. Fiory and A. F. Hebard, Phys. Rev. Lett. **52**, 2057 (1984).
[62] H. M. Jaeger, D. B. Haviland, A. M. Goldman, and B. G. Orr, Phys. Rev. B **34**, 4920 (1986).
[63] S. Ezaki, K. Makise, B. Shinozaki, T. Odo, T. Asano, H. Terai, T. Yamashita, S. Miki, and Z. Wang, J. Phys.: Condens. Matter **24**, 475702 (2012).
[64] J. M. Valles, R. C. Dynes, and J. P. Garno, Phys. Rev. B **40**, 6680 (1989).
[65] J. Graybeal, Physica B **135**, 113 (1985).
[66] O. Crauste, C. Marrache-Kikuchi, L. Bergé, S. Collin, Y. Dolgorouky, S. Marnieros, C. Nones, and L. Dumoulin, J. Low Temp. Phys. **163**, 60 (2011).

## 4.3 What is the meaning of "disorder" ? (cont'd)

### 4.3.1 Presentation of the paper

The following paper, presented at the LT26 conference in August 2011 by Olivier Crauste, is a preliminary report on the work that led to the previous article.

Although it also shows, more sketchily, how the effect of the thickness reduction is different from a change in composition or annealing temperature, I have included it in this manuscript for it focuses on the scaling near the SIT, following the relations mentioned in section 3.2. It shows how a scaling analysis confirms the specific role of the thickness : the critical exponent product obtained for the thickness-tuned transition ($\nu_d z_d \sim 0.4$) is different from the one obtained when the SIT is driven by the annealing temperature ($\nu_\theta z_\theta \sim 1$). The two transitions therefore belong to two different universality classes.

### 4.3.2 Paper ♯6 : Crauste et al., *J. Phys : Conf. Series*, 400, 022012, 2012

# Superconductor-Insulator Transition in Amorphous $Nb_xSi_{1-x}$ Thin Films. Comparison between Thickness, Density of State and Microscopic Disorder.

**O Crauste[1,2,⋆], F Couedo[1,2], L Bergé[1,2], C Marrache[1,2,†] and L Dumoulin[1,2]**

[1] Univ Paris-Sud, CSNSM, UMR8609, Orsay, F-91405;
[2] CNRS-IN2P3, Orsay, F-91405

E-mail: ⋆ Olivier.Crauste@csnsm.in2p3.fr

E-mail: † Claire.Marrache@csnsm.in2p3.fr

**Abstract.** We report on the study of the Disordered-induced Superconductor-Insulator Transition (D-SIT) in $Nb_xSi_{1-x}$ thin films. These films, synthesized by electron-beam co-deposition, are continuous, amorphous, homogeneously disordered and structurally stable for a wide range of compositions, thicknesses and annealing temperature and thus particularly well suited for the study of D-SIT.

We present an analysis of the D-SIT induced by three different parameters: the thickness, the Nb composition that changes the electronic density of states and the annealing temperature that changes the microscopic disorder. The annealing changes quantum interference patterns that decreases the local conductance. Our results show that the effect of the thickness on the destruction of superconductivity is very distinct from those of the composition or the annealing. We point out this material is particularly interesting to disentangle the effect of the parameters driving this quantum phase transition.

## 1. Introduction

The understanding of the interplay between disorder and the superconductivity in 2D systems is a long-standing problem [1, 2, 3, 4, 5], relying on the competition between the disorder that increases the localization and leads to an insulator and the Cooper pairing that leads to an infinite conductivity. In 2D systems, this competition is exacerbated as it is the lowest dimension for both these effects. In these systems, the disorder is evaluated through the measurement of $R_\square = \rho/d$ which is proportional to $1/k_F l$, $k_F$ the Fermi wave vector and $l$ the electronic mean free path. Since the work of Goldman [1], the thickness has been considered as a parameter for the study of the disordered-induced SIT. We here report on two other parameters allowing the tunning of disorder : the density of state and the microscopic disorder.

## 2. Experimental Setup

The $Nb_xSi_{1-x}$ thin films are synthesized by electron-beam co-deposition process in an ultra-high vacuum setup ($10^{-8}$ mbar) at room temperature. The samples thickness $d$ and composition $x$ are determined by the Nb and Si deposition rates which are finely controlled in-situ by two pairs of piezo-electric quartz during the deposition process. These parameters are controlled ex-situ by Rutherford Back-Scattering. The $Nb_xSi_{1-x}$ thin films were deposited onto a sapphire substrate initially prepared with a 250 Å SiO under-layer. After the deposition, a protective cap of 250 Å of SiO is deposited to avoid the oxidation of the $Nb_xSi_{1-x}$ thin film.

The transport measurements were carried with four-probe technique on a dilution fridge down to 7 mK.

Moreover, the samples of composition $x = 13.5\%$ and $x = 18\%$ were studied at different annealing temperature. These samples are annealed under a flowing $N_2$ atmosphere 1 hour at a temperature up to 250°C.

Microscopic measurements show the $Nb_xSi_{1-x}$ thin films are continuous, homogeneous in thickness and amorphous even down to 25 Å. This is confirmed by the absence of reentrant behavior of the transport measurement at low temperature. Transmission Electronic Microscope measurement on 25 Å thick sample show no evidence of crystallization up to 500°C where crystallites of $Nb_3Si$ appears. For the studied range of annealing temperature, the samples remains homogeneously disordered [6].

## 3. Experimental Results

With the deposition process, we can probe the Disordered-induced Superconductor-Insulator Transition (D-SIT) on $Nb_xSi_{1-x}$ thin films with the composition $x$ or the thickness $d$.

### *3.1. Disordered-induced Superconductor-Insulator Transition*

We observe a D-SIT for the composition-tuned sets (Fig. 1a) or the thickness-tuned sets of samples (Fig. 1b). With the annealing, we observe a linear decrease of the conductivity with the annealing temperature (Fig. 1d). Starting from a superconducting sample, the annealing decreases its critical temperature ($T_c$) (Fig. 1c), leading the sample towards the SIT. According to the Béal & Friedel's model[7], the annealing of a binary alloy slightly changes the position of the atoms due to the relaxation of the structural stress, this lead to a change of the electronic interference pattern and thus a decrease of the local conductance. No change on the Hall conductivity was observed on $Nb_xSi_{1-x}$ system by annealing [8], the annealing has then no effect on the material's carrier density Our interpretation of the annealing process is that it changes the local disorder of the samples, i.e. its electronic mean-free path, whereas the composition changes the electronic properties and hence $k_F$.

Fisher's model [2] describes the D-SIT as a Quantum Phase Transition. In the vicinity of the transition, the transport behavior is then described by a scaling law : $R(\delta,T)/R_c = f\left(\delta T^{-1/\nu.z}\right)$, with $\delta$ the distance to the critical point, $\nu$ the correlation length exponent, $z$ the dynamical critical exponent and $R_c$ the critical resistance. The critical point of the transition can be determined by the crossing-point on the $(R_n, d)$ plane, Fig. 2a.

First for the scaling analysis with the thickness as the parameter, we only consider superconducting films close enough of the D-SIT, i.e. where $\delta = \frac{d_\perp - d_c}{d_c} < 3$, to be described by the scaling law (Fig 2b). To successfully overlap the $R_\square(T)$ curves, we obtain a critical exponents product $\nu_d z_d = 0.43 \pm 0.03$ for the thickness-tuned SIT which is coherent with previous work at different composition [9]. The thickness-tuned SIT is then coherent with the disordered-induced SIT description of Fisher's model.

Then we consider the annealing-tuned transition. No superconducting sample undergo the SIT, we thus determine the critical point by extrapolating the linear behavior of the annealing temperature where $T_c$ is canceled. The $\nu_\theta z_\theta$ critical exponent product obtained for the best overlap (Fig. 2c) is very close to 1.0. Considering their experimental uncertainty, these product are incompatible and outlines the thickness-induced and the annealing-induced transitions do not belong to the same universality class.

Published under licence by IOP Publishing Ltd

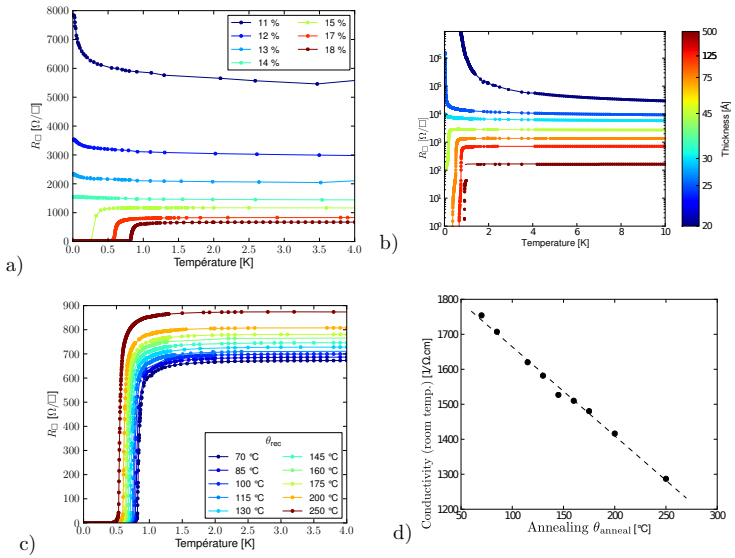



**Figure 1.** The $Nb_xSi_{1-x}$ undergo a Superconductor-Insulator Transition either by tuning the composition $x$ (a), the thickness $d_\perp$ (b) or the annealing temperature $\theta_{\text{anneal}}$ (c). (d) The normal state conductivity decreases linearly with the annealing temperature.

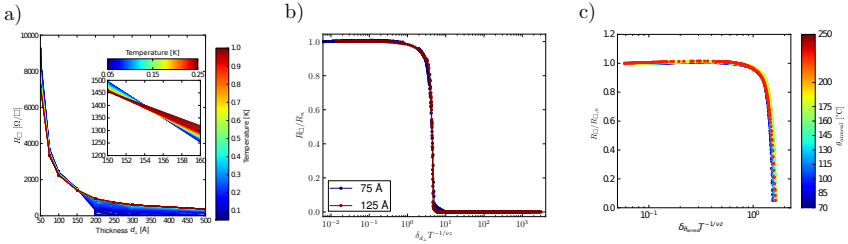



**Figure 2.** a) The crossing point in the $(R_\square, d_\perp)$ plan defines the critical point of the transition (zoom of the crossing point in insert), $x = 13.5\%$. b) The best overlap for renormalized $R_\square/Rn$ vs $\delta T^{-1/\nu z}$ is obtained for $\nu z = 0.43 \pm 0.03$, $x = 18\%, \theta_{\text{anneal}} = 70°\text{C}$. c) Scaling with the annealing temperature as the tunning parameter. The best overlap is obtained with $\nu_\theta z_\theta = 1.0 \pm 0.1$, here $x = 18\%$, $d = 75\mathring{A}, \theta_c = 520C$.





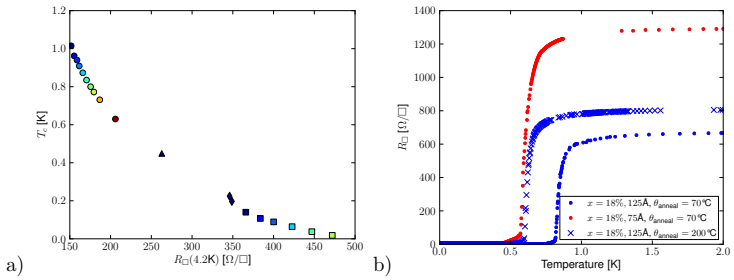



**Figure 3.** a) We obtain a bi-univocal relation between $T_c$ and $R_\square$ (here for $d = 500$Å) either by changing the composition, plot with different shape, and the annealing temperature plot with different color. b) Starting from one reference sample, we cannot obtain the same $T_c$ reduction and the same $R_\square$ increase either by changing the thickness (blue to red circles) or the annealing temperature (blue circles to crosses). The thickness has a specific effect compared to composition and annealing.

### *3.2. Comparison between parameters*

One main advantage of the $Nb_xSi_{1-x}$ is that we can compare the effect of each of the parameters. We first compare the evolution of the superconducting temperature transition $T_c$ with $R_\square$ gathering the different composition and annealing temperature for a given thickness (Fig 3a). All the data align on the same curve, for each thicknesses. This is coherent with our interpretation of the effect of these parameters. As the composition changes the electronic properties ($k_F$) and the annealing affects the local disorder ($l$), they both affect the same disorder parameter $k_F l$: they have a joint role on the disorder parameter.

However, this analysis cannot be reproduced with the thickness $d$ and the annealing temperature $\theta_{\text{anneal}}$. Starting from a reference sample (blue circle), we cannot obtain the same $T_c$ reduction with the same $R_n$ increase either by changing $\theta_{\text{anneal}}$ (from blue circle to blue cross) or by the thickness (blue circle to red circle).

## 4. Conclusion

The structural stability of the $Nb_xSi_{1-x}$ material over a wide range of composition, thickness and annealing brings us the ability to tune the samples towards the D-SIT with these three parameters. This allow us to disentangle the effect of these parameters on the disorder. Our results outline the specific role of the thickness compared to the composition and the annealing temperature on the disorder parameter.

## References

[1] Haviland D B, Liu Y and Goldman A M 1989 *Phys. Rev. Lett.* **62** 2180
[2] Fisher M P A 1990 *Phys. Rev. Lett.* **65** 923–926
[3] Anderson P W 1959 *Journal of Physics and Chemistry of Solids* **11** 26–30
[4] Maekawa S and Fukuyama H 1981 *J. Phys. Soc. Japan* **51** 1380–1385
[5] Feigel'man M V, Ioffe L B and Mézard M 2010 Superconductor-Insulator transition and energy localization (*Preprint* 1006.5767)
[6] Crauste O 2010 Ph.D. thesis Univ Paris-Sud
[7] Béal M T and Friedel J 1964 *Phys. Rev.* **135** –466
[8] Nava F, Psaras P A, Takai H and Tu K N 1986 *Journal Material Research* **1** 327
[9] Marrache-Kikuchi C A, Aubin H, Pourret A, Behnia K, Lesueur J, Bergé L and Dumoulin L 2008 *Phys. Rev. B* **78** 144520

# Chapter 5

# Application to particle detectors

In this chapter, I will describe the work we have undertaken in relation with different applications in astroparticle detection, and more specifically for detectors operating in the sub-millimeter domain.

Indeed, some very promising sub-millimeter detectors currently use superconducting films as thermometers. Understanding the response of such systems to an incoming wave is of crucial importance in order to achieve a highest sensitivity and meet the future challenging detection goals. This domain has therefore common interest with ongoing research on superconducting thin films, although for different purposes. This is one of the many reasons for the close links between fundamental solid state physics research and Research and Development for astroparticle detection in our group.

I will first put our activity in the sub-millimeter detection domain into perspective and outline the main challenges faced by the detector community in this field, before presenting our contributions.

## 5.1 Background on the CSNSM *Cryogenic Detectors Group*

The *Cryogenic Detectors Group* is part of the *Solid State Physics Group* of the CSNSM. The group has been created in the early 1990's by Louis Dumoulin, based on the observation that particle detectors had reached sensitivities such that they had to deal with solid-state physics issues in order to make any significant progress. The founding of the group aimed at gathering solid state physicists who would both study specific materials for their solid-state properties, and use them to create innovative detectors for astrophysics and astroparticle physics experiments that require ultimate performances.

The group's activity in detectors R&D currently revolves around three main components [1] :

1. **Direct Dark Matter search**

   In order to reconcile astrophysical observations (rotation curves of galaxies, gravitational lensing observations, cosmic microwave background measurements, ...) with current astrophysics theories, one must postulate the existence of a new category of particles, very different from the so-called baryonic particles that form our day-to-day environment : Dark Matter. There are several proposals for the nature and properties of these very elusive particles, one of which consists of WIMP (Weakly Interacting Massive Particles) [2].

   The EDELWEISS experiment (*Expérience pour DÉtecter Les Wimps En SIte Souterrain* [3]) aims at the direct detection of these WIMPs through their interaction with a large mass of cryogenic ionization-heat bolometers. The signals induced by WIMPs are predicted to be of very weak energy (tens of keV) and very rare (less than one interaction per kg of detector per year). However, should a WIMP interact with the detector, it should deposit its energy (leading to a rise in temperature of a few nK to a few $\mu$K) and create an electron-hole pair within the bolometer. The deposited energy is then converted into heat and measured by a thermometer, whereas the electron and the hole drift in different directions through the application of an electric field. The charges are subsequently measured by a charge amplifier via dedicated electrodes (see figure 5.1). This double measurement enables the efficient discrimination (better than 99,98%) between signals due to WIMPs and those due to the residual radioactivity.

   The *Cryogenic Detectors Group* at CSNSM is responsible for the detectors R&D for the EDELWEISS experiment and has developed, amongst other things, an extensive study on the charge drift and scattering

1. These three axis have all been identified as priorities both for French and European Astroparticle Physics communities. See for example the scientific priorities as set up by the IN2P3 (Institut National de Physique Nucléaire et de Physique des Particules : `http://www.in2p3.fr/presentation/politique/questions_majeures_en.htm` or the ASPERA roadmap for Astroparticle Physics European funding : `http://www.aspera-eu.org/images/stories/files/Roadmap.pdf`.
2. For a review, see for example [Sadoulet, 1999]
3. Experiment for WIMPs detection in an underground site.

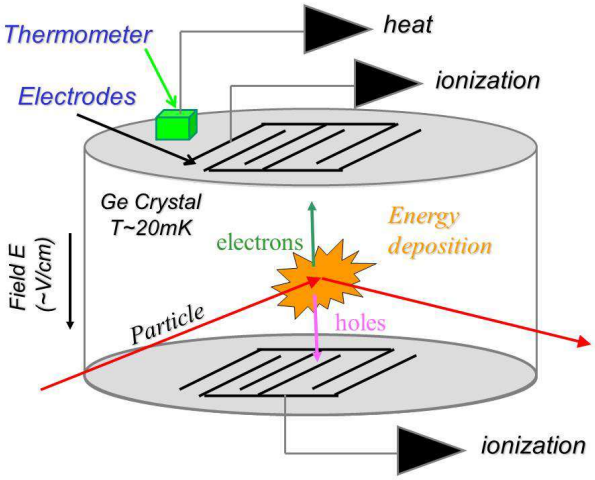



Figure 5.1: Schematic diagram of an ionization-heat bolometer.

in high purity germanium (of which is made the bolometer's absorber) [4]. The group is also currently interested in developing dedicated amplification electronics based on mesoscopic circuits [5].

2. **Double beta decay experiments**

   Recent advances in particle physics have shown that the so-called *Standard Model*, through which most of particle physics results have so far been explained, is incomplete. Indeed, this model cannot account for the Neutrino Flavor Oscillations observed for the first time by the Super-Kamiokande experiment in 1998. A generic neutrino can be represented as the superposition of three distinct neutrino flavor states (electronic, muonic and tauonic). The probability to measure one flavor state has been shown to vary in time, which implies that the neutrino has a mass, in contradiction with the *Standard Model*. The measurement of the absolute mass of the different neutrino states is an important particle physics issue and represents a strong motivation for particle physics experiments that explore beyond the *Standard Model* [6].

   If the neutrino is a Majorana particle, i.e. if it is its own antiparticle, a measurement of its absolute mass scale is possible, for example through a neutrinoless double beta decay experiment. In this hypothetic reaction that can only, and very rarely, occur in certain nuclides such as $^{130}$Te or $^{100}$Mo, one neutron, after absorbing a virtual neutrino produced by the beta decay of another neutron, converts into a proton and another beta electron. If the nuclides under discussion are contained in as scintillating single crystal cooled down to very low temperature, the heat and light releases due to this process can then be measured by extremely sensitive detectors. The challenge consists in measuring these rare events via the reduction of the background, due, in our case, to alpha particles. The double readout used here indeed allows to tag and reject alpha events.

   Our group has recently developed heat/light bolometers in order to achieve this discrimination. We are testing the use of superconducting thermometers, instead of resistive NTDs [7], to increase the resolution and the speed of both the heat and light detection, thus taking advantage of the tunability of the NbSi superconducting thin films, as will be explained in the following sections.

3. **Measurement of the Cosmic Microwave Background (CMB)**

   The first observation of the temperature anisotropies of the CMB by the COBE satellite in the 1990s has launched a entire new field in astronomy and cosmology : the use of far-infrared, sub-millimeter and millimeter waves to study the history of the Universe. The majority of the photon energy in the Universe lies within the Cosmic Optical, Infrared and Microwave radiation bands (COB, CIB and CMB). The brightness of the corresponding radiations are shown in Figure 5.2. Each radiation band constitutes a picture of the Universe at a particular stage of its development : the CMB (its inhomogeneity and polarization notably) gives information on the very early stage of the Universe, when the decoupling between matter and photons occurred ; CIB provides insight on the early galaxies formation by accretion ; and the COB records the total light emission from galaxies mainly due to stellar nucleosynthesis. In the last two decades, many experiments, whether ground-, balloon- or satellite-borne [8], have been launched

4. See for example [Olivieri et al., 2012].
5. See Hélène le Sueur's ANR projet COCA for example.
6. For a review, see for example [Gatti, 2009]
7. Neutron Transmutation Doped germanium resistors.
8. One can cite the WMAP, Planck, Archeops, Boomerang, ... experiments for instance.

in order to measure the Cosmic Background in these wavelengths [9].

Low temperature detectors have proved to be particularly interesting for this application, since they combine a large spectral bandwidth within this frequency range, and a sensitivity potentially only limited by the photon noise. In all cases, light collection efficiency is a primary concern and optimization of the focal plane coverage a goal in itself.

The *Cryogenic Detectors Group* has initiated numerous instrumental developments in this field, notably to propose large bolometer arrays adapted to the specifications of the different astrophysics projects.

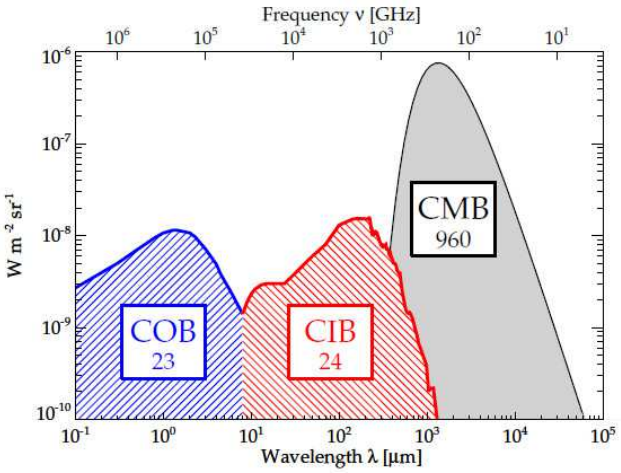



Figure 5.2: Schematic spectral energy distributions of the most important backgrounds in the Universe : Cosmic Optical, Infrared, and Microwave Background radiations. Taken from [Dole et al., 2006].

In the following sections, I will detail the work we have undertaken regarding detectors for the CMB measurements.

## 5.2 Challenges in CMB and sub-millimeter astroparticle detection

### 5.2.1 Scientific challenges

The Cosmic Microwave Background has been theoretically predicted as a major consequence of the Big Bang by George Gamow in 1948 and experimentally (and accidentally) measured by Penzias and Wilson in 1964. In 1993, the satellite COBE [10] measured some fluctuations in the CMB intensity. These anisotropies have subsequently been confirmed by WMAP [11] and, more recently, by the Planck satellite.

As previously stated, a careful analysis of the Cosmic Microwave Background and of the sub-millimeter radiation is crucial for a better understanding of the early stages of our Universe. They will enable to address critical cosmological and astrophysical issues, such as :

- The age of the Universe
- The value of cosmological constants (such as the Hubble constant)
- Study the formation of galaxies (in particular through the measurement of the polarization of the CMB)
- Study interstellar medium
- The ratio of dark versus baryonic matter

The community is now preparing new experiments, focusing on the measurement of the B-mode polarization, due to primordial gravitational waves created by the inflation as early as $10^{-35}$ s after the Big Bang [12].

### 5.2.2 Instrumental challenges

#### Interest of low temperature detectors

As can be seen Figure 5.2, the brightness of the CMB, CIB and COB radiations are very low and extend over a very large spectrum. Cryogenic detectors provide a natural choice for these measurements, for three main reasons :

- They are broadband : they are competitive in the range 90 GHz $\sim$ 5 THz (or 60 $\mu$m $\sim$ 3 mm).

9. For a review, see for example [Golwala, 2009]
10. COsmic Background Explorer
11. Wilkinson Microwave Anisotropy Probe
12. For more details : `http://www.sciops.esa.int/SA/PLANCK/docs/Bluebook-ESA-SCI(2005)1_V2.pdf` and [Coll., 2013]

– In this range, cryogenic detectors are extremely efficient. Since the mid-1990s, most bolometric detectors even have a noise level below the fundamental photon background noise.
– They are compatible with array structures, which allow high read-out speed while still maintaining a large radiation collecting area [Moseley, 2009]. This is particularly important : the detectors having performances close to being set by the background noise, any significant improvement will come from a more rapid collection time.

The current trend in CMB and sub-millimeter radiation measurements is therefore to develop large arrays of detectors, similar to CCDs in the optical domain, in order to collect more light and fill efficiently the entire telescope focal plane.

### General structure of a low temperature bolometer

A standard low temperature detector is made out of three elements, shown Figure 5.3:
– An **absorber** with which the incoming radiation or particle interacts and where the energy exchange takes place.
– An **thermal link** through which the absorber is connected to the cold bath. The energy absorbed by the absorber eventually relaxes through this thermal conductance $G$ into the cold bath.
– A **thermometer** to monitor the absorber temperature and retrieve the information on the deposited energy.

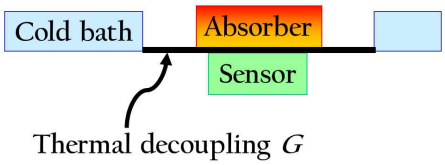



Figure 5.3: Schematic representation of a low temperature bolometer.

### Performance indicators

As often, the design of cryogenic detectors results from a compromise between several antagonistic performance indicators, each of which is subject to optimization [Golwala, 2009] :

1. The **Noise Equivalent Power** (NEP) is an indicator of the *individual* detector sensitivity. For low temperature bolometers, working at a temperature $T$, the NEP is limited by the thermal conductance $G$:

$$NEP_G = \sqrt{4k_B T^2 G} \tag{5.1}$$

This is due to the fluctuations in energy exchanges between the absorber and the cold bath. The corresponding temperature fluctuations cannot be distinguished from variations in radiation power. The evolution of bolometer NEP in time is given Figure 5.4.

2. For astrophysical measurements, the NEP is fundamentally limited by the **photon background power**, also called Background Limited Infrared Photometer (**BLIP**), due to the discrete nature of photons that arrive on the detector.

$$NEP_{BLIP} = \sqrt{2h\nu Q + \frac{Q^2}{\Delta\nu}} \tag{5.2}$$

where the bolometer receives a radiation load $Q$ in a spectral bandwidth $\Delta\nu$, centered about a frequency $\nu$.

This NEP depends on the frequency and on the bandwidth, and therefore the BLIP limit varies, depending on the application. For terrestrial observations in the sub-millimeter and far-infrared range, the BLIP limit is of the order of $10^{-17}$ W/$\sqrt{\text{Hz}}$. This limit is 10 times lower for space-borne imaging. For space spectroscopy the BLIP limit can be as low as a few $10^{-21}$ W/$\sqrt{\text{Hz}}$.

3. The **response time** of the detector - of total heat capacity $C$ - is given by :

$$\tau = \frac{C}{G} \tag{5.3}$$

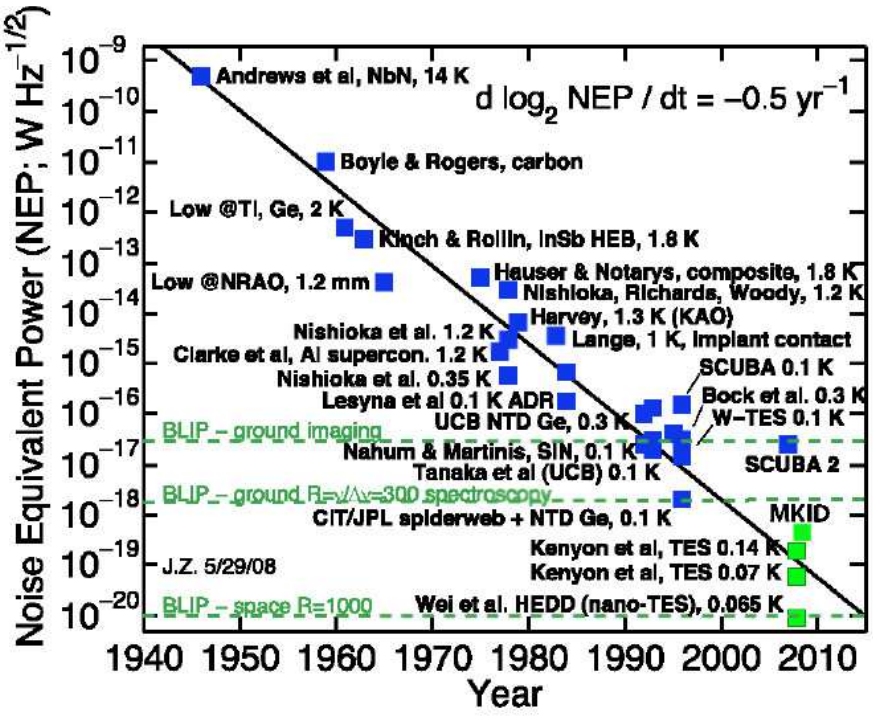



Figure 5.4: Bolometer NEP as a function of time. The photon noise (BLIP) for different applications are also shown. Taken from [Golwala, 2009].

4. The **bolometer sensitivity** is partly determined by the ratio between the temperature increase $\partial T$ due to a change in the photon flux and $\partial P$ :

$$S = \frac{\partial T}{\partial P} = \frac{1}{G_{thermo}} \tag{5.4}$$

where $G_{thermo}$ is the thermal conductance of the thermometer. The conversion of the obtained temperature increase into a measurable electrical signal is also of importance but depends on the read-out of the thermometer.

These performance indicators show the advantage of working at low temperature : since the NEP and the heat capacity of any given material decrease with temperature, a low working temperature improves the response time as well as the bolometer signal to noise ratio.

**What solutions ?**

The challenge is therefore to optimize $NEP_G$ through the reduction of the thermal conductivity $G$, while keeping the detector's response time $\tau$ within reason. One can achieve this by reducing the heat capacity of the absorber and the detector $C$. Moreover, the ideal detector should be suitable for large array fabrication. Solutions proposed by the detection community include:

1. **Reduce $G$ by using spiderwebs -** In order to decrease the thermal conductivity linking the absorber to the cold bath, the absorber is deposited onto a membrane suspended by fine support legs. An example of such a detector is shown Figure 5.5. The draw-back of such structures is the very delicate clean room process that is required to fabricate them.
2. **Reduce $C$ by using membranes -** Membranes are also useful since they reduce the detector total heat capacity $C$ that intervenes in the response time.
3. **Use Transition Edge Sensors (TES) to increase the thermometer sensitivity -** Voltage-biased TES are currently widely used. They are placed at a working temperature at the middle of their superconducting transition, and thus have a very good sensitivity. These sensors tend to replace doped semiconductors and NTD germanium thermometers, thanks to the predictability of their performances [Sadoulet, 2009] and the fact that they can easily be lithographied and hence are suitable for array fabrication. However, this promising technology suffers from three main drawbacks. The first resides in the excess noise observed in several of these sensors. This feature, represented in Figure 5.6, increases with the TES sensitivity and is still unexplained. The second drawback is their low impedance and the need to

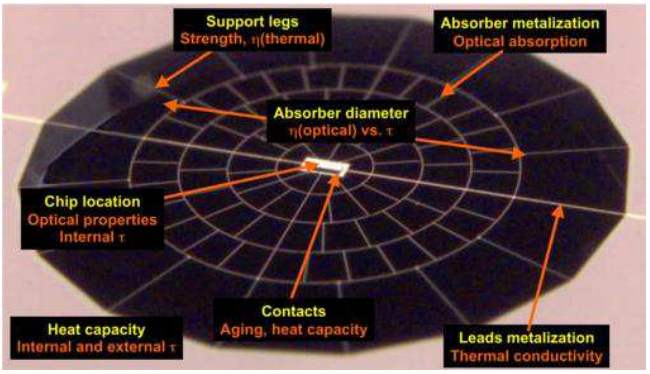



Figure 5.5: Example of a sub-millimeter wave detector used by Planck satellite. Taken from `http://hfi.planck.fr/article227.html`.

implement a SQUID read-out for each detector [13]. Thirdly, the tunability of the TES critical temperature to suit the different possible applications is still an issue : either TES are made out of single elements, such as W or Ti, and have therefore a operating temperature dictated by the $T_c$ of these materials ; or they use bilayers in order to have more flexibility in the choice of $T_c$, which comes at the price of reproducibility and ease of fabrication.

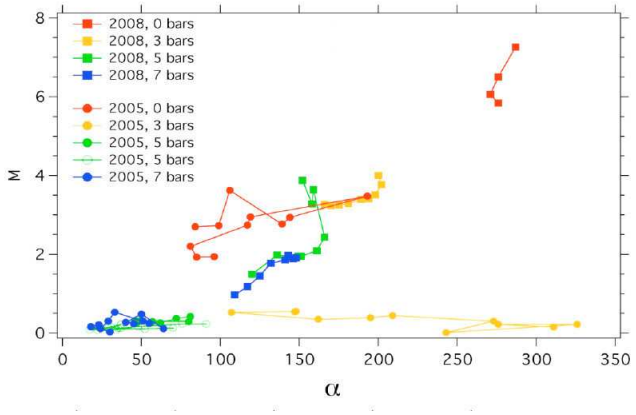



Figure 5.6: Excess noise parameterized by $M$ as a function of $\alpha = \frac{\partial log(R)}{\partial log(T)}$ for different TES geometries. $M$ is such that the voltage noise is $S_v = 4k_BTR\left(1 + 2\frac{\partial log(R)}{\partial log(I)}\right)\left(1 + M^2\right)$, with $R$ the resistance, $T$ the operating temperature and $I$ the current. Taken from [Jethava et al., 2009].

## 5.3 A proposal for a new kind of solid-state sub-millimeter particle detector

### 5.3.1 Presentation of the proposal

The following paper, presented at the LT25 conference in August 2008, is a proposal, based on an original idea by Louis Dumoulin and Stefanos Marnieros, for a new kind of bolometer structure that takes advantage of solid-state physics properties to address the following issues :

1. **Reduce the thermal decoupling $G$ -** In the proposed device, the thermal decoupling $G$ is replaced by the electron-phonon decoupling. This would facilitate the detector fabrication which would no longer need to sit on a fine membrane. The typical electron-phonon decoupling that can thus be achieved in NbSi films depends on the temperature ($G_{e-ph} \propto T^4$) and is typically of $G_{e-ph} = 50$ pW.K$^{-1}$ at 100 mK, very much in line with the best thermal decoupling that is currently achieved through delicate mechanical structures ($G_{e-ph} = 50 - 100$ pW.K$^{-1}$ [Golwala, 2009]). This idea can be adapted both for high-impedance thermometers and TES. The schematic representation of Figure 5.3 is then replaced by the one given Figure 5.7.

13. SQUID multiplexing is still quite difficult to implement for very large bolometer arrays.

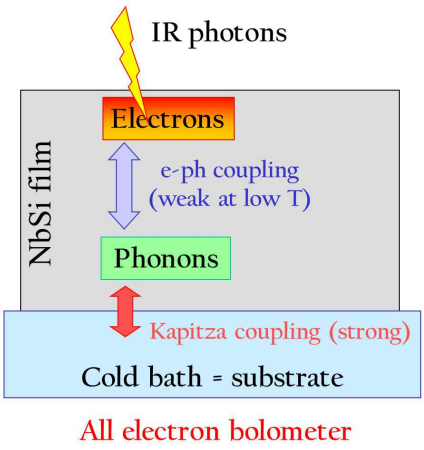



Figure 5.7: Schematic representation of an "All Electron Bolometer".

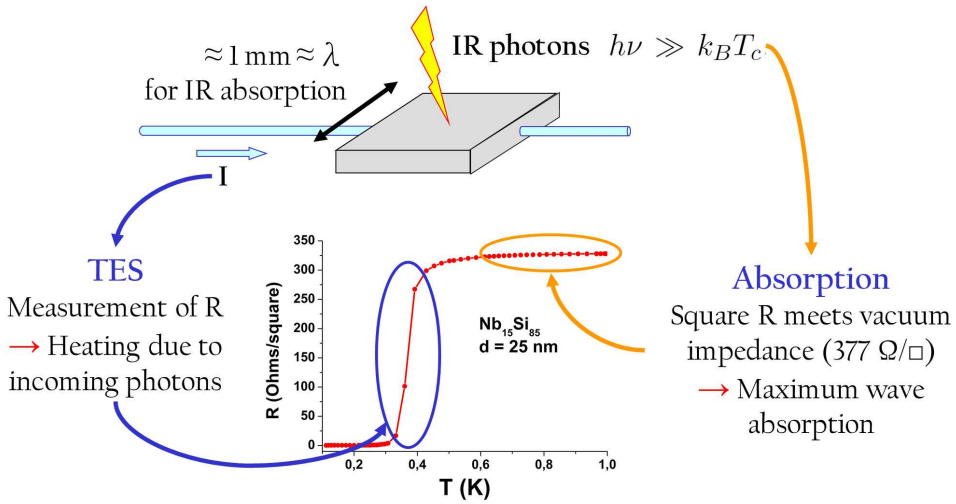



Figure 5.8: Working principle of an "All Electron Bolometer" in the case of a superconducting a-NbSi thin film. The same could be applied for an insulating a-NbSi film.

2. **Facilitate the detector fabrication -** For this, we propose to combine the three functions of a bolometer ("absorber", "thermometer" and "thermal decoupling") into a single film. The incoming wave is therefore directly absorbed into the electron bath of the thermometric material, here NbSi thin films. This is based on studies on NbSi thin films near the Metal-to-Insulator Transition in the 100-1000 GHz region [Lee et al., 2000], showing that the conductivity of the films only depends on the ratio $\frac{h\nu}{k_B T}$. In other words, sub-millimeter photons, due to their energy $h\nu$, are sensitive to the high-temperature impedance of the film where $k_B T_{equiv} = h\nu$. This high-temperature impedance can therefore be designed to match the vacuum impedance (377 Ω per square) for optimum wave absorption. On the other hand, the thermometer function of the device is governed by the electronic temperature of the material, which corresponds to the cold bath temperature. Then the photons release their energy into the electronic bath, the corresponding temperature increase is therefore measured very precisely. The working principle of the proposed device is shown Figure 5.8 and can be adapted to both high-impedance or superconducting materials.

### 5.3.2 Paper ♯7 : Marnieros et al., *J. Phys. Conf. Series*, 150, 012027, 2009

# All electron bolometer for radiation detection

**S. Marnieros[1], L. Dumoulin[2], A. Benoit[2], L. Berge[1], P. Camus[2], S. Collin[1], A. Juillard[1] and C.A. Marrache-Kikuchi[1]**

1 CSNSM, CNRS-IN2P3, Paris 11 University, Orsay, France
2 CRTBT, CNRS, Grenoble, France

E-mail: Stefanos.Marnieros@csnsm.in2p3.fr

**Abstract.** In order to measure the Cosmological Microwave Background (CMB), high performance "bolometric cameras" similar to CCDs are currently developed. They are made out of thousands of pixels, each of which is a bolometer on its own. In order to meet the requirements for future CMB experiments - notably the measurement of the CMB B-mode polarization - the sensitivity of each pixel should be improved by one or two orders of magnitude compared to what now exists. Taking advantage of the solid-state properties of amorphous $Nb_xSi_{1-x}$ thin films, we here present a proposal for a new bolometer structure that would increase the pixels' sensitivity, its response time and allow a simplification of the fabrication process. In this resistive detector (that can be either high impedance or TES) the three functions of a classical bolometer (wave absorption, temperature measurement and thermal decoupling) are achieved in a single $Nb_xSi_{1-x}$ film. The frequency properties of this material allow the merger of the two first functions. The natural thermal decoupling between electrons and phonons at low temperature then makes it possible to use this single object as bolometer. This new type of detector solely uses the electronic properties of the $Nb_xSi_{1-x}$ thin films and is free of any phononic mediation of the energy.

## 1. Scientific context

The measurement of the Cosmological Microwave Background (CMB) is now reaching the sensitivity limit of single bolometer-type detectors. Numerous observations related to the millimetric domain are limited by the photon noise and further improvement of the detectors imply optimizing the focal plane filling factor by the use of large bolometric matrices. Among all CMB measurements that the scientific community has not yet been able to perform, the CMB B-mode polarization is probably the most constraining from the instrumental point of view. The signature of primordial gravitational waves which give a B-type polarization, is one of the utmost goals in today's cosmology and amongst the first objectives in the field.

The current European Spatial Agency Planck satellite program, which will perform measurements of the CMB temperature with a resolution down to 5 arc minutes, already has 52 detectors in the telescope's focal plane. However, for future programs which will focus on the detection of the CMB B-mode polarization, the sensitivity of the angular power spectrum measurement will have to be improved by at least two orders of magnitude. The noise equivalent power sensitivity (NEP) will have to be kept down to about $10^{-18}$ W/$\sqrt{Hz}$ , and the number of detectors in the telescope's focal plane will have to be drastically increased up to many thousands. A number of solutions are currently being developed by the different collaborations to achieve fabrication of high performance "bolometric cameras" similar to CCDs. This implies

© 2009 IOP Publishing Ltd


25th International Conference on Low Temperature Physics (LT25) IOP Publishing
Journal of Physics: Conference Series **150** (2009) 012027 doi:10.1088/1742-6596/150/1/012027

fabricating matrixes with thousands of pixels, each pixel having performances at the level of the experimental photon noise. The structure of a single pixel must therefore be compatible with a highly-reliable collective fabrication and multiplexed readout electronics.

## 2. Principle of operation of an all electron bolometer

The base structure of a single pixel for submillimetric measurements is composed of three important elements : a radiation absorber, a thermometer and a thermally isolated holder enabling a very weak coupling of the former two with respect to the cold bath. The different existing detectors differ in the nature of the absorber (horns, absorbing films, antennas), the nature of the thermometer (high impedance-type, or superconducting Transition Edge Sensors) and in the answer given to the thermal decoupling problem (diversely manufactured membranes, micromesh membranes). The latter is an extremely critical point : the sensitivity of a bolometer to an incident power $P$ is limited by its Noise Equivalent Power : $NEP^2 = 4k_BT^2G$ and therefore directly depends on the thermal decoupling $G$ between the absorber and the thermometer on the one hand and the cold bath on the other. Moreover, in order to experimentally realize this thermal decoupling, very delicate clean room processes is required. In the Planck experiment, for example, the bolometer is placed at the center of a spider web-shaped membrane which decouples the bolometer from the cold bath. Its extremely weak thermal coupling of $10^{-11}$ W.K$^{-1}$ is perfectly matched to the value of the Planck CMB background power of the order of pW but the fabrication of such structures is difficult and many groups worldwide are currently making huge efforts to obtain high performance membranes for bolometer matrixes. All currently investigated devices have in common to use phonons as vectors for energy transport between the different parts.

We here present a proposal for an innovative device which replaces these delicate membrane-based structures and eliminates the mediation of phonons : the incoming energy will be directly captured and measured in the electron bath of an appropriate sensor and the thermal decoupling will be achieved via the natural decoupling that exists between electrons and phonons of the sensor at very low temperature. This has been studied in detail for amorphous $Nb_xSi_{1-x}$ thin films [1] [2] giving: $G_{eph} = \partial P/\partial T = KT^4$ and $K = 500$ W.K$^{-4}$.cm$^{-3}$ (figure 1.a.). It follows that $G_{eph} = 5.10^{-11}$ W.K$^{-1}$ at 100 mK for a 100 nm thick 100 $\mu$m x 100 $\mu$m thermometer. Because $G_{eph}$ varies proportionally to $T^4$, the performances of such a detector are directly linked to the possibility of working at very low temperature, a constraint which is anyhow unavoidable in order to improve the performances of existing detectors. The use of temperatures below 100 mK (Planck's nominal temperature) will be necessary in order to maintain the sensor's thermodynamical noise - called "phonon noise" - below the "photon noise" due to the measured light sources when the latter becomes very weak. The limitation in the operation temperature is then set by the desired response time : the intrinsic relaxation time of NbSi thin films is of the order of 10 ms at 30 mK and varies proportionally to $T^{-4}$ (figure 1.b.).

In order to use the natural electron-phonon decoupling as the bolometric thermal decoupling, it is crucial to absorb the wave directly into the electron bath of the thermometric material used. Recent studies [3] on a-$Nb_xSi_{1-x}$ thin films, known to undergo a superconductor-metal-insulator transition when the niobium concentration or the thickness is varied, allow us to propose different answers to this question. We consider detectors where the absorption is achieved by the thermometer alone or by the thermometer electrically coupled to antennas. For either case, our proposal can adapt to high-impedance (R>100 kΩ) or SQUID-based readouts (R<1 Ω).

## 3. A single superconducting thin film for the absorber and the thermometer

A first possible device consists in a single superconducting thin film which both absorbs the wave and measures the temperature. In order to be suitable for matrix fabrication, the absorber

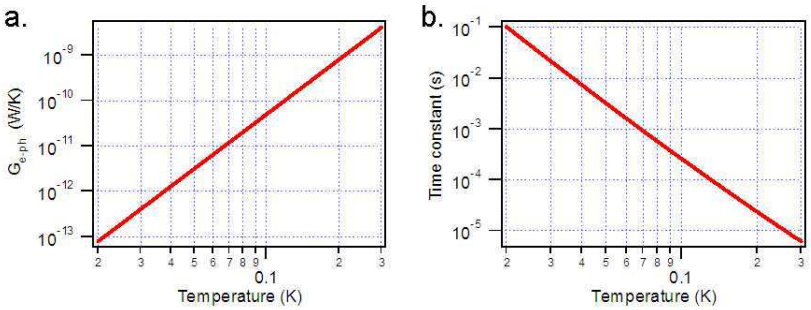



**Figure 1.** a. Electron-phonon thermal coupling constant $G_{eph}$ for a 100 nm thick, 100 $\mu$m x 100$\mu$m NbSi thermometer ($G_{eph}$ is proportional to the film volume). b. Intrinsic response time of a NbSi insulator thin film. In our case the time constant is independent of the size of the film.

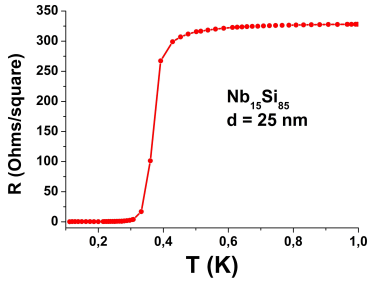



**Figure 2.** Square resistance versus temperature of a 25 nm $Nb_{15}Si_{85}$ thin film.

must have a size of the order of the wavelength ($\simeq$ 1 mm) and meet the vacuum impedance (377 $\Omega$ per square) so that the wave absorption is optimum. In the case of a superconducting absorber, the detected incoming photons will see the normal resistance since they have energies larger than the superconducting gap : $h\nu \gg k_B T_c$. We have previously shown [2] [3] that a-$Nb_xSi_{1-x}$ is a compound where the superconducting temperature $T_c$ and the normal resistance can be separately tuned through the composition of the alloy $x$ and the film thickness $d$. Figure 2 shows the superconducting transition of a a-$Nb_xSi_{1-x}$ 25nm thin film which normal resistance is optimum for the absorption and could be used as a TES at the temperature of $^3$He (300mK). However, the composition and thickness of the alloy could also be adapted in order to fabricate a TES working around 50 mK, which is the optimum temperature for a performant thermal decoupling and a not-too-long response time.

This device could, in principle, be combined to an optimal readout system. Keeping a constant normal impedance with respect to the incoming electromagnetic wave, the TES transition resistance could both be adapted to a SQUID-based readout - via interdigited electrodes - or to classic transistor readout - via a meander shape of the film.



25th International Conference on Low Temperature Physics (LT25) IOP Publishing
Journal of Physics: Conference Series **150** (2009) 012027 doi:10.1088/1742-6596/150/1/012027

## 4. Antennas and TES

A second possible device consists of an antenna coupled to a superconducting film. Antennas are made out of superconducting films having a specially designed geometry in order to absorb the incident radiation with high selectivity with respect to the energy spectrum and polarization. In standard existing devices, the absorbed power is routed via superconducting strips towards a resistive load where dissipation occurs. The thermometer and the resistive load are designed to be very close although they stay (in principle) electrically decoupled. Thus, the energy transfer is phonon-mediated. Some attempts have already been made [4] to transfer the absorbed energy from antennas directly to the electrons in a TES. However high-frequency impedance matching of antennas to conventional TES is difficult because of their low normal state impedance. The properties of a-$Nb_xSi_{1-x}$ thin films enable such a fine tuning since its normal impedance is rather high (a 100 nm thick TES film has a normal square resistance of typically 150 $\Omega$ per square). In addition to the intrinsic advantages of using antennas - high selectivity, good filling coefficient - they would in our case enable to reduce the size of the thermometric thin film and thus decrease the value of the equivalent thermal leak $G_{eph}$ which is proportional to the volume of the film.

## 5. Absorbers and thermometers are Anderson insulators

Last, the absorber and the thermometer could be made out of an Anderson insulator. Indeed, low temperature fundamental studies on Anderson insulators and most particularly on a-$Nb_xSi_{1-x}$ [5] at concentrations where it is insulating (x<9%) show that the real part of the impedance at a high frequency $h\nu$ is essentially the same as the low frequency impedance at a temperature $T$ given by $k_B T = h\nu$. This means that at 150 GHz, the value of the film resistivity is equal to the one measured with DC bias at a temperature of 10 K. This is independent of the DC film resistance at the working temperature which can be of a few M$\Omega$ at 50 mK and hence perfectly suitable for a JFET type electronic readout.

## 6. Conclusion

Many groups throughout the world (including the French DCMB collaboration) work on the realization of matrixes under the very classical scheme of absorber-thermometer-decoupling device. The present project which proposes to gather all three functions in one material presents a original way to improve and simplify the detectors so that, in particular, to meet the challenge of the B-mode CMB polarisation measurement.

## Acknowledgments

This research has been partially funded by ANR-06-BLAN-0326.

## References

[1] Marnieros S, Berge L, Juillard A and Dumoulin L 2000 *Phys. Rev. Lett.* **84** 2469
[2] Marnieros S 1998 *PhD thesis*
[3] Marrache-Kikuchi CA, Berge L, Collin S, Dobrea C, Dumoulin L, Juillard A, Marnieros S 2006 NIMA **559** 579
[4] Ali S et al. 2004 *NIMA* **520** 490
[5] Lee H L, Carini D, Baxter V, Henderson W and Gruner G 2000 *Science* **287** 633

## 5.4 Thermometry for particle and light detectors : superconducting NbSi

### 5.4.1 Presentation of the paper

As seen in section 5.2, the thermometer is a crucial component of a bolometer and much efforts have been devoted to find an ideal material for temperature measurements that would present the following characteristics:
- Important sensitivity
- Low heat capacity
- Tunable operating temperature
- Adaptability to JFET electronics
- Low noise level
- Reproducibility and ease in fabrication

Our group had already shown [Dumoulin et al., 1993, Dumoulin et al., 1996] that NbSi films were particularly well suited for resistive thermometry. Taking advantage of the Anderson Metal-to-Insulator Transition at low enough niobium content, one could have an important sensitivity using the exponential variation of the resistance with the temperature. Moreover, the operating temperature could be tuned through the niobium content.

In a subsequent paper [Marrache-Kikuchi et al., 2006], we had shown that the reduction of the film thickness lowered the heat capacity without damaging the electron-phonon coupling or the noise characteristics.

The following paper proposes a characterization of *superconducting* NbSi thin films from the point of view of thermometry. It addresses the following issues :

1. **Tunability -** As we have shown earlier, the superconducting properties of NbSi thin films can be tuned through a change of composition, thickness or annealing.

   For CMB measurements, in order to maximize the incoming wave absorption, it is important that the sheet resistance of the absorber be close to the vacuum impedance ($Z_0 = 377\ \Omega$ per square).

   We show that the sheet resistance and the critical temperature (i.e. the operating temperature) could be *separately* tuned through an adjustment of the composition and thickness of the film. These superconducting films could therefore be used for CMB measurements, in all-electron bolometers (see section 5.3), but also for a variety of different applications requiring different operating temperatures (due to diverse constraints).
2. **Adaptability to different electronics -** We also show that NbSi thermometers allow different options for the signal read-out. By varying the length-to-width ratio (through inter-leaved or meander-shaped electrodes), the same film can be made high impedance for JFET-based electronics, or low impedance of a read-out via SQUIDS (see examples in Figure 5.9).

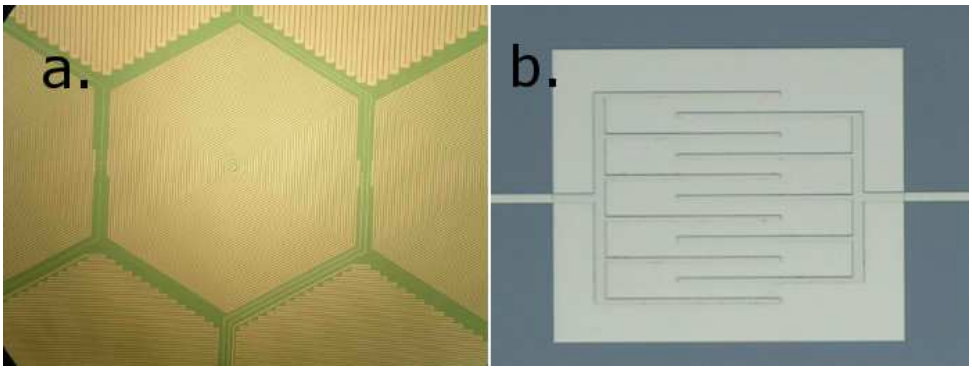



Figure 5.9: a. High-impedance meander-shaped NbSi film. b. Inter-leaved electrodes for low-impedance films.

### 5.4.2 Paper ♯8 : Crauste et al., *J. Low Temp. Phys.*, 163, 60, 2011

J Low Temp Phys (2011) 163: 60–66
DOI 10.1007/s10909-010-0284-2

# Tunable Superconducting Properties of a-NbSi Thin Films and Application to Detection in Astrophysics

**Olivier Crauste · Claire A. Marrache-Kikuchi · Laurent Bergé · Sophie Collin · Youri Dolgorouky · Stefanos Marnieros · Claudia Nones · Louis Dumoulin**

Received: 7 June 2010 / Accepted: 7 November 2010 / Published online: 12 November 2010
© Springer Science+Business Media, LLC 2010

**Abstract** We report on the superconducting properties of amorphous $Nb_xSi_{1-x}$ thin films. The normal-state resistance and critical temperatures can be separately adjusted to suit the desired application. Notably, the relatively low electron–phonon coupling of these films makes them good candidates for an "all electron bolometer" for Cosmological Microwave Background radiation detection. Moreover, this device can be made to suit both high and low impedance readouts.

**Keywords** Transition-edge sensors · Electron–phonon coupling · Superconductivity · Bolometer

## 1 Introduction

One of the long-standing challenges of cosmology is the comprehension of the forming of the Universe. In this field, the study of the Cosmological Microwave Background (CMB) is a precious source of information. However, the measurement of this primordial radiation is now reaching the sensitivity limit of single pixel bolometer-type detectors. Numerous observations related to the millimetric domain are indeed limited by the photon noise and further improvement of the detectors therefore implies optimizing the focal plane filling factor by the use of large bolometric matrices. Amongst all CMB measurements that the scientific community has yet to perform, the CMB B-mode polarization is probably the most constraining from the instrumental point of view. Detecting the signature of primordial gravitational waves yielding a B-type polarization is one of the utmost goals in today's cosmology and amongst the first objectives in the field.

In order to meet this scientific challenge, the current trend followed by different collaborations is to develop a "bolometric camera" similar to CCDs. Each pixel of this camera will consist in a single detector which sensitivity—measured through its noise equivalent power sensitivity (NEP)—will be at the level of the experimental photon noise : about $10^{-17}$ W/$\sqrt{\text{Hz}}$ for terrestrial use and ten times lower for space-based use. By filling the telescope focal plane with thousands of such pixels, the instrument overall performance will thus be considerably increased.

The base structure of a single pixel for submillimetric measurements requires three components: a radiation absorber, a thermometer and a thermally isolated holder enabling a very weak coupling of the former two with respect to the cold bath. The problem of the thermal decoupling is extremely critical since the sensitivity of a bolometer to an incident power $P$ is limited by its NEP: $\text{NEP}^2 = 4k_BT^2G$ and therefore directly depends on the thermal decoupling $G$ between the absorber and the thermometer on the one hand and the cold bath on the other. To date, all devices designed for this application are based on using phonons as vectors for energy transport between the different parts of the bolometer. This implies that the thermal decoupling is achieved through very thin mechanical structures involving delicate clean room processes that are difficult to implement on macroscopic lengths such as those needed for this particular application.

We have recently proposed an innovative solution to this problem [1] where these caveats are lifted: in the envisioned "all electron bolometer", the incoming energy will be directly captured and measured in the sensor electron bath and the thermal decoupling will be ensured via electron–phonon decoupling at low temperature. The idea of using electron–phonon decoupling has been introduced earlier [2], but in our imagined device, the absorption will also take place within the superconducting film, so that complicated antenna designs are no longer needed. One possible device consists in a single superconducting thin film combining the absorber and the thermometer functions. The incoming photons having energies larger than the superconducting gap ($h\nu \gg k_BT_c$) [3], they will see the film normal resistance and the electromagnetic wave will be absorbed by the electrons. The radiation-induced electronic temperature increase will be measured by the resistivity variation of the superconducting film, similarly to a Transition-Edge-Sensor [4]. The superconducting film then has to meet four requirements: (1) In order to be suitable for matrix fabrication, it must have a size of the order of the wavelength ($\simeq$1 mm); (2) For the wave absorption to be optimum, the film must meet the vacuum impedance (i.e. a sheet resistance of 377 Ω per square); (3) It must have a competitive electron–phonon decoupling in order to ensure a small enough NEP; (4) Its response time must be suitable for experimental observation (typically, a few ms is acceptable). The first condition is easily met thanks to standard evaporation or lithography techniques. In the present paper, we will focus on the three other pre-requisites.

This work has been partially supported by the ANR (grant No. ANR-06-BLAN-0326), by the Triangle de la Physique (grant No. 2009-019T-TSI2D) and by a Marie Curie Intra European Fellowship within the 7th European Community Framework Programme FP7/2007-2013 (Proposal No. 236122).

O. Crauste · C.A. Marrache-Kikuchi (✉) · L. Bergé · S. Collin · Y. Dolgorouky · S. Marnieros · C. Nones · L. Dumoulin
Univ Paris-Sud, CSNSM, UMR 8609, Orsay, 91405, France
e-mail: claire.marrache@csnsm.in2p3.fr

O. Crauste · C.A. Marrache-Kikuchi · L. Bergé · S. Collin · Y. Dolgorouky · S. Marnieros · C. Nones · L. Dumoulin
CNRS, Orsay, 91405, France

The present work centers on superconducting amorphous $Nb_xSi_{1-x}$ thin films that have already shown interesting properties as thermometric thin films [5, 6]. By carefully adjusting the films composition $x$ and thickness $d$, we show that the superconducting properties, namely the normal sheet resistance $R_n$ and the critical temperature $T_c$ can be independently adjusted to build a detector suitable for submillimetric measurements.

## 2 Experimental Procedure

The amorphous NbSi thin films have been synthesized under ultrahigh vacuum ($10^{-8}$ to $10^{-7}$ mbar) by electron beam (e-beam) co-deposition of Nb and Si onto sapphire substrates coated with a 50-nm-thick SiO underlayer. Each evaporation was controlled in situ by a dedicated set of piezoelectric quartz in order to precisely monitor the composition and the thickness of the deposition. Its homogeneity throughout the film volume was also carefully checked. The in situ measurements were then systematically and successfully compared to ex situ Rutherford Back Scattering (RBS) measurements. The compositions ranged from 14% to 18% and thicknesses $d$ ranging from 45 Å to 1000 Å. The films size was of a few $mm^2$ and the samples have all been annealed at 70°C.

The electrical characteristics of the films have been measured down to below 10 mK using a dilution refrigerator. Resistance measurements were performed using a standard ac lock-in detection technique and all electrical leads were filtered from radio frequency at room temperature.

## 3 Results

The results for the studied superconducting thin films are summarized in Table 1. The superconducting critical temperature strongly depends on the niobium composition: for the studied samples, it has been varied from 34 mK (for the 105 Å thick $Nb_{14}Si_{86}$ sample) to 840 mK (for the 125 Å thick $Nb_{18}Si_{82}$ sample). "Thick" films ($d > 75$ Å) have a constant resistivity, and hence a normal sheet resistance $R_n$ inversely proportional to the thickness. Thinner films have a resistivity larger than the bulk value due to prominent 2D effects. As can be seen from Fig. 1.a, $T_c$ and $R_n$ can thus be separately tuned and adapted to the desired application. Regarding sub-millimetric measurements, the 500 Å thick $Nb_{14}Si_{86}$ sample is an optimal candidate for wave absorption, while the 175 Å thick $Nb_{14}Si_{86}$ sample has a $T_c$ suitable for an operating temperature of 100 mK (the working temperature for the Planck satellite experiment [8]) (Fig. 1.b).

Furthermore, it must be noted that the characteristics are here given for films annealed at 70°C. A heat treatment at higher temperature renders the sample more insulating: the critical temperature is lowered and the normal resistance enhanced. The annealing can therefore be used to fine-tune the desired $T_c$ and film resistance (see for example [9]). It has been shown elsewhere [10] that, for a 500 Å-thick $Nb_{13.5}Si_{86.5}$ sample, the resistivity and the superconducting critical temperature can be linearly





**Table 1** Superconducting properties of the $Nb_xSi_{1-x}$ samples: composition $x$, thickness $d$, normal sheet resistance $R_n$ (at 4.2 K) and critical temperature $T_c$

| $x$ (%) | $d$ (Å) | $R_n$ (Ω) | $T_c$ (mK) |
|---|---|---|---|
| 14 | 105 | 1896 | 34 |
| 14 | 150 | 1128 | 73 |
| 14 | 175 | 1065 | 92 |
| 14 | 500 | 349 | 236 |
| 15 | 75 | 2256 | 200 |
| 15 | 100 | 1476 | 250 |
| 15 | 250 | 630 | 335 |
| 15 | 500 | 287 | 470 |
| 15 | 1000 | 152 | 525 |
| 17 | 75 | 1615 | 375 |
| 17 | 125 | 831 | 600 |
| 18 | 45 | 2637 | 225 |
| 18 | 75 | 1291 | 604 |
| 18 | 125 | 673 | 840 |

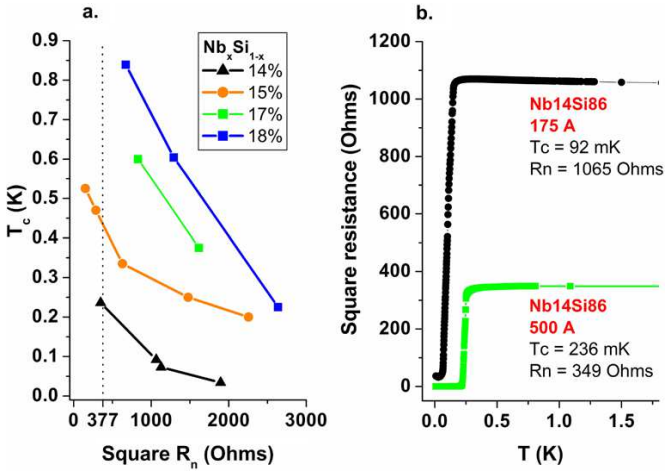



**Fig. 1** (Color online) **a**. Superconducting critical temperature as a function of the normal sheet resistance for different compositions. The two parameters can thus be independently tuned. The lines are guides to the eye. **b**. Resistance characteristics of the 175 Å and 500 Å thick $Nb_{14}Si_{86}$ samples

tuned by the annealing temperature. When the annealing temperature is varied from 70°C to 250°C, the resistivity increases by 17% while the $T_c$ drops by 61%. It is therefore conceivable that the annealing be used at the end of the detector fabrication process to fine-tune the adaptation to the operating temperature, without much affecting the normal resistance.

**Table 2** Thermal properties of the 175 Å thick $Nb_{14}Si_{86}$ sample: electron–phonon coupling constant $g_{e-ph}$, thermal conductivity $G_{e-ph}$, estimated electron–phonon response time $\tau_{e-ph}$ and NEP

| T (mK) | $g_{e-ph}$ ($W K^{-5} cm^{-3}$) | $G_{e-ph}$ ($W K^{-1}$) | $\tau_{e-ph}$ (ms) | NEP ($W\sqrt{Hz}$) |
|---|---|---|---|---|
| 50 | 26.8 | $10^{-9}$ | 0.97 | $2.3\times10^{-17}$ |
| 100 | 41.8 | $9.8\times10^{-11}$ | 8.4 | $3.7\times10^{-18}$ |

In order to test the competitiveness of these films as detectors, electron–phonon coupling measurements have been performed using $I$–$V$ characteristics, following the procedure described in [7]. Note that the films were current-biased, so that no phase separation (such as reported in [11]) was observed. For the considered samples, the electron–phonon coupling weakly depends on the niobium concentration or the film thickness. As is usual for disordered materials, the relation between the applied power $P$ on a film of volume $\Omega$ and the electron and phonon temperatures is given by [7]:

$$\frac{P}{\Omega} = g_{e-ph}\left(T_e^5 - T_{ph}^5\right) \tag{1}$$

with $g_{e-ph}$ the electron–phonon coupling constant. The thermal conductivity is then given by $G_{e-ph} = \frac{\partial P}{\partial T_e}V$ where $V$ is the thin film volume. The response time $\tau_{e-ph} = \frac{C_e}{G_{e-ph}}$ then has been evaluated considering the relevant temperature dependance of the specific heat $C_e$ [7]. Typical results are given in Table 2 for the 175 Å thick $Nb_{14}Si_{86}$ film at 50 and 100 mK. At 100 mK, this film is still close to mid-transition and has both a NEP suitable for terrestrial telescope applications and a sufficiently short response time. The NEP can be improved down to a few $10^{-18}$ $W/\sqrt{Hz}$ by lowering the operating temperature to 50 mK, however at the cost of a slightly longer—but still acceptable—response time. These films thus have performances comparable to currently used state-of-the-art bolometers and present the advantage of a relatively simple fabrication process. They indeed can be synthesized on a regular substrate and do not require the use of membranes. This considerably simplifies the fabrication of bolometer matrices with a large number of pixels.

## 4 Future Prospects

Regarding possible applications for radiation detection, the tunable superconducting properties of amorphous $Nb_xSi_{1-x}$ thin films allow the tuning of the operating temperature while maintaining an optimal incoming wave absorption. Moreover, the low electron–phonon coupling in these films enable us to take advantage from the electron–phonon decoupling to build an efficient bolometer with state-of-the-art NEP and which does not require elaborate fabrication process. Another concern for these bolometer matrices fabrication is the adaptation of the pixel to the readout electronics. Indeed, if thousands of pixels are to be implemented, the readout multiplexing is an important technological issue. Currently, the TES are mainly measured by a





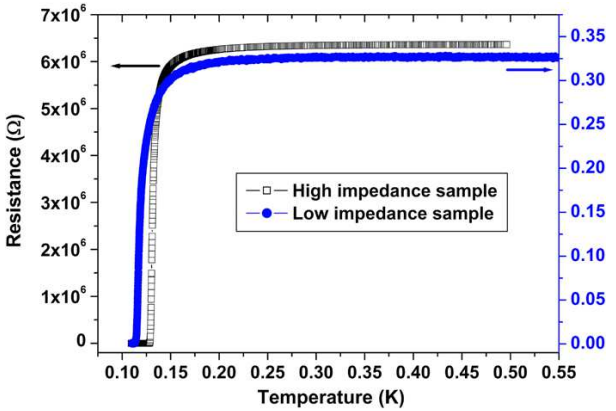



**Fig. 2** (Color online) Resistance as a function of temperature for superconducting films which design has been adapted for either JFET or SQUID readout

SQUID-based electronics. However a JFET-based electronics could be an interesting alternative.

An notable feature of the a-$Nb_xSi_{1-x}$ films concerns their adaptability to both considered electronic readouts. Indeed, the important parameter for radiation absorption is the sheet resistance. However, the films can be designed to yield a high resistance sample (typically a few MΩ) suitable for JFET readout through a large Length/Width ratio. On the contrary, a small value of such a ratio will give a low resistance (typically less than 1 Ω) sample that could be probed by a SQUID readout. We have fabricated two such geometries (Fig. 2), based on 50 nm-thick a-$Nb_{14}Si_{86}$ films which superconducting temperatures have been tuned around 100 mK by a specific annealing at 120°C.

The flexibility of these a-$Nb_xSi_{1-x}$ superconducting films and the versatility of the readout systems that could be used make them particularly interesting for applications in detection that could extend beyond CMB measurements.

## References

1. S. Marnieros, L. Dumoulin, A. Benoit, L. Berge, P. Camus, S. Collin, A. Juillard, C.A. Marrache-Kikuchi, All electron bolometer for radiation detection. J. Phys. Conf. Ser. **150**, 012027 (2009)
2. Y.P. Gousev, G.N. Gol'tsman, B.S. Karasik, E.M. Gershenzon, A.D. Semenov, H.S. Barowski, R.S. Nebosis, K.F. Renk, Quasioptical superconducting hot electron bolometer for submillimeter wave. Int. J. Infrared Millim. Waves **17**, 317 (1996)
3. H.L. Lee, D. Carini, V. Baxter, W. Henderson, G. Gruner, Quantum-critical conductivity scaling for a metal-insulator transition. Science **287**, 663 (2000)
4. K.D. Irwin, G.C. Hilton, in *Cryogenic Particle Detection*, ed. by C. Enss (Springer, Heidelberg, 2005), pp. 63–150
5. L. Dumoulin, L. Berge, J. Lesueur et al., NbSi thin films as thermometers for low temperature bolometers. J. Low Temp. Phys. **93**, 301 (1993)
6. G. Hertel, D.J. Bisthop, E.G. Spencer, J.M. Rowell, R.C. Dynes, Tunneling and transport measurements at the metal-insulator transition of amorphous Nb:Si. Phys. Rev. Lett. **50**, 743 (1983)

7. S. Marnieros, L. Berge, A. Juillard, L. Dumoulin, Dynamical properties near the metal-insulator transition: evidence for electron-assisted variable range hopping. Phys. Rev. Lett. **84**, 2469 (2000)
8. G. Morgante, D. Pearson, F. Melot, P. Stassi, L. Terenzi, P. Wilson, B. Hernandez, L. Wade, A. Gregorio, M. Bersanelli, C. Butler, N. Mandolesi, Cryogenic characterization of the Planck sorption cooler system flight model. J. Inst. **4**, T12016 (2009)
9. D. Querlioz, E. Helgren, D.R. Queen, F. Hellman, Beneficial effects of annealing on amorphous Nb-Si thin-film thermometers. Appl. Phys. Lett. **87**, 221901 (2005)
10. O. Crauste, Étude des transitions de phase quantiques supraconducteur-isolant, métal-isolant dans des matériaux amorphes désordonnés proches de la dimension 2, Ph.D. dissertation, Université Paris-Sud XI (2010)
11. B. Cabrera, Design considerations for TES and QET sensors. Nucl. Instr. Meth. Phys. Res. A **444**, 304 (2000)

# Chapter 6

# Experimental development : a cryogen free dilution refrigerator

I would like to end this manuscript by a few pages on a recent experimental development that we have undertaken in the group. Building new equipments and setting up a new experiment are too rarely spoken of nor taken into account in the assessment of a experimentalist's activity. However, I strongly feel it is one of the cores of our work and that it helps build up a group's experimental strength.

Putting together a cryogen-free dilution refrigerator from scratch was one of the projects I enjoyed most in the last few years, through the interactions with my partner in this entreprise, Emiliano Olivieri ; with the mastermind behind this new cryostat design, Patrick Pari ; with his group of the *Service de Cryogénie* [1], Philippe Forget and Matthieu de Combarieu ; with Philippe Bonnet from Integrelec and Cryoconcept ; with all engineers and staff at Cryoconcept : Julien Paris, Olivier Guia, Christian Laurent and Pascale Peron [2] ; and thanks to discussions and wise advice from Maurice Chapellier and Louis Dumoulin.

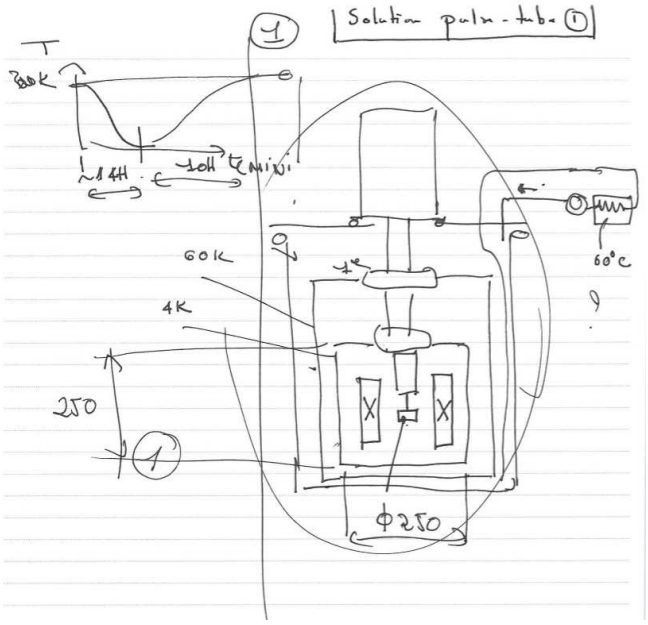



Figure 6.1: First sketch of a magnet-bearing cryogen-free dilution unit by Patrick Pari (2008).

The ***He free*** project has much evolved since its genesis in 2008. From the start, it was conceived as a collaboration between Patrick Pari's group and the CSNSM. The aim was to develop a cryogen-free dilution refrigerator with a 7 T magnet and a cooling power larger than 100 $\mu$W at 100 mK. The design was initially meant to be very simple, as can be seen from the very first sketches drawn by Patrick Pari (figure 6.1). Although Patrick Pari's group and Cryoconcept were already building a prototype dilution unit that used a Pulse Tube Refrigerator, this project would be one of the first to cool down a relatively large superconducting magnet.

Rapidly, however, it became clear to us that the cooling time of the cryostat would be an issue due to the magnet weight (18 kg in our case). The project would therefore be greatly improved if the cooling time could

1. SPEC, IRAMIS, CEA
2. `http://www.cryoconcept.com/`

be optimized. This became a second goal in this project.

After finding partial funding for the so-called ***He free*** project, we were able to launch it in mid-2009[3]. Once the cryostat structure and the magnet configuration were defined, the first tests at 4 K were performed in summer 2011. The dilution unit was subsequently mounted and tested. The cryostat was operating in early 2012.

In the following, I will describe the main characteristics of this cryostat, its performances, what I feel the advantages of using such a system are, and the few drawbacks that we have identified and that we are currently trying to remedy.

## 6.1 Characteristics

### 6.1.1 Pulse tube-based pre-cooling

The main characteristic of the ***He free*** project is the use of a Pulse Tube Refrigerator (PTR). PTRs - or Pulse Tubes (PTs) - are based on a thermo-acoustic refrigeration process where $^4$He gas is cooled down by undergoing a Stirling cycle. PTs are usually composed of two stages : one working at $\sim$ 60 K and the second at $\sim$ 3 K. This newly expanding technique for cryogenics offers numerous advantages :

1. First of all, PTRs are particularly convenient since they allow cooling down to 4K without any cryogenic liquids. More specifically no liquid $^4$He bath is needed.
2. The absence of $^4$He bath allows for a single vacuum which both suppresses the need for a indium-sealed Internal Vacuum Chamber and allows for a very large experimental space. We are currently working with a 10 mK plate of 300 mm in diameter, which is very rare in the case of liquid helium-based systems.
3. Since the vector of the cold in the PT is the $^4$He gas itself, there is no mechanical part moving on the low temperature side of the device, hence a greater reliability. Moreover, this technology is particularly well suited for pre-cooling dilution units since, a priori, the vibrations induced by the moving mechanical parts could be reduced to a minimum. In our case, we have chosen have the rotary van distributing the $^4$He in the PT remote. Since the major part of the PT-induced vibrations comes from this element, this solution is known to reduce the vibration level on the cryostat. In practice, we will see that the situation is more complex.
4. In order to weaken the residual vibrations which are induced by the movement of the $^4$He gas inside the PT even more, Patrick Pari has developed a radiator-based technique which allows the heat exchange without, in principle, any mechanical contact between the PT and the cryostat. The heat exchange is mediated by the $^3$He-$^4$He mixture. The space between the PT and the cryostat plates then serves as the dilution unit pumping line. A schematic representation is given figure 6.2 (right).

### 6.1.2 Double still technique

Alain Benoit, of Institut Néel, has developed a variation on the standard dilution unit that allows for a quicker cool down, based on the use of a second still. This technique is particularly useful for cryogen-free systems where there is no exchange gas to thermalize the dilution unit during the cool down to 4 K : the $^3$He-$^4$He mixture is injected through the pumping line (used in "reverse" mode), without passing through the injection impedance, into the mixing chamber. The mixture is then pumped through the second still. The schematic representation of this rapid cool down technique is given figure 6.2 (left)[Pari, 1990]. When cooling down from 300 K to 4 K, the entire dilution unit then is roughly at the same temperature. Hence a quicker cool down time. At about 4 K, this "rapid" mode is reversed and the $^3$He-$^4$He mixture is brought in through the injection line, into a Joule-Thomson stage [Pari, 1987], and pumped through the pumping line, as usual in a dilution unit. The second still has to be pumped during normal dilution cycles in order to prevent any additional heat load due to the Rolin film.

### 6.1.3 Superconducting magnet in parallel to the dilution unit

As soon as we started to define the cryostat, together with Patrick Pari's group and Cryoconcept, the idea of installing a magnet parallel to the dilution unit, and not in its alignment, soon arose. The main advantage was to simplify the thermalization of the magnet itself, since it could then be directly screwed on the 4K plate (and not hanging on a copper rod of length $L$, which would slow down the cooling time proportionally to $L^2$). Additionally, it allowed to shorten the 4 K and 1 K copper thermal shields and hence to decrease the cooling time of the cryostat.

3. This project was partially financed by RTRA Triangle de la Physique (grant 2009-019T-TSI2D), ANR (grant ANR-2010-BLANC-0403-01).

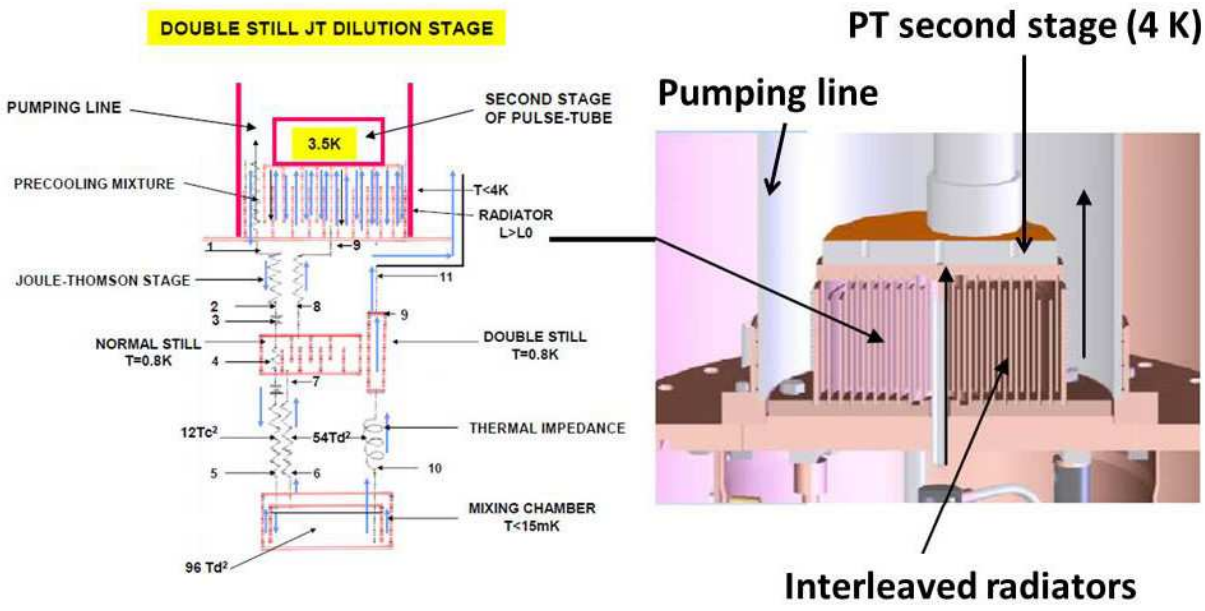



Figure 6.2: Left : Schematic representation of a double still Joule-Thomson dilution stage. The blue arrows indicate the flow of the $^3$He-$^4$He mixture during the pre-cooling (down to 4K) sequence. Right : Schematic representation of the heat exchange between the second stage of the PT and the 4 K plate of the cryostat. Both by Patrick Pari and Matthieu de Combarieu.

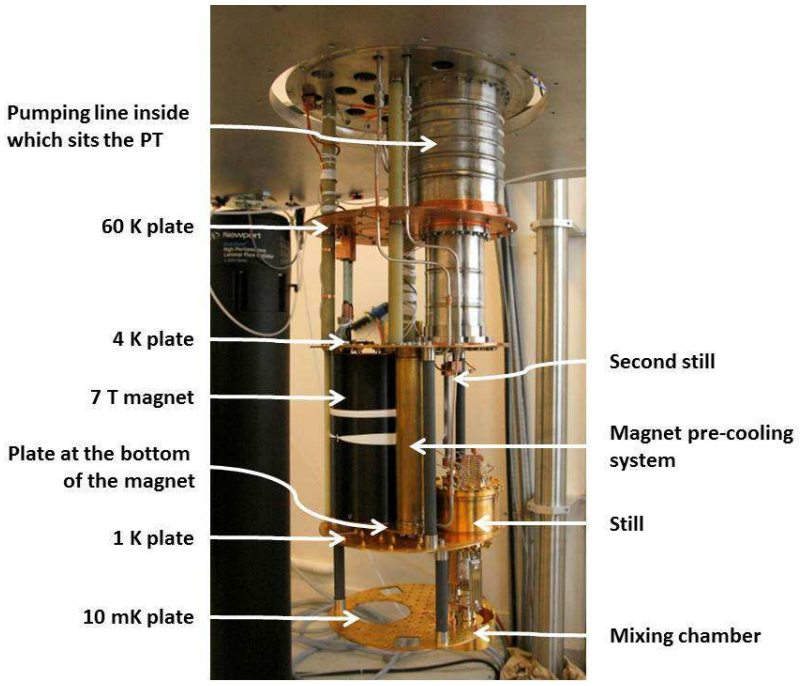



Figure 6.3: Main elements of the ***He free*** *cryostat*. Picture by Anne-Sophie Pari.

As can be seen from the picture figure 6.3, in this configuration, a sample sitting in the center of the magnet is normally cooled down by a cold finger coming *up* from the 10 mK plate which sits below. In the future, it will be possible to place a sample inside the magnet via a *clear shot* insert for which a direct line of sight has been planned.

### 6.1.4 Magnet pre-cooling system

Having a cryogen-free superconducting magnet raises one concern : how long will the magnet take to cool down to 4 K and will it significantly hinder the cooling time of the cryostat and hence its competitiveness compared to a system using liquid helium ? In this instance, our 7 T superconducting magnet weighs 18 kg

which is more than the whole dilution unit and the corresponding plates put together. We have therefore decided to install a pre-cooling system in order to facilitate the magnet cool down. As shown figure 6.3, it consists in a copper heat exchanger thermally linking the 4 K plate and the bottom of the magnet. It has two functions :

1. When not in usage, the copper tube provides a thermal link between both sides of the magnet, helping to reduce the thermal gradient along the magnet.
2. In a standard cryogen-free cryostat, the magnet is only cooled down by the PT. With our pre-cooling system, developed by Patrick Pari and his lab, in usage, we can inject liquid nitrogen at the bottom of the heat exchanger, at a typical pressure of 1 bar. It cools down the magnet, but also thermally drags the 4 K plate, so that this technique speeds up the entire dilution unit cooling down time, as we will see. Of course, the drawback is the use of liquid nitrogen, so that the system is no longer entirely cryogen-free...

### 6.1.5 Thermal switches

Having the objective to cool down as rapidly as possible, we have installed two thermal switches between the 4 K and the 1 K plates and between the 1 K and the 10 mK plates, as featured figure 6.4. They consist of a thin stainless tube containing copper radiators. The tube is filled with 2 bars of helium. A high temperature, the helium is gaseous and ensures a thermal link between the two stages. All the dilution unit is therefore cooled at approximately the same speed, the lower plates being thermally dragged by the second stage of the PT. Below $\sim$ 25 K, the helium is pumped by a charcoal pump placed at the bottom of the switches. The residual conduction at low temperature is due to the stainless tube, which is negligible.

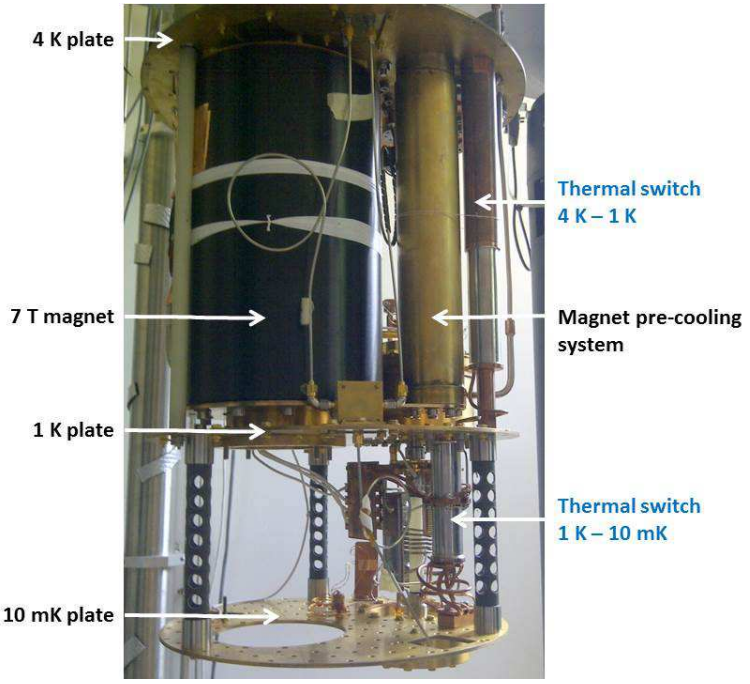



Figure 6.4: Thermal switches installed between the 4 K and the 1 K plates and between the 1 K and the 10 mK plates.

## 6.2 Performances

### 6.2.1 General performances

The initial specifications for this ***He free*** project were the following :

- Base temperature below 10 mK
- Operation of a 7 T magnet
- A cooling power above 100 $\mu$W at 100 mK

The actual cryostat fulfills all the above points :

- **The lowest temperature achieved to date is of 8.9 mK**, measured by a Matsushita Carbon Glass thermometer, calibrated in separate cryostat. We have also operated a precision thermometry system, the SRD1000 [4], that uses calibrated reference points. The ***He free*** mixing chamber temperature has then been measured to be lower than the last reference point, at 13 mK.
- **The Cryomagnetics NbTi magnet has been operated up to a magnetic field of 6 T** [5]. Due to Eddy currents, the temperature of the coil is about 5 K when ramping up the field at a rate of 0.011 A/s (or 1.6 mT/s). In all cases, the 4 K plate and the magnet temperature are well below the critical temperature of the NbTi wire. The stray field outside the cryostat has been measured with a Hall probe, both on the 300 K plate (above a 2 cm-thick aluminum plate) and on the side of the cryostat, at the point where the stray field was maximum (near the center of the magnet). Results are given figure 6.5.

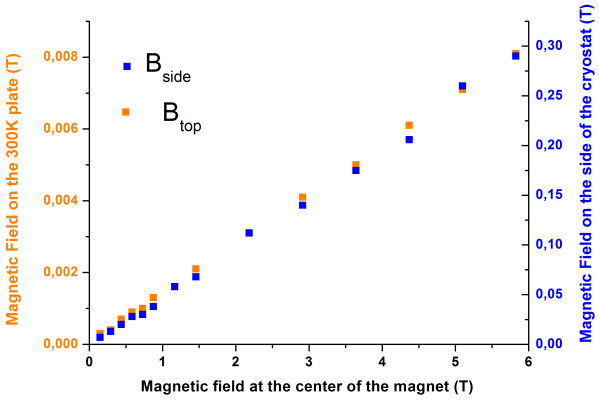



Figure 6.5: Stray field on the 300 K plate and on the side of the cryostat as a function of the field at the center of the magnet.

- **At 5 K, the cooling power on the first stage of the PT is 300 mW** with a pumping pressure of $6\times10^{-2}$ mbar, but this value depends on the pumping pressure.
- **The cryostat has a cooling power of about 260 $\mu$W at 100 mK**. The power curve is given figure 6.6 for two different pumping pressures. The mixing chamber temperature varies with $\sqrt{P}$ as theoretically expected [6].

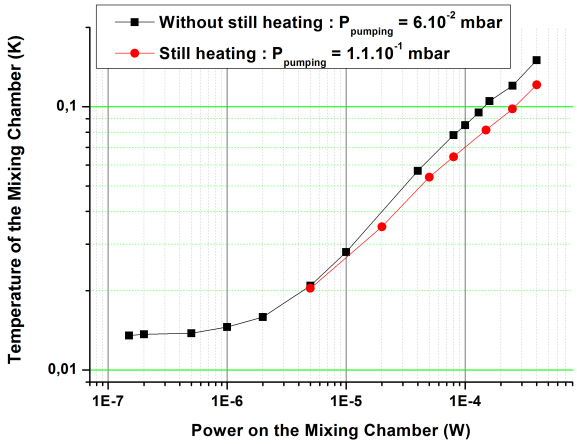



Figure 6.6: Power curve for the ***He free*** cryostat with and without heating the still (i.e. at two different pumping pressures).

4. `http://hdleiden.home.xs4all.nl/srd1000/`
5. To avoid any risk of quenching, we did not try to increase the magnetic field above this value.
6. It was obtained for the following impedance values : $Z_1$, placed at the exit of the Joule-Thomson stage and made out of sintered alumina, is $Z_1$=54 L/h ; $Z_2$, placed at the still outlet and made out of a squeezed 0.3×0.5 mm CuNi capillary, is $Z_2$=26 cm$^3$/min. The base temperature of 8.9 mK was subsequently obtained by changing $Z_1$ to a squeezed 0.2×0.5 mm CuNi capillary of 9 cm$^3$/min.

– For the record, the typical temperature and pressures of the system, during a normal dilution cycle, are the following :

$$\begin{aligned} T_{\text{PT first stage}} &\simeq 65 \text{ K} \\ T_{\text{PT second stage}} &\simeq 4 \text{ K} \\ T_{\text{still}} &\simeq 750 - 850 \text{ mK} \\ T_{\text{double still}} &\simeq 1.2 \text{ K} \\ P_{\text{pumping}} &\simeq 0.1 \text{ mbar} \\ P_{\text{injection}} &\simeq 500 - 700 \text{ mbar} \end{aligned}$$

### 6.2.2 Cooling down time

The ***He free*** cryostat has been optimized to minimize the cooling time, notably through the use of various thermal switches and of the magnet $N_2$ pre-cooling system. The efficiency of this additional cooling system can be appreciated figure 6.7.a. : the pulse tube alone (without magnet or dilution unit attached to it, but with the 50 K and 4 K shields) takes 8 hours to cool down the 4K plate ; the pulse tube with the 18 kg superconducting magnet attached to it, but no pre-cooling system, takes more than 18 hours to cool down to 4 K ; however, the $N_2$ pre-cooling system working at 1 bar reduces this **cooling time to 12.5 hours**. **The mixing chamber reaches 100 mK two hours later**. To our knowledge, this is one of the most rapid cool downs attained for a cryostat bearing a 18 kg magnet and a mixing chamber of 300 mm in diameter. Let us also appreciate Patrick Pari's clairvoyance in his estimation of this cooling time more than 3 years before the actual experiment (cf prediction figure 6.1 top left corner)...

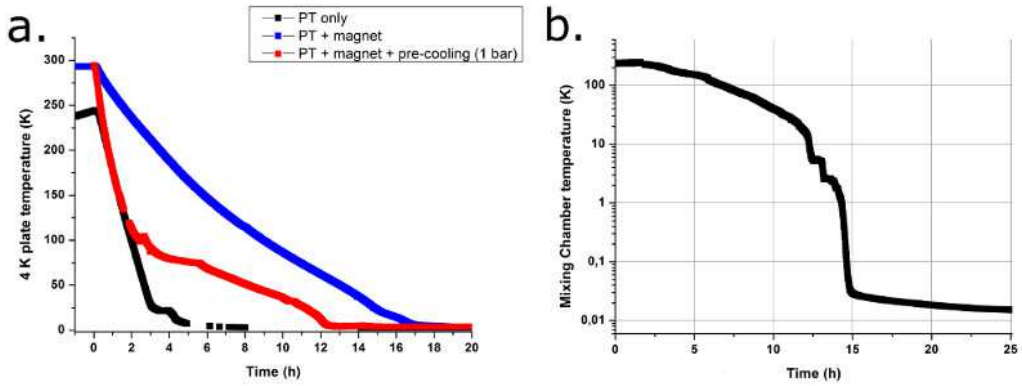



Figure 6.7: a. Cooling time for the 4 K plate for different cryostat configurations (see text). b. Cooling time for the mixing chamber with the magnet pre-cooling system working at 1 bar.

## 6.3 Advantages

As has already been seen, there are numerous advantages to this ***He free*** cryostat :

- The rapidity and simplicity of operation.
- The computer interface and the use of pneumatic valves on the gas handling system enable the remote control of the cryostat.
- The near-absence of cryogenic fluids makes it simpler to use. In particular, not having to manage liquid helium supplies and transfers is appreciable.
- The large working space at the lowest temperature. This is a true revolution for someone used to working with liquid-helium based dilution units : there is no need to worry about the volume of any additional component put at low temperature.

## 6.4 Ongoing improvements

As all real projects, the ***He free*** project presents a couple of drawbacks, one minor, and a more serious one, especially considering the experiments the group wants to run with this instrument :

1. The drawback from having a single vacuum space is that the "natural" insulation from infrared photons, that was secured by the Internal Vacuum Chamber in traditional liquid helium-based cryostats, no longer

exists. One therefore has to re-create a infrared photon-tight space at low temperature to prevent any unwanted heating on the samples or the mixing chamber. Careful thermal shielding as of 1 K, including anti-infrared paint, solves this issue.

2. Moreover, there is no exchange gas to thermalize the samples when cooling down from 300 K to 4 K. This could be an issue for weakly thermally coupled samples, such as massive bolometers.
3. Despite the use of radiators to decouple the vibrations of the PT from the cryostat, there still remain some movements on the mixing chamber, that may prove prohibitive for low noise bolometric measurements. Indeed, we have measured a resistive NTD [7] thermometer placed on a bolometer that is weakly coupled to the mixing chamber, with the PT "on" and then "off". The result is given figure 6.8.a. As can be seen, the resistance of the NTD measured with the PT "off" is higher than when the PT is in operation, indicating an effective temperature of the NTD that is higher when the PT is "on". This is due to the PT vibrations, enhanced by the fact that, in this configuration, the NTD is weakly coupled to the cold bath.

   This vibration problem has long been known to PT users. It is not problematic for a sample strongly thermally coupled to the mixing chamber but all bolometric measurements require a vibration level much lower than the one achieved to date.

   To solve this, Emiliano Olivieri, together with Patrick Pari's group, has undertaken a research program in order to quantify the problem and, if possible, offer a solution to it. The first step was to mechanically decouple the mixing chamber from the cryostat in the hope to reduce the vibrations transmitted from the PT to the lower parts of the cryostat. The encouraging results are summarized figure .b. The Power Spectral Density (PSD) has been measured by an accelerometer placed on the 10 mK plate in three different configurations [8] :

   - PT off
   - PT on and the 10 mK plate rigidly attached by fiberglass posts to the dilution unit
   - PT on and the 10 mK plate non-rigidly suspended to the dilution unit by Kevlar wires

   As can been seen, the suspension of the 10 mK plate improves the PSD, although not completely satisfactory to run bolometers. Further improvements are under way.

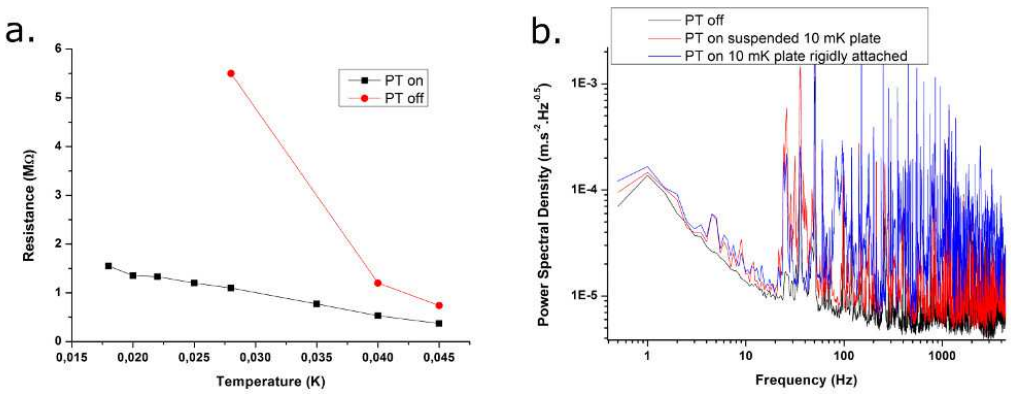



Figure 6.8: a. Measured resistance of a NTD with the PT on or off. b. Power Spectral Density (PSD) along the $z$-axis for different configurations of the system (see text).

7. Neutron Transmutation Doped Germanium.
8. Typically the measured acceleration of the 10 mK plate in the $z$-axis corresponds to a displacement of a few $\mu$m.

# Part III

# Future Perspectives

# Chapter 7

# Future work and outlook

In this chapter, I would like to enumerate the questions I personally find interesting and important to address to fully grasp the basic phenomena driving the response of disordered systems at very low temperature. Some of them we are currently trying to address experimentally, either in our group at CSNSM, or in collaboration. Some of them I would like to undertake in the future. And some of them are complicated issues which will probably only be solved by concurring experiments from different groups and by theoretical developments.

## 7.1 Elucidation of the effect of the thickness

As mentioned in section 4.2, we have shown that what is usually called *disorder* in the literature embraces different phenomena. More specifically, a reduction in the film thickness seems to have a very distinct effect from the one induced by other disorder-tuning parameters, such as the composition or the annealing temperature, at least in a-NbSi thin films.

This result is the starting point for a reflection on the specific role of the thickness. In particular, we would like to see if a change in thickness influences other parameters in the system. Indeed, it has been suggested [Simonin, 1986] that decreasing the sample thickness increases the relative importance of the surfaces in such a manner that the depletion of $T_c$ could be explained. This hypothesis, although rarely mentioned, is very appealing and we would like to engage a study in this direction. The first step is to re-analyze our data along this theoretical proposition and see if this could explain the phenomenological difference we observe between annealing or composition on the one hand, and thickness on the other. Ultimately, this could guide us towards a more quantitative definition of *disorder*.

## 7.2 Study of the dynamic properties of disordered superconductors

We are currently investigating the high frequency conductivity (100 MHz-8 GHz) response of thin a-NbSi films down to 15 mK. This work is performed in close collaboration with the Nanostructures à la Nanoseconde group at the Laboratoire de Physique des Solides in Orsay [1], and mainly involves François Couëdo and Pascale Diener [2].

The aim of these experiments is to check the quantum nature of the Superconductor-to-Insulator Transition and to measure the electrodynamic response of the superconducting phase. The work goes along three axes :

1. **Understanding the transition(s) - a quantum phase transition point of view**
   - If the studied transition(s) indeed are Quantum Phase Transitions, we should observe a crossover in the conductivity between a classical and a quantum regime (no microscopic scattering time involved) at $\hbar\omega \simeq k_B T$ [Sondhi et al., 1997, Damle and Sachdev, 1997] [3] :
     i. When $\hbar\omega \ll k_B T$, the behavior of the system is governed by the $\omega = 0$ limit and is therefore dominated by temperature effects.
     ii. When $\hbar\omega \gg k_B T$, the behavior is dominated by quantum fluctuations, and limited by the frequency of the measurement, independently of the temperature.
   - At finite temperature, one should observe, in the critical regime corresponding to the SIT, a dependence of the conductivity which should scale with $\frac{\hbar\omega}{k_B T}$. This important theoretical prediction

1. Julien Gabelli and Marco Aprili notably.
2. This work has partially been funded by the RTRA Triangle de la Physique (grant No. 2009-019T-TSI2D) and by the ANR (grant No. ANR-2010-BLANC-0403-01).
3. 1 GHz corresponds to 48 mK (through the conversion $\hbar\omega \equiv k_B T$, whereas 8 GHz corresponds to 380 mK.

[Damle and Sachdev, 1997] establishing the crucial role of the interactions has never been clearly verified.

2. **Studying the fluctuations and measurement of the superfluid density**
Finite frequency measurements allow to probe the complex electrodynamic response of both the superconducting and the normal components [Crane et al., 2007]. It is therefore possible to address both paired and unpaired electron dynamics and eventually their interference beyond the BCS theory. We hope to clarify the microscopic nature of the different ground states close to the SIT (localized or delocalized). The two-fluid model AC conductivity below the superconducting gap is given by:

$$\begin{aligned} \sigma_1 &= Re(\sigma) = \frac{\pi n_s e^2}{2m}\delta(\omega) + n_n \frac{e^2 \tau_n}{m} \\ \sigma_2 &= Im(\sigma) = \frac{n_s e^2}{m\omega} \end{aligned}$$

where $\sigma_1$ is the real part of the complex conductivity, $\sigma_2$ its imaginary part, $n_s$ the density of superfluid electrons, $n_n$ the density of normal electrons, $\tau_n$ the relaxation time for normal electrons and $\delta(\omega)$ is the Dirac function. One can thus probe the different fluctuation regimes and the nature of the carriers in this phase, notably:
- Whether $n_s$ survives beyond the destruction of the superconductivity, which would mean that short-lived Cooper pairs exist even when there is no long-range superconductivity. One could then verify whether the universal relation between $n_s(T = 0)$ and $T_c$ observed in high $T_c$ superconductors [Uemura et al., 1989, Uemura, 1997, Tashiro et al., 2008] holds in these systems. The Kosterlitz-Thouless transition could also be probed [Crane et al., 2007].
- Whether $n_n$ survives at low temperature, even for superconducting samples, thus accrediting the fermionic channel scenario [Yazdani and Kapitulnik, 1995] which has only been probed by DC transport experiments.
- For a BCS superconductor, the energy scale for the imaginary and real part of the conductivity is set by the energy gap. We would like to investigate whether a lower energy scale appears in $\sigma_2$, characteristic of the apparition of a long-range order at the Kosterlitz-Thouless transition.
- Knowing $n_n$, the scattering rate and its energy dependence can be obtained from the Drude term in $\sigma_1$. The nature of the state ensuing the suppression of the superconductivity could hence be probed.

3. **Building a dedicated AC measurement set-up for low temperature measurements**
In order to measure the GHz conductivity of the system, we needed to perform absolute measurements of the complex impedance at very low temperature. This requires to subtract from the measured reflection coefficient the signal coming from the the microwave circuit (cables, amplifier, connectors, coupler, ...). One way to proceed is to develop a very careful calibration procedure that could be used at low temperature, be reproductible, and which allows to measure the sample after having calibrated the setup thanks to an open circuit, a short circuit and a load, all in a single cool-down run. This *calibrator* is not available commercially, and Pascale Diener has built a prototype of such a device, based on a mechanical switching, and which could be used in a dilution unit (figure 7.1). The first design and tests are reported in `http://arxiv.org/pdf/1309.4321`

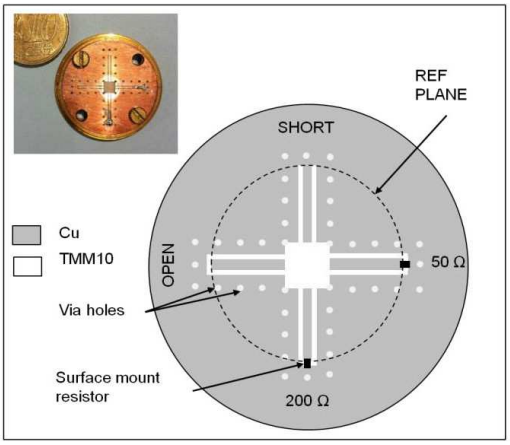



Figure 7.1: Picture and schematic representation of the *calibrator*. The microwave signal is injected at the center of the dial. A right-angled connector drives the microwave to one of the four circuits : open, short, load, or sample (here a 200 Ω resistance). Both by Pascale Diener.

## 7.3 Probing the density of state near the SIT

Measuring the density of state (DOS) at low temperature near the SIT would provide important insight both on the existing ground states and on the physical processes driving the transition. With this aim in mind, we have started a collaboration with Claude Chapelier (INAC, CEA, Grenoble) [4] in order to compare the DOS in a-NbSi thin films measured by local Scanning Tunneling Microscopy (STM) and by macroscopic tunnel junctions. The project has two main objectives :

1. **Understanding the nature of the phase**
   Both on the superconducting side and on the metallic (or insulating) side, tunneling experiments should be useful. We plan to start macroscopic tunneling experiments and complete those with local STM measurements. In the superconducting phase, one should observe the superconducting gap in the DOS and it would be interesting to see what this gap becomes as the samples are more and more disordered:
   - At the transition, it would be noteworthy to see whether states appear in the gap, indicating a metallic behavior, or if it smears, indicating short-lived Cooper pairs.
   - The relation between the gap and the superconducting critical temperature should give an indication on the nature of the superconductivity (BCS or abnormal).
   - If the macroscopic tunneling experiments observe a smearing of the gap, it would be interesting to compare with STM measurements of the local DOS to see if this smearing is intrinsic to the material or due to order parameter spatial inhomogeneities (as explained below).
   - In the case of a fermionic metallic state, one should be able to observe a correlation pseudo-gap [Lesueur et al., 1985, Hertel et al., 1983] which would be interesting to characterize.
2. **Understanding the nature of the fluctuations**
   - A corollary to the above-mentioned tunneling experiment is that an insight on the fermionic or bosonic nature of the mechanism responsible for the Tc suppression could be gained through tunneling measurement of the gap evolution with disorder.
   - One of the important questions to solve for a complete understanding of these disordered systems is the notion of homogeneity. Previous experiments on superconducting thin films analyzed in the SIT picture have shown percolation-like features (notably the value of the correlation length critical exponent $\nu \simeq \frac{4}{3}$ in TiN films for example). STM measurements [Sacépé et al., 2008] on those systems have shown that superconducting islands form even for materials that are claimed to be non-granular. This would point to an intrinsic inhomogeneity of the phase itself, independently of whether the material is structurally homogeneous or not. In a-NbSi, we did not find any percolation-like features in transport properties nor in TEM clichés, so that measurements on those films would be particularly interesting, especially regarding the validity of the pseudo-spin scenario (see section 1.2).
   - We also plan to intentionally synthesize granular films by nanostructuring NbSi films (see section 7.7). The correlation between the structural and the order parameter inhomogeneities would be interesting to study, along with the comparison with STM measurements on the same non-nanostructured NbSi films.
   - Above $T_c$, the thermal evolution of the DOS at the Fermi energy, in a regime where a pseudogap has been observed in TiN or InO [Sacépé et al., 2010], is also expected to give information on the nature of the fluctuations. In particular, superconducting fluctuations in two dimensions can thus be unveiled.

On a more prospective level, once the STM and macroscopic tunneling experiments are set up, all equipments will be available for tunneling measurements under a magnetic field. To date, it seems to us that the interpretation of such experiments is not straight-forward, but should be interesting to monitor the fluctuations and the superfluid response when the destruction of the superconductivity is tuned by the application of a magnetic field. Moreover, the one particle DOS in the non-superconducting state together with the thermal dependence of the conductance of the film should give us information on the nature of the charge carriers above the critical field of the QPT, in particular on their bosonic or fermionic character. At an even higher field it would be interested to compare the field dependence of the DOS at the Fermi level in NbSi films with the measured one in a-Bi films where an intriguing "quantum metal" has been discovered [Butko and Adams, 2001].

## 7.4 Influence of Coulomb interactions in disordered systems

Although the subject is debated [Feigel'man et al., 2010, Finkel'stein, 1994], I feel it is likely that Coulomb interactions play a role in the properties of thin disordered films. We would therefore like to study the strength of electron-electron interactions by putting superconducting a-NbSi films near a metallic gate. A backgate voltage could then tune the screening [5]. This would aim at :

4. This work has partially been funded by the ANR (grant No. ANR-2010-BLANC-0403-01)
5. The effect of screening will however have to be distinguished from electrostatic doping.

1. **Exploring the phase diagram**
   Changing the effective Coulomb interactions will be an extremely important test to determine their importance for tuning the transitions. In particular, we will test the validity of the pseudo-spin scenario in contrast to other Superconductor-Insulator Transitions theories for which these interactions are believed to be crucial. We will determine what becomes of the various ground states under an electric field-effect. This should be especially interesting in the case of the possible quantum metal phase.
2. **Understanding the transitions**
   Experiments under an electric field are complementary to magnetoresistance measurements that will allow the separate determination of the correlation length critical exponent $\nu$ and to the dynamical exponent $z$ that characterize the SIT universality class.

## 7.5 Characterization of the hypothetic metallic state(s)

The characteristics of the metallic behavior evoked in section 3.2 are to be explored.

The first step is to carefully determine the phase diagram of a-NbSi thin films. In parallel, the above-mentioned experiments (GHz transport measurements, tunneling experiments, ...) will provide more precisions on the exact nature of the dissipative phase(s) and on the relevant parameters for their apparition.

## 7.6 Towards an understanding of the specificity of the materials

As mentioned in section 1.1, disordered superconductors can be divided into different sub-categories, depending on their properties. For instance :

- When submitted to a **magnetic field**, some materials, like $InO_x$ and TiN, present a giant magnetoresistance at high magnetic field ; and others, such as a-MoGe or a-NbSi, have only a weak magnetoresistance.
- When the **thickness is reduced**, some materials, like a-Bi or Pb, have sheet resistances varying by orders of magnitude for a thickness difference of less than 1 Å; others, like MoRu or a-NbSi, have a more progressive variation.

Like many others in the field, I feel that understanding the parameters driving these differences between materials might provide interesting insight on the mechanisms at play. One possible preliminary step towards this aim is to characterize, as can be, one material through different means. This is the approach we have chosen for the ANR POSTIT project, where we chose to tackle the SIT in a-NbSi by various techniques (transport measurements in DC and the GHz regime, STM, macroscopic tunneling effect, ...), so as to corroborate the different results. This will hopefully give us a clearer vision of this material, which could then be compared to other compounds.

## 7.7 Nanostructured films

Nanostructured films offer possibilities to explore ground states that would not be accessible with the same non-structured material. These have been explored through two complementary approaches :

1. **Nano-honeycomb films**
   Jim Valles and his group have shown [Stewart et al., 2007, Hollen et al., 2011] that amorphous thin films or nano-patterned films of the same material did not obligatorily present the same properties[6]. Indeed, in their case, a-Bi homogeneous films presented a SIT with a small positive magnetoresistance and characteristics compatible with a fermionic scenario for the destruction of superconductivity. Nano-honeycomb a-Bi films (see figure 7.2), however, have a large negative magnetoresistance, and transport characteristics more compatible with a bosonic scenario. In this case, they have also shown that there were signs of Cooper pairs persisting in the insulating phase. They explain these different *flavors* for the SIT through a small variation in the film thickness near the holes of the nano-honeycomb structure. The film then seems to be controlled by weak links which conductance is comparable to the quantum conductance for pairs. This result shows one step towards the understanding of the mechanism that allows the evolution towards an insulating phase while keeping the Cooper pairs formed.
   We would like to look if we can also access a bosonic insulator with nano-patterned a-NbSi films [Kopnov et al., 2012]. We feel these experiments could provide an interesting insight on the similarities and differences between materials exhibiting SITs (see section 7.6).
2. **Mesoscopic superconductor-normal-superconductor arrays**
   More recently, Nadya Mason's group has used superconductor-normal-superconductor arrays (see figure

6. A clear summary of the different experiments on this system, either granular, homogeneous or nano-patterned, can be found in `http://www.lorentzcenter.nl/lc/web/2011/449/presentations/index.php3?wsid=449&type=presentations`.

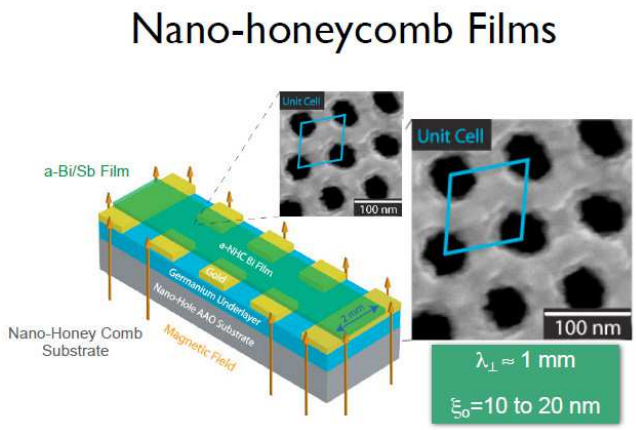



Figure 7.2: Schematic representation and AFM picture of a nano-honecomb Bi film. Taken from Jim Valles' presentation (`http://www.lorentzcenter.nl/lc/web/2011/449/presentations/index.php3?wsid=449&type=presentations`).

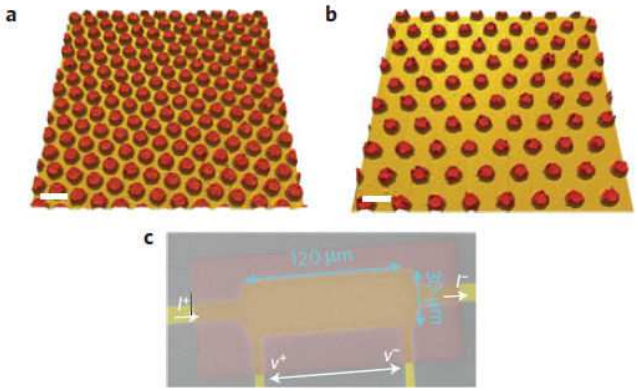



Figure 7.3: AFM picture of a device composed of an superconductor-normal-superconductor array. Taken from [Eley et al., 2011]. a. arrays of 87-nm-thick Nb dots (red) on 10-nm-thick Au underlayer (yellow). The spacing between each dot is of 140nm. b. Idem with a dot spacing of 340nm. c. SEM image of the device. The Au ground plane is painted in yellow and the red plane corresponds to the island array.

7.3) to study a two-dimensional metallic state [Eley et al., 2011, Eley et al., 2012]. This system is a convenient way to engineer a structurally inhomogeneous, yet controlled, superconducting state. When the dots are larger the superconducting coherence length $\xi_{SC}$ of the dot - here Nb -, the proximity effect ensures that the system as a whole is superconducting. The originality of this work is to synthesize dots of the sizes comparable to $\xi_{SC}$. Mesoscopic fluctuations then allow the existence of a metallic ground state [Spivak et al., 2001, Spivak et al., 2008].

With Vincent Humbert, we are starting a work to investigate this possibly new metallic state and compare it to what we have previously found in two-dimensional homogeneous systems (see section 7.5).

## 7.8 Disordered materials on the insulating side

Disordered insulating systems ($InO_x$, granular aluminum or non-continuous metallic films, ...) are ideal candidates for the observation of electron glasses [Ovadyahu, 2006]. This phase has been theoretically predicted 30 years ago [Davies et al., 1984, Pollak and Ortuño, 1984] to result from Coulomb interactions between localized carriers. However, subsequent experimental studies, such as the "field-effect experiment" described below, exhibited features that are still unsatisfactorily explained. Since 2011, we have an ongoing collaboration with Julien Delahaye and Thierry Grenet (Institut Néel, Grenoble) to investigate whether a-NbSi films, in the insulating regime, exhibit such properties. To date, there has been two types of experiments :

1. **Relaxation of the conductance**

   After being quench-cooled to liquid $^4$He temperature, the conductance $G$ of the films is measured at a 4.2 K. In electron glasses, $G$ slowly relaxes in a logarithmic manner with time. This behavior is characteristic

of a glassy behavior and has been observed over more than five decades in time in crystalline $InO_x$ films [Ovadyahu and Pollak, 2003].

2. **Field-effect**
   When used as the channel in a field-effect device, electron glasses present a gate voltage dependant conductance. When the sample is quench-cooled to low temperature and equilibrates at a given temperature, $G(V_g)$ has a minimum centered around the gate voltage $V_g^0$ at which the sample has been cooled down. In the so-called "two-dip experiment", when the gate voltage is subsequently modified to $V_g^n$, the conductance exhibit two conductance minima at $V_g^0$ and $V_g^n$. The dip at $V_g^0$ then slowly fades away with time [Grenet et al., 2007].

Measurements at the Institut Néel have shown that a-NbSi films indeed display a relaxing behavior analogous to what has been observed in other systems. However the magnitude and the dynamics of the relaxation present distinctive features that makes a-NbSi an interesting system for these studies. The first results have been presented by Julien Delahaye at the TIDS15 conference in September 2013 [7].

## 7.9 Application to detectors : Kinetic Inductance Detectors

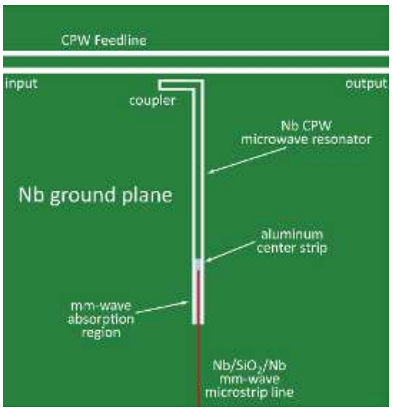



Figure 7.4: A picture of a Al/Nb resonator. Taken from [Maloney et al., 2009].

One interesting application of the properties of disordered superconductors in the GHz regime (see section 7.2) relies in Kinetic Inductance Detectors. The working principle of these detectors, developed in the early 00's by Caltech and the Jet Propulsion Laboratory [Day et al., 2003], is the following : a photon of energy $h\nu > 2\Delta$ is absorbed by a superconducting film of superconducting energy gap $\Delta$, thus modifying the surface resistance and inductance of the film. If the superconducting film is capacitively coupled to a microwave feedline, as shown figure 7.4, the superconducting film acts like a resonator which absorbs all energy coming from the feedline at its resonance frequency. This translates into a dip in the transmission factor of the feedline (see figure 7.5).

These photon detectors are particularly interesting because they combine the high sensitivity of resonators and the possibility of multiplexing the detectors : multiple resonators can be coupled to a single feedline, provided they work at slightly different frequencies. They are currently developed for photon frequencies ranging from the far-infrared to X-Rays.

In our group, Hélène le Sueur has started to study resonators made out of a-NbSi. The corresponding results will be interesting to follow, both for potential applications to high-sensitivity detectors, and for the fundamental superconducting parameters that could be extracted from these measurements.

## 7.10 Towards lower dimensions

The KIDs also offer a natural pathway towards the study of disordered superconductors in 1D. There has been a renewed interest for this subject since Mooij and Nazarov proposed disordered superconductors as interesting candidates for an experimental realization of Quantum Phase Slips [Mooij and Harmans, 2005, Mooij and Nazarov, 2006] - the dual counterpart of the Josephson junction [8] - where fluctuations in the order parameter can cause a macroscopic quantum tunneling of the phase across a current-biased superconducting nanowire. When the device is operated near the critical current, these topological excitations can cause the

7. Transport in Interacting Disordered Systems : `http://www.ub.edu/tids15/index.php/conference-program`
8. Phase and charge are conjugate quantities.

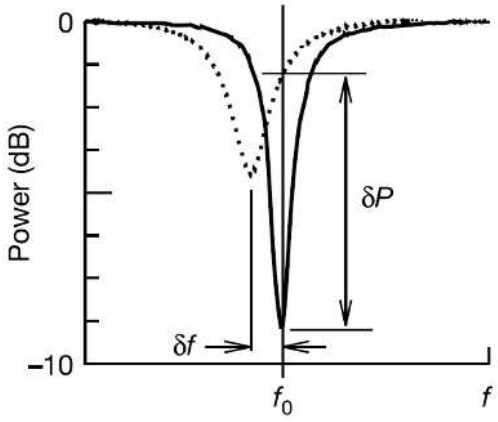



Figure 7.5: On resonance, the superconducting resonator, which acts as a $LC$ circuit, loads the feedline, producing a dip in its transmission. The incoming photons, when absorbed by the resonator, change the surface resistance and inductance, so that the resonance is moved to lower frequency (effect of $L$) and broadened (effect of $R$). Taken from [Day et al., 2003].

appearance of a *hotspot*, inducing a non-zero resistance state. This allows the phase to "slip" in such a way that the phase difference between the two ends of the wire changes by $\pm 2\pi$.

Recently, some experimental realization have demonstrated the feasibility of Quantum Phase Slips, using disordered superconductors such as a-NbSi [Hongisto and Zorin, 2012], a-MoGe [Aref et al., 2012] or $InO_x$ [Astafiev et al., 2012].

Studies on Quantum Phase Slips are of considerable interest, both for a fundamental understanding of the SIT in nanowires [Bezryadin et al., 2000, Herzog et al., 1998, Johansson et al., 2005, Bollinger et al., 2008], and for applications, such as the establishment of a standard for current [Webster et al., 2013].

# Bibliography


[A. Kapitulnik and Chakravarty, 2001] A. Kapitulnik, N. Mason, S. K. and Chakravarty, S. (2001). Effects of dissipation on quantum phase transitions. *Phys. Rev. B*, 63:125322.

[Abrahams et al., 1979] Abrahams, E., Anderson, P., Licciardello, D., and Ramakrishnan, T. (1979). Scaling theory of localization: Absence of quantum diffusion in two dimensions. *Phys. Rev. Lett.*, 42:673.

[Anderson, 1958] Anderson, P. (1958). Absence of diffusion in certain random lattices. *Phys. Rev.*, 109:1492.

[Anderson, 1959] Anderson, P. (1959). Theory of dirty superconductors. *J. Phys. Chem. Solids*, 11:26.

[Anderson et al., 1983] Anderson, P. W., Muttalib, K. A., and Ramakrishnan, T. V. (1983). Theory of the "universal" degradation of $T_c$ in high-temperature superconductors. *Phys. Rev. B*, 28:117–120.

[Aref et al., 2012] Aref, T., Levchenko, A., Vakaryuk, V., and Bezryadin, A. (2012). Quantitative analysis of quantum phase slips in superconducting mo_ {76} ge_ {24} nanowires revealed by switching-current statistics. *Physical Review B*, 86(2):024507.

[Astafiev et al., 2012] Astafiev, O., Ioffe, L., Kafanov, S., Pashkin, Y. A., Arutyunov, K. Y., Shahar, D., Cohen, O., and Tsai, J. (2012). Coherent quantum phase slip. *Nature*, 484(7394):355–358.

[Aubin et al., 2006] Aubin, H., Marrache-Kikuchi, C., Pourret, A., Behnia, K., Berge, L., Dumoulin, L., and Lesueur, J. (2006). Magnetic-field-induced quantum superconductor-insulator transition in nb0.15si0.85. *Phys. Rev. B*, 73:094521.

[Baturina et al., 2007] Baturina, T. I., Strunk, C., Baklanov, M. R., and Satta, A. (2007). Quantum metallicity on the high-field side of the superconductor-insulator transition. *Phys. Rev. Lett.*, 98:127003.

[Béal and Friedel, 1964] Béal, M. and Friedel, J. (1964). Relation between local order and interference effects in electrical resistivity for metallic alloys. *Phys. Rev.*, 135:A466.

[Bezryadin et al., 2000] Bezryadin, A., Lau, C., and Tinkham, M. (2000). Quantum suppression of superconductivity in ultrathin nanowires. *Nature*, 404(6781):971–974.

[Bielejec and Wu, 2002] Bielejec, E. and Wu, W. (2002). Field-tuned superconductor-insulator transition with and without current bias. *Phys. Rev. Lett.*, 88:206802.

[Bollinger et al., 2008] Bollinger, A. T., Dinsmore, R. C., Rogachev, A., and Bezryadin, A. (2008). Determination of the superconductor-insulator phase diagram for one-dimensional wires. *Phys. Rev. Lett.*, 101:227003.

[Butko and Adams, 2001] Butko, V. and Adams, P. (2001). Quantum metallicity in a two-dimensional insulator. *Nature*, 409:161.

[Cha et al., 1991] Cha, M., Fisher, M., Girvin, S., Wallin, M., and Young, A. (1991). Universal conductivity of two-dimensional films at the superconductor-insulator transition. *Phys. Rev. B*, 44:6883.

[Chayes et al., 1986] Chayes, J., Chayes, L., and Fisher, D. (1986). Finite-size scaling and correlation lengths for disordered systems. *Phys. Rev. Lett.*, 57:2999.

[Coll., 2013] Coll., P. (2013). Planck 2013 results. i. overview of products and scientific results. *ArXiv*, page 1303.5062.

[Crane et al., 2007] Crane, R., Armitage, N. P., Johansson, A., Sambandamurthy, G., Shahar, D., and Grüner, G. (2007). Survival of superconducting correlations across the two-dimensional superconductor-insulator transition: A finite-frequency study. *Phys. Rev. B*, 75:184530.

[Crow et al., 1969] Crow, J., Strongin, M., Thompson, R., and Kammerer, O. (1969). The superconducting transition temperatures of disordered nb, w, and mo films. *Phys. Lett. A*, 30A:161.

[Damle and Sachdev, 1997] Damle, K. and Sachdev, S. (1997). Nonzero-temperature transport near quantum critical points. *Phys. Rev. B*, 56:8714.

[Das and Doniach, 1999] Das, D. and Doniach, S. (1999). Existence of a bose metal at t=0. *Phys. Rev. B*, 60:1261.

[Davies et al., 1984] Davies, J., Lee, P., and Rice, T. (1984). Properties of the electron glass. *Physical Review B*, 29(8):4260.

[Day et al., 2003] Day, P. K., LeDuc, H. G., Mazin, B. A., Vayonakis, A., and Zmuidzinas, J. (2003). A broadband superconducting detector suitable for use in large arrays. *Nature*, 425(6960):817–821.

[Deutscher et al., 1980] Deutscher, G., Bandyopadhyay, B., Chui, T., Lindenfeld, P., McLean, W., and Worthington, T. (1980). Transition to localization in granular aluminum films. *Phys. Rev. Lett.*, 44:1150.

[Dole et al., 2006] Dole, H., Lagache, G., Puget, J.-L., Caputi, K. I., Fernández-Conde, N., Floc'h, E. L., Papovich, C., Pérez-González, P. G., Rieke, G. H., , and Blaylock, M. (2006). The cosmic infrared background resolved by spitzer. *Astron. Astroph.*, 451:417.

[Dumoulin et al., 1993] Dumoulin, L., Bergé, L., Lesueur, J., Bernas, H., and Chapellier, M. (1993). Nb-si thin films as thermometers for low-temperature bolometers. *J. Low. Temp. Phys.*, 93:301.

[Dumoulin et al., 1996] Dumoulin, L., Bergé, L., Marnieros, S., and Lesueur, J. (1996). Progress in low temperature thin film thermometers. *Nucl. Instr. Meth. A*, 370:211.

[Dynes et al., 1978] Dynes, R. C., Garno, J. P., and Rowell, J. M. (1978). Two-dimensional electrical conductivity in quench-condensed metal films. *Phys. Rev. Lett.*, 40:479–482.

[Eley et al., 2011] Eley, S., Gopalakrishnan, S., Goldbart, P. M., and Mason, N. (2011). Approaching zero-temperature metallic states in mesoscopic superconductor-normal-superconductor arrays. *Nature Physics*, 8(1):59–62.

[Eley et al., 2012] Eley, S., Gopalakrishnan, S., Goldbart, P. M., and Mason, N. (2012). Fate of global superconductivity in arrays of long sns junctions. *arXiv preprint arXiv:1206.5999*.

[Feigel'man et al., 2010] Feigel'man, M., Ioffe, L., Kravtsov, V., and Cuevas, E. (2010). Fractal superconductivity near localization threshold. *Ann. Phys.*, 325:1390.

[Feigel'Man et al., 2001] Feigel'Man, M., Larkin, A., and Skvortsov, M. (2001). Quantum superconductor–metal transition in a proximity array. *Physics-Uspekhi*, 44(10S):99.

[Feigel'man and Larkin, 1998] Feigel'man, M. and Larkin, A. I. (1998). Quantum superconductor–metal transition in a 2d proximity-coupled array. *Chemical physics*, 235(1):107–114.

[Finkel'stein, 1994] Finkel'stein, A. (1994). Suppression of superconductivity in homogeneously disordered systems. *Physica B*, 197:636.

[Finkel'stein, 1987] Finkel'stein, A. M. (1987). Superconducting transition temperature in amorphous films. *JETP Lett.*, 45:46.

[Fisher et al., 1990] Fisher, M., Grinstein, G., and Girvin, S. (1990). Presence of quantum diffustion in two dimensions : universal resistance at the superconductor-insulator transition. *Phys. Rev. Lett.*, 64:587.

[Fisher and Lee, 1989] Fisher, M. and Lee, D. (1989). Correspondence between two-dimensional bosons and a bulk superconductor in a magnetic field. *Phys. Rev. B*, 39:2756.

[Gantmakher, 1998] Gantmakher, V. (1998). Transport properties of normal and quasinormal states of poor superconductors. *International Journal of Modern Physics B*, 12(29n31):3151–3156.

[Gantmakher, 2004] Gantmakher, V. (2004). Traits of the insulator formed under the superconductor-insulator transition. *Physica C*, 404:176.

[Gantmakher and Dolgopolov, 2010] Gantmakher, V. and Dolgopolov, V. (2010). Superconductor-insulator quantum phase transition. *Physics-Uspekhi*, 53:1.

[Gantmakher et al., 2000] Gantmakher, V., Golubkov, M., Dolgopolov, V., Tsydynzhapov, G., and Shashkin, A. (2000). Superconductor-insulator transition in amorphous in-o films. *Physica B*, 284:649.

[Gantmakher and Dolgopolov, 2008] Gantmakher, V. F. and Dolgopolov, V. T. (2008). Localized-delocalized electron quantum phase transitions. *Physics-Uspekhi*, 51(1):3–22.

[Gatti, 2009] Gatti, F. (2009). Contributions of low temperature detectors to neutrino physics. *AIP Conf. Proc.*, 1185:553.

[Ghosal et al., 2001] Ghosal, A., Randeria, M., and Trivedi, N. (2001). Inhomogeneous pairing in highly disordered s-wave superconductors. *Physical Review B*, 65(1):014501.

[Giamarchi, 2009] Giamarchi, T. (2009). Experimental and theoretical developments in dirty bosons.

[Golwala, 2009] Golwala, S. (2009). Future developments in low temperature detectors for cmb and submm astronomy. *AIP Conf. Proc.*, 1185:773.

[Grenet et al., 2007] Grenet, T., Delahaye, J., Sabra, M., and Gay, F. (2007). Anomalous electric-field effect and glassy behaviour in granular aluminium thin films: electron glass? *The European Physical Journal B*, 56(3):183–197.

[Haviland et al., 1989] Haviland, D., Liu, Y., and Goldman, A. (1989). Onset of superconductivity in the two-dimensional limit. *Phys. Rev. Lett.*, 62:2180.

[Hebard and Vandenberg, 1980] Hebard, A. F. and Vandenberg, J. M. (1980). Role of clusters in the approach to localization of josephson-coupled granular lead films. *Phys. Rev. Lett.*, 44:50–54.

[Hertel et al., 1983] Hertel, G., Bishop, D., Spencer, E., Rowell, J., and Dynes, R. (1983). Tunneling and transport measurements at the metal-insulator transition of amorphous nb: Si. *Phys. Rev. Lett.*, 50:743.

[Herzog et al., 1998] Herzog, A. V., Xiong, P., and Dynes, R. C. (1998). Magnetoresistance oscillations in granular sn wires near the superconductor-insulator transition. *Phys. Rev. B*, 58:14199–14202.

[Hirakawa et al., 2008] Hirakawa, A., Makise, K., Kawaguti, T., and Shinozaki, B. (2008). Thickness-tuned superconductor–insulator transitions in quench-condensed mo and moru films. *Journal of Physics: Condensed Matter*, 20(48):485206.

[Hollen et al., 2011] Hollen, S., Nguyen, H., Rudisaile, E., Stewart Jr, M., Shainline, J., Xu, J., and Valles Jr, J. (2011). Cooper-pair insulator phase in superconducting amorphous bi films induced by nanometer-scale thickness variations. *Physical Review B*, 84(6):064528.

[Hongisto and Zorin, 2012] Hongisto, T. T. and Zorin, A. B. (2012). Single-charge transistor based on the charge-phase duality of a superconducting nanowire circuit. *Phys. Rev. Lett.*, 108:097001.

[Jaeger et al., 1986] Jaeger, H., Haviland, D., Goldman, A. M., and Orr, B. (1986). Threshold for superconductivity in ultrathin amorphous gallium films. *Phys. Rev. B*, 34:4920.

[Jethava et al., 2009] Jethava, N., Ullom, J., Irwin, K., Doriese, W., Beall, J., Hilton, G., Vale, L., and Zink, B. (2009). Dependence of excess noise on the partial derivatives of resistance in superconducting transition edge sensors. *AIP Conf. Proc.*, 1185:31.

[Johansson et al., 2005] Johansson, A., Sambandamurthy, G., Shahar, D., Jacobson, N., and Tenne, R. (2005). Nanowire acting as a superconducting quantum interference device. *Phys. Rev. Lett.*, 95:116805.

[Kapitulnik et al., 1985] Kapitulnik, A., Kotliar, G., et al. (1985). Anderson localization and the theory of dirty superconductors. *Physical review letters*, 54(5):473–476.

[Kopnov et al., 2012] Kopnov, G., Cohen, O., Ovadia, M., Lee, K. H., Wong, C. C., and Shahar, D. (2012). Little-parks oscillations in an insulator. *Physical review letters*, 109(16):167002.

[Kravchenko et al., 1994] Kravchenko, S., Kravchenko, G., Furneaux, J., Pudalov, V., and D'Iorio, M. (1994). Possible metal-insulator transition at b=0 in 2 dimensions. *Phys. Rev. B*, 50:8039.

[Larkin, 1999] Larkin, A. (1999). Superconductor-insulator transitions in films and bulk materials. *Ann. Phys.*, 8:785.

[Lee et al., 2000] Lee, H. L., Carini, J. P., Baxter, D. V., Henderson, W., and Gruner, G. (2000). Quantum-critical conductivity scaling for a metal-insulator transition. *Science*, 287:633.

[Lee and Ramakrishnan, 1985] Lee, P. and Ramakrishnan, T. (1985). Disordered electronic systems. *Rev. Mod. Phys.*, 57:287.

[Lesueur et al., 1985] Lesueur, J., Dumoulin, L., and Nedellec, P. (1985). Metal-insulator transition in quench-condensed $\mathrm{al}_x\mathrm{ge}_{1-x}$ : Scaling and tunneling experiments. *Phys. Rev. Lett.*, 55:2355.

[Ma and Lee, 1985] Ma, M. and Lee, P. (1985). Localized superconductors. *Phys. Rev. B*, 32:5658.

[Maekawa et al., 1983] Maekawa, S., Ebisawa, H., and Fukuyama, H. (1983). Upper critical field in two-dimensional superconductors. *J. Phys. Soc. Jpn.*, 52:1352.

[Maekawa and Fukuyama, 1982] Maekawa, S. and Fukuyama, H. (1982). Localization effects in two-dimensional superconductors. *J. Phys. Soc. Jpn.*, 51:1380.

[Maloney et al., 2009] Maloney, P., Czakon, N., Day, P., Duan, R., Gao, J., Glenn, J., Golwala, S., Hollister, M., LeDuc, H., Mazin, B., et al. (2009). The mkid camera. In *AIP Conference Proceedings*, volume 1185, page 176.

[Markovic et al., 1998] Markovic, N., Christiansen, C., and Goldman, A. (1998). Thickness-magnetic field phase diagram at the superconductor-insulator transition in 2d. *Phys. Rev. Lett.*, 81:5217.

[Marnieros, 1998] Marnieros, S. (1998). *Couches minces d'isolant d'Anderson. Application à la bolométrie à très basse température*. PhD thesis, Paris XI, Orsay.

[Marrache-Kikuchi, 2006] Marrache-Kikuchi, C. (2006). *Effets dimensionnels dans un système désordonné au voisinage des transitions métal-isolant et supraconducteur-isolant*. PhD thesis, Paris XI, Orsay.

[Marrache-Kikuchi et al., 2008] Marrache-Kikuchi, C., Aubin, H., Pourret, A., Behnia, K., Lesueur, J., Bergé, L., and Dumoulin, L. (2008). Thickness-tuned superconductor-insulator transitions under magnetic field in a-nbsi. *Phys. Rev. B*, 78:144520.

[Marrache-Kikuchi et al., 2006] Marrache-Kikuchi, C., Berge, L., Collin, S., Dobrea, C., Dumoulin, L., Juillard, A., and Marnieros, S. (2006). Properties of thermometric nbsi thin films and application to detection in astrophysics. *Nucl. Instr. and Meth. in Phys. Res. A*, 559:579.

[Mooij and Harmans, 2005] Mooij, J. E. and Harmans, C. J. P. M. (2005). Phase-slip flux qubits. *New Journal of Physics*, 7(1):219.

[Mooij and Nazarov, 2006] Mooij, J. E. and Nazarov, Y. V. (2006). Superconducting nanowires as quantum phase-slip junctions. *Nat. Phys.*, 2:169.

[Moseley, 2009] Moseley, S. (2009). Scientific applications and promise of cryogenic detector arrays. *AIP Conf. Proc.*, 1185:9.

[Olivieri et al., 2012] Olivieri, E., Domange, J., Dumoulin, L., Marnieros, S., and Broniatowski, A. (2012). Transport anisotropy and impurity scattering in ge at millikelvin temperatures : Experimental study. *J. Low Temp. Phys.*, 167:1137.

[Ovadia et al., 2009] Ovadia, M., Sacépé, B., and Shahar, D. (2009). Electron-phonon decoupling in disordered insulators. *Physical review letters*, 102(17):176802.

[Ovadyahu, 1993] Ovadyahu, Z. (1993). Optical absorption and disorder in an amorphous metal. *Phys. Rev. B*, 47:6161–6164.

[Ovadyahu, 2006] Ovadyahu, Z. (2006). Temperature- and field-dependence of dynamics in electron glasses. *Phys. Rev. B*, 73:214208.

[Ovadyahu and Pollak, 2003] Ovadyahu, Z. and Pollak, M. (2003). History-dependent relaxation and the energy scale of correlation in the electron glass. *Physical Review B*, 68(18):184204.

[Pari, 1987] Pari, P. (1987). *Réfrigeration $^3$He-$^4$He sans étage de condensation séparé*. PhD thesis, CNAM.

[Pari, 1990] Pari, P. (1990). Dilution refrigerator with no liquid helium supply. *Adv. Cryo. Eng.*, 35:1079.

[Pollak and Ortuño, 1984] Pollak, M. and Ortuño, M. (1984). Sol. energy mater., 8, 81 (1982); m. pollak. *Philos. Mag. B*, 50:265.

[Punnoose and Finkel'stein, 2005] Punnoose, A. and Finkel'stein, A. (2005). Metal-insulator transition in disordered two-dimensional electron systems. *Science*, 310:289.

[Qin et al., 2006] Qin, Y., Vicente, C. L., and Yoon, J. (2006). Magnetically induced metallic phase in superconducting tantalum films. *Physical Review B*, 73(10):100505.

[Sacépé, 2007] Sacépé, B. (2007). *Spectroscopie tunnel dans les films minces proches de la transition supraconducteur-isolant*. PhD thesis, Joseph Fourier, Grenoble.

[Sacépé et al., 2008] Sacépé, B., Chapelier, C., Baturina, T., Vinokur, V., Baklanov, M., and Sanquer, M. (2008). Disorder-induced inhomogeneities of the superconducting state close to the superconductor-insulator transition. *Phys. Rev. Lett.*, 101:157006.

[Sacépé et al., 2010] Sacépé, B., Chapelier, C., Baturina, T., Vinokur, V., Baklanov, M., and Sanquer, M. (2010). Pseudogap in a thin film of a conventional superconductor. *Nature Communications*, 1:140.

[Sachdev, 1999] Sachdev, S. (1999). *Quantum Phase Transitions*. Cambridge University Press.

[Sadoulet, 1999] Sadoulet, B. (1999). Deciphering the nature of dark matter. *Rev. Mod. Phys.*, 71:S197.

[Sadoulet, 2009] Sadoulet, B. (2009). Recent progress with low temperature particle detectors. *AIP Conf. Proc.*, 1185:785.

[Sambandamurthy et al., 2004] Sambandamurthy, G., L.W. Engel, A. J., and Shahar, D. (2004). Superconductivity-related insulating behavior. *Phys. Rev. Lett.*, 92:107005.

[Shahar and Ovadyahu, 1992] Shahar, D. and Ovadyahu, Z. (1992). Superconductivity near the mobility edge. *Phys. Rev. B*, 46:10917.

[Simonin, 1986] Simonin, J. (1986). Surface term in the superconductive ginzburg-landau free energy : Application to thin films. *Phys. Rev. B*, 33:7830.

[Sondhi et al., 1997] Sondhi, S., Girvin, S., Carini, J., and Shahar, D. (1997). Continuous quantum phase transitions. *Rev. Mod. Phys.*, 69:315.

[Spivak et al., 2008] Spivak, B., Oreto, P., and Kivelson, S. (2008). Theory of quantum metal to superconductor transitions in highly conducting systems. *Physical Review B*, 77(21):214523.

[Spivak et al., 2001] Spivak, B., Zyuzin, A., and Hruska, M. (2001). Quantum superconductor-metal transition. *Phys. Rev. B*, 64:132502.

[Stewart et al., 2007] Stewart, M., Yin, A., Xu, J., and Valles, J. M. (2007). Superconducting pair correlations in an amorphous insulating nanohoneycomb film. *Science*, 318(5854):1273–1275.

[Strongin et al., 1970] Strongin, M., Thompson, R., Kammerer, O., and Crow, J. (1970). Destruction of superconductivity in disordered near-monolayer films. *Phys. Rev. B*, 1:1078.

[Tashiro et al., 2008] Tashiro, H., Graybeal, J. M., Tanner, D. B., Nicol, E. J., Carbotte, J. P., and Carr, G. L. (2008). Unusual thickness dependence of the superconducting transition of a-moge thin films. *Phys. Rev. B*, 78:014509.

[Uemura, 1997] Uemura, Y. J. (1997). Bose-einstein crossover picture for high-$T_c$ cuprates. *Physica C*, 282:194.

[Uemura et al., 1989] Uemura, Y. J., Luke, G. M., Sternlieb, B. J., Brewer, J. H., Carolan, J. F., Hardy, W. N., Kadono, R., Kempton, J. R., Kiefl, R. F., Kreitzman, S. R., Mulhern, P., Riseman, T. M., Williams, D. L., Yang, B. X., Uchida, S., Takagi, H., Gopalakrishnan, J., Sleight, A. W., Subramanian, M. A., Chien, C. L., Cieplak, M. Z., Xiao, G., Lee, V. Y., Statt, B. W., Stronach, C. E., Kossler, W. J., and Yu, X. H. (1989). Universal correlations between $T_c$ and $\frac{n_s}{m^*}$ (carrier density over effective mass) in high-$T_c$ cuprate superconductors. *Phys. Rev. Lett.*, 62:2317–2320.

[van der Zant et al., 1996] van der Zant, H. S. J., Elion, W. J., Geerligs, L. J., and Mooij, J. E. (1996). Quantum phase transitions in two dimensions: Experiments in josephson-junction arrays. *Phys. Rev. B*, 54:10081–10093.

[Webster et al., 2013] Webster, C., Fenton, J., Hongisto, T., Giblin, S., Zorin, A., and Warburton, P. (2013). Nbsi nanowire quantum phase-slip circuits: dc supercurrent blockade, microwave measurements, and thermal analysis. *Physical Review B*, 87(14):144510.

[Yazdani and Kapitulnik, 1995] Yazdani, A. and Kapitulnik, A. (1995). Superconducting-insulating transition in two-dimensional a-moge thin films. *Phys. Rev. Lett.*, 74:3037.